Application of Commingled Thermoplastic Composites on an Airline Seat Backrest

Richard Mattheyse

Thesis presented at the University of Stellenbosch in partial fulfilment of the requirements for the degree of

Master of Science in Mechanical Engineering

Department of Mechanical and Mechatronic Engineering
Stellenbosch University
Private Bag X1, 7602 Matieland, South Africa

Supervisors:

Mr. Kobus van der Westhuizen   Stellenbosch University

Dr. Ir. Kjelt van Rijswijk   Aerosud Innovation and Training Centre

December 2009

DECLARATION

By submitting this thesis electronically, I declare that the entirety of the work contained therein is my own, original work, that I am the owner of the copyright thereof (unless to the extent explicitly otherwise stated) and that I have not previously in its entirety or in part submitted it for obtaining any qualification.

Date: 23 Nov. 09

ABSTRACT

Thermoplastic composites (TPCs) have shown significant advantages over thermosetting composites. They have only been put into use recently and global knowledge in TPCs is often proprietary, therefore a study into the application, processing and properties is of importance. The aim of the study is to contribute knowledge in TPCs for South African industry and academic institutions.

This thesis studies continuous fibre reinforced thermoplastics (CFRTPs), focussing on the autoclave processing of commingled CFRTPs. A literature study provided background knowledge to CFRTPs regarding processing techniques and mechanics.

Flexural testing and impact testing were performed on a variety of CFRTPs and thermosetting composites (TSCs). These tests were performed to further understand CFRTPs as well as to compare CFRTPs and TSCs. The flexural testing revealed that CFRTPs have comparable strength and stiffness to the TSCs that were tested. They also revealed that pre-consolidated sheets showed better and more consistent properties than sheets made from commingled fabric. The impact testing revealed that the tested CFRTPs and TSCs had similar impact resistance even though thermoplastic composites are supposed to be more impact resistant. The tests also showed that thick unreinforced thermoplastics had much higher impact resistance than the reinforced materials.

Manufacturing experiments were performed to establish sound processing methods of CFRTPs. It was realised here that the high temperatures required to process the materials require specific processing consumables and tooling. The experiments began by processing flat panels in a convection oven with vacuum bagging techniques. They then progressed to autoclave processing of parts with complex geometry.

An airline seat backrest was chosen as the case study in the application of CFRTPs. This application requires structural strength and stiffness and also has strict fire, smoke, toxicity and heat release (FSTH) requirements. Its geometry was sufficiently complex to demonstrate the use of commingled CFRTP material. Backrests were made from both CFRTPs and TSCs so that a comparison could be made between the two types.

The backrest was modelled using finite element methods (FEM) to determine an adequate lay-up. This lay-up was then used for both the CFRTP and TSC backrests to ensure similarity between the backrests of both materials. LPET (modified polyethylene terephthalate) was the chosen thermoplastic matrix as it was more attainable than PPS (polyphenylene sulphide) CFRTPs. The backrests of both materials were manufactured in an autoclave with a vacuum bag method and then assembled using adhesives and bonding jigs. Testing revealed that the stiffness and mass of the CFRTP backrests were very similar to the epoxy backrests. This implies that commingled CFRTPs can replace the use of TSCs in similar applications.

A basic cost comparison was also performed to compare the manufacture of CFRTP backrests to TSC backrests.

Further work is needed to optimise processing time of these materials to make them more competitive with TSCs. The processing time of commingled materials will probably never be as quick as that of press formed pre-consolidated sheets. Their ability to be formed into more complex parts does however make their use advantageous.

OPSOMMING

Termoplastiese saamgestelde materiale (Engels: thermoplastic composites (TPCs)) toon beduidende voordele bo termoverhardbare saamgestelde materiale. Hulle word eers sedert onlangs benut en algemene kennis in TPCs is dikwels patentregtelik, dus is 'n studie van die aanwending, prosessering en eienskappe daarvan van belang. Die doel van hierdie studie is om 'n bydrae te lewer tot die kennis van TPCs vir die Suid-Afrikaanse industrie en akademiese instellings.

Hierdie tesis ondersoek kontinue veselversterkte termoplastieke (Engels: continuous fibre reinforced thermoplastics (CFRTPs)) en fokus op die outoklaafprosessering van vermengde (Engels: commingled) CFRTPs. 'n Literatuurstudie het die agtergrondkennis rakende die prosesseringstegnieke en meganika van CFRTPs verskaf.

Buigtoetsing en impaktoetsing is op 'n verskeidenheid CFRTPs en termoverhardbare saamgestelde materiale (Engels: thermosetting composites (TSCs)) uitgevoer. Hierdie toetse is uitgevoer om CFRTPs beter te verstaan asook om CFRTPs en TSCs te vergelyk. Die buigtoetsing het onthul dat CFRTPs ooreenstemmende sterkte en styfheid het as die TSCs wat getoets is. Dit het ook getoon dat vooraf-gekonsolideerde plate beter en meer konsekwente eienskappe getoon het as plate wat van vermengde materiaal gemaak is. Die impaktoetsing het onthul dat die CFRTPs en TSCs wat getoets is soortgelyke impakweerstand gehad het, selfs al is termoplastiese saamgestelde materiale veronderstel om meer impakweerstand te toon. Die toetse het ook getoon dat dik onversterkte termoplastieke veel hoër impakweerstand gehad het as die versterkte materiale.

Vervaardigingseksperimente is uitgevoer om betroubare prosesseringsmetodes vir CFRTPs vas te stel. Daar is besef dat die hoër temperature wat vereis word om die materiale te prosesseer ook spesifieke prosesseringsverbruiksware en -gereedskap benodig. Die eksperimente het begin met die prosessering van reguit panele in 'n konveksie-oond met vakuumsaktegnieke. Daar is toe aanbeweeg na die outoklaafprosessering van onderdele met komplekse geometrie.

Die rugleuning van 'n vliegtuigsitplek is gekies as die gevallestudie in die gebruik van CFRTPs. Hierdie toepassing vereis strukturele sterkte en styfheid en is ook onderhewig aan streng vereistes t.o.v. brand, rook, toksisiteit en hittevrystellimg (Engels FSTH). Die geometrie daarvan was kompleks genoeg om die gebruik van vermengde CFRTP-materiaal te demonstreer. Rugleunings is gemaak van beide CFRTPs en TSCs sodat 'n vergelyking tussen die twee tipes gemaak kon word.

Die rugleuning is gemodelleer deur eindige element metodes (EEM) te gebruik om 'n aanvaarbare oplegging te bepaal. Hierdie oplegging is toe gebruik vir beide die CFRTP en TSC rugleunings om die gelykvormigheid tussen die rugleunings van beide materiale te verseker. LPET (Engels: modified polyethylene terephthalate) was die gekose termoplastiese matriks aangesien dit meer verkrygbaar was as PPS (Engels: polyphenylene sulphide) CFRTPs. Die rugleunings van beide materiale is vervaardig in 'n outoklaaf met 'n vakuumsakmetode en toe geintegreer deur die gebruik van kleefstowwe en setmate. Toetsing het getoon dat die styfheid en massa van die CFRTP rugleunings baie soortgelyk was aan die epoksie rugleunings. Dit impliseer dat vermengde CFRTP die plek van TSCs in soortgelyke gebruike kan inneem.

'n Basiese kostevergelyking is ook gedoen om die vervaardiging van CFRTP-rugleunings teenoor TSC-rugleunings te vergelyk.

Verdere studie is nodig om die prosesseringstyd van hierdie materiale te optimeer om hulle meer kompeterend met TSCs te maak. Die prosesseringstyd van vermengde materiale sal waarskynlik nooit so vinnig as dié van persgevormde vooraf-gekonsolideerde plate wees nie. Hul vermoë om in meer komplekse onderdele gevorm te word, maak hul gebruik egter meer voordelig.

ACKNOWLEDGEMENTS

CONTENTS

LIST OF FIGURES

LIST OF TABLES

LIST OF ABBREVIATIONS AND NOMENCLATURE

CF	-	Carbon fibre
CFRTP	-	Continuous fibre reinforced thermoplastic
DSC	-	Differential scanning calorimetry
E	-	Young's modulus (tensile modulus of elasticity)
EMI	-	Electromagnetic interference
FEA	-	Finite element analysis
FEM	-	Finite element methods
FSTH	-	Fire, smoke, toxicity and heat release
G	-	Shear modulus of elasticity
GF	-	Glass fibre
GW	-	Glass weave (also used as subscript)
LPET	-	An amorphous form of PET (Polyethylene terephthalate) modified to be processed at 200 °C - 230 °C.
PA 6	-	Polyamide 6
PA 66	-	Polyamide 66
PBT	-	Polybutylene terephthalate
PEEK	-	Polyether-etherketone
PEI	-	Polyetherimide
PET	-	Polyethylene terephthalate
PP	-	Polypropylene
PPS	-	Polyphenylene sulphide
SG	-	Specific gravity
Tg	-	Glass transition temperature
TGA	-	Thermo-gravimetric analysis
Tm	-	Melting temperature
TP	-	Thermoplastic
TPC	-	Thermoplastic composite
TS	-	Thermoset
TSC	-	Thermosetting composite
UD	-	Unidirectional – a composite material with all fibres in one direction (also used as subscript)

1   INTRODUCTION

Thermoplastic composites (TPCs) have shown significant advantages over thermosetting composites. They have only been put into use relatively recently (about 20 years ago, E-Composites, 2003) and global knowledge in TPCs is often proprietary, therefore a study into the application, processing and properties is of importance. The aim of the study is to contribute knowledge in TPCs for South African industry and academic institutions. It was written as part of the requirements for an MScEng (Mechanical) degree at Stellenbosch University, South Africa. The research was part of the CFRTP research group (AMTS 07-04-M) of the AMTS (Advanced Manufacturing Technology Strategy) initiative funded by the Department of Science and Technology.

Continuous fibre reinforced thermoplastics (CFRTPs) have shown major advantages for the aviation industry. These advantages include rapid processing cycles instead of the long curing cycles for thermosetting composites (TSCs). Airbus alone produces about 480 aircraft a year (Kingsley-Jones, 2009) and each aircraft requires between 100 and 525 seats. These seats require backrests with strict FSTH (fire, smoke, toxicity and heat release) properties, structural strength and rigidity and impact resistance which are all related to passenger safety. Thus it was decided to investigate CFRTPs with the focus application of airline seat backrests.

Airline backrests have complex geometry which would make them difficult to produce by press-forming pre-consolidated CFRTPs – a method commonly used in the aerospace industry. It was therefore decided to focus this study on the vacuum bag processing of commingled CFRTP material. These materials allow easily customisable lay-ups and their drapability makes it possible to manufacture parts with complex geometry.

The aim of this study was to gain an understanding of commingled CFRTPs and compare them to composite materials currently used to make backrests. A literature study was performed to gain current knowledge on the subject including types of thermoplastics, raw material forms, processing methods and characteristics of CFRTPs that affect their processing.

Manufacturing experiments were performed to establish sound processing methods of CFRTPs. These started with vacuum bag processing in a convection oven and progressed to autoclave processing methods. Flat panels were first produced, followed by parts with complex geometry.

Flexural tests were performed on a variety of composite materials. Pre-consolidated CFRTPs and TSCs currently used in the aerospace industry were tested and compared with commingled materials. These tests provided a good general impression of the mechanical properties of the materials.

Low velocity, small-impactor impact tests were also performed on a variety of CFRTP and TSC materials. The aim of these tests was to quantify the impact resistance of the materials and make a comparison between them.

The case study backrests were manufactured after the initial research into CFRTPs was complete. The backrest was based on a design previously produced for airline companies. Its geometry was sufficiently complex to demonstrate the use of commingled CFRTP material. It was decided to produce backrests with both CFRTPs and TSCs so that a comparison could be made between the two types of materials.

The backrest was modelled using finite element methods (FEM) to determine an adequate lay-up. This lay-up was then used for both the CFRTP and TSC backrests to ensure similarity between the backrests of both materials.

The backrests of both materials were manufactured in an autoclave with a vacuum bag method and then assembled using adhesives and bonding jigs. These manufactured backrests were then mechanically tested so that the stiffness of CFRTP and TSC components could be compared.

A basic cost comparison was also performed to compare the manufacture of CFRTP backrests to TSC backrests.

2   LITERATURE STUDY

2.1   Background

Continuous fibre reinforced thermoplastic composites (CFRTPs) have had a relatively short history of about 20 years. They began receiving attention in the military aviation industry in the 1980s because the first generation thermosetting composites (TSCs) were showing signs of delamination from low-velocity impacts such as those from dropped tools (Hannsman, 2003). CFRTPs were thus identified as materials having higher damage tolerance.

E-Composites, Inc. (2003) reported that the market for CFRTPs has grown rapidly with a reported growth rate of 105 % between 1998 and 2002 and that this growth is due to low-cost commingled materials becoming available in recent years. 13.4 million lbs of commingled CFRTPs alone were shipped in 2002 and it was predicted that the use of CFRTPs would be over 80 million lbs in 2008. Thus, the CFRTP industry has grown rapidly and this growth is predicted to increase in the future.

2.2   Benefits of CFRTPs

The benefits and disadvantages of thermoplastic composites (TPCs) compared to thermosetting composites (TSCs) are listed in the section below. These are sourced from the following references: Bigg et al (1988), Svensson et al (1988), Bourban et al (2001), McDonnell et al (2001), Hansmann (2003), E-Composites, Inc. (2003):

2.2.1   Benefits of Thermoplastic Composites

- Thermoplastic composites have better impact strength and chemical resistance over most TSCs.
- They have an unlimited shelf life.
- They require only heat and pressure to process whereas TSCs require time for the curing process.
- They are suited to high volume production.
- There is no need for cooled storage and transport.
- Their manufacturing is 'clean' without solvents or fumes.
- They are easier to recycle.
- Their processing times are faster.
- Certain TPCs have better fire, smoke, toxicity and heat (FSTH) properties than TSCs.
- They can be re-melted for fusion bonding or secondary shaping. This can eliminate the need for drilling holes for fasteners when parts need joining.

2.2.2   Disadvantages of Thermoplastic Composites

- They require higher temperature and pressure to process than TSCs – their processing temperature must be much higher than their intended use temperature.
- High melt viscosities of molten polymers (500 – 5000 Pa.s) compared to uncured TSs (100 Pa.s) cause difficult/slower impregnation (fibre wetting).
- It is more difficult to pre-impregnate the fibres (to make a prepreg).
- Vacuum bagging consumables need to withstand much higher temperatures and are therefore more expensive and more difficult to work with.
- TPs' mechanical performance decreases as their T_g is approached

- Lack of tackiness can make lay-ups difficult.
- Thermoplastics show poor creep resistance, especially at elevated temperature, compared to thermosetting plastics.
- Tooling can be expensive due to the high temperatures and pressures required in processing.

2.3   Thermoplastics Used in CFRTPs

Thermoplastics are divided into categories depending on their morphology. These morphologies are described as crystalline, semi-crystalline and amorphous (Hansmann, 2003). It is, however, not possible to obtain 100 % crystallinity due to the complex nature of thermoplastic molecules. Therefore, only semi-crystalline and amorphous thermoplastics will be discussed.

Semi-crystalline TPs have areas of ordered molecular structure and exhibit well-defined melting points. Cooling rate affects crystallinity as it is a transport and thermodynamic phenomenon. Crystallinity has similar effects to the cross-linking in TSs as it increases the stiffness and solvent resistance of the polymer. Softening occurs more gradually as the temperature increases above T_g for semi-crystalline materials than amorphous materials and progresses toward a sudden change to an apparent liquid state. Semi-crystalline materials usually show good chemical resistance.

Amorphous TPs have a random molecular structure. They do not show a sharp melting point but instead soften gradually with rising temperature. Their strength decreases rapidly above their T_g even when reinforced with continuous fibres. They are also more susceptible to physical aging effects, creep and fatigue at elevated temperatures.

Table 1 lists and describes thermoplastics that are used currently in CFRTPs. This list does not contain all the thermoplastics that could possibly be used in CFRTPs. It only lists those that are commonly used. The contents of the table and the following paragraphs are referenced from Comfil ApS (Polymer Types) and E-Composites, Inc. (2003).

Table 1: Thermoplastics commonly used in CFRTPs

Material	Processing Temperature [°C]	Continuous Use Temperature [°C]	Uses	Comments
Polyamide 6 (PA 6)	240	120	Anti-ballistics, sports equipment, automotive components	Good price/performance ratio
Polyamide 66 (PA 66)	280	130	Sports equipment, industrial applications, automotive components	Good price/performance ratio
PBT (Polybutylene terephthalate)	250-280	110	Automotive components	Commonly used. Good chemical resistance
PEEK (Polyether-etherketone)	365-380	250	Oil and aviation industry	"Extraordinary" mechanical properties. High chemical resistance. High impact strength. Very good flame retardance. Expensive
PEI (Polyether-imide)	370-400	200	Aviation industry	Slightly lower properties than PEEK. Excellent flame retardance. Cheaper than PEEK.
PP (Polypropyl-ene)	185-200	90	Automotive components	Most commonly used. One of the cheapest thermoplastic matrix
PPS (Polyphenylene-sulphide)	310	220	Aviation industry, automotive components	"Exceptional" chemical resistance, high mechanical properties and excellent flame retardance

As the focus application for this project is aviation interior components, specifically backrests, the most suitable materials would be PPS, PEI and PEEK. This is because they have excellent fire, smoke, toxicity and heat release (FSTH) ratings and high mechanical properties.

The author believes PPS is the ideal material for aircraft backrests as its processing temperature of 310 °C is much lower than that of PEEK and PEI (365 °C – 400 °C) which makes the cost and ease of manufacture favourable. It is not as tough as the other high performance matrices but its modulus and strength are within 20 % of PEEK. Another

advantage is that it can be used above its T_g due to its semi-crystalline nature. It is also about half the price of PEEK.

2.4   Material Preforms

2.4.1   Mixed Fibres

This category of CFRTPs has the reinforcing fibres mixed with polymer fibres in a yarn which is then woven or stitched into a fabric. There are four categories of yarns containing mixed fibres, namely: Commingled, co-wrapped, core-spun and non-commingled (Svensson et al, 1998 and Bourban et al, 2001). The aim of the yarns is to uniformly distribute the matrix and reinforcement fibres and to protect the reinforcement fibres from damage.

Commingled yarns have continuous reinforcement and matrix fibres mixed at the fibre level. This process allows much freedom in the type and combination of materials. Another form of commingling described by McDonnell et al (2001) consists of stretch broken reinforcing fibres with an average length of 80 mm that are blended using a textile spinning technique. This form is reported to have comparable strength to continuous fibres. Figure 1 shows examples of commingled material including woven fabric and stitched unidirectional and multiaxial fabrics.

Figure 1: Examples of commingled fabric

Co-wrapping involves wrapping thermoplastic fibres around a core of reinforcement fibres. This provides good protection for the reinforcement fibres during weaving or braiding of yarns, but has poor fibre distribution which requires higher processing temperatures and pressures.

Laminates made from commingled yarns have less voids and higher strengths than those made from co-wrapped yarns.

Combining commingling and co-wrapping gives a yarn with good reinforcement protection and fibre distribution.

Core-spun yarns have short thermoplastic fibres spun around a core of reinforcement fibres. These yarns have similar properties to co-wrapped yarns but are more flexible allowing easier post-processing.

Non-commingled yarns simply consist of a thermoplastic bundle and a reinforcing fibre bundle placed next to each other without them being intimately mixed.

Commingled yarns, woven into fabric provide a drapable material that can be handled easily during processing. Lystrup (2006) reported that it can be processed with pressure as low as 0.1 MPa (vacuum only). He also reported that it can be used for large parts of complex geometry and thick lay-ups (100 mm after consolidation).

Commingled roving and fabrics offer extremely fast processing via filament winding, compression moulding, pultrusion and vacuum moulding (E-Composite, 2003).

2.4.2 Powder Impregnation

Reinforcement fibres can be powder-coated and mingled into yarns for further weaving, stitching or braiding (Svensson et al, 1998 and Bourban et al, 2001). These yarns have higher friction which causes difficulties in textile processing such as fibre breakage, powder fall-off and entanglement. Powder-coated fabrics are also more bulky than commingled fabrics which results in more movement during moulding and possibly more complex tooling. The production of powders with small particle sizes is also more expensive than producing polymer fibres as reported by Hansmann (2003).

2.4.3 Consolidated and Semi-Consolidated Sheets

Thermoplastic prepreg is typically sold in sheet form. These sheets are supplied as pre-consolidated material and can come in various thicknesses with specified fibre orientations. They can also be supplied as custom/tailored lay-ups where the thicknesses and ply orientations vary over a sheet as reported by Cramer (2003).

Prepreg is produced by layering the reinforcing fabric with sheets of polymer. The polymer is then heated above its melting or softening temperature and then forced into the fabric with applied pressure.

Sometimes, the plastic is only part-melted into the fabric to form a flexible sheet known as semi-preg. This material form is useful for large parts of simple curvature and can be processed in an autoclave. Semi-preg also allows varied lay-ups throughout the part.

2.5 Processing Methods

2.5.1 Vacuum/Autoclave Consolidation

Vacuum consolidation involves heating the laminate in a one sided mould to melting temperature under vacuum. The vacuum is usually applied using a plastic vacuum bag with sealant tape in a process similar to that used for TSCs. Lystrup (2006) reported that this method can be used to produce very large parts, such as wind turbine blades, as it does not require an autoclave or press. The mould can either contain its own heat source or can be placed in a convection oven.

Vacuum consolidation of commingled materials is limited to parts with simple geometry because a maximum pressure of only 0.1 MPa (atmospheric pressure) is applied. There are methods to overcome this limitation as discussed in the following section.

Parts with complex geometry require additional pressure to ensure complete consolidation and to prevent bridging (where the fibres do not follow the contours/corners of a mould completely). This can be provided by performing the vacuum consolidation in an autoclave to apply a pressure higher than atmospheric pressure.

2.5.2 Compression Moulding

Compression moulding or press moulding applies pressure to the molten laminate with matched male and female moulds (E-Composites, 2003). One mould can be made of an elastomeric material to improve pressure application on steep faces. This method can be used with all thermoplastic sheet and fabric forms.

The process involves melting the laminate– in the mould for commingled fabrics and outside for prepregs – then closing the mould on the laminate, waiting for the laminate to solidify sufficiently under pressure and then removing the part from the mould.

Press moulding provides good surface finishes on both sides of a laminate.

2.5.3 Miscellaneous Methods

The methods described in this section are either less commonly used or irrelevant to this project. The section is referenced from E-Composites (2003).

Panel lamination can be used to make flat sheets with or without cores. The panels are produced by feeding rolls of CFRTP flexible sheets (and core material if applicable) into rollers where heating is applied for consolidation followed by cooling. These panels can be used as-is or for a secondary process such as compression moulding.

Roll forming is similar to panel lamination where sheet stock is preheated above the melting point. Instead of just making flat panels, the sheets stock is run through a series of rollers that form the material into a final shape. Various beam shapes are produced with this method.

Tape winding involves laying a narrow strip of CFRTP sheet onto a mandrel. Heating occurs at the roller that applies pressure to the tape on the mandrel. The process can be automated and results in few residual stresses due to localised and fast heating and cooling of the plastic.

Filament winding is similar to tape winding except that commingled roving is used for raw material. The rovings are pulled through a heater onto a mandrel where pressure is applied to consolidate the material. It is used to make cylindrical structures such as storage tanks and pressure vessels.

Bladder forming is similar in principle to autoclave processing. It is used to make hollow parts. A silicone bladder is inserted into a braided or filament wound preform. This is then placed into a solid mould where the laminate is heated and pressure is applied to the inside of the bladder which forces the laminate against the mould surface.

2.5.4 Post-Processing and Bonding

Fusion bonding involves the same principles as other CFRTP processes, namely, the application of heat and pressure. The components to be joined can be heated with externally applied methods such as resistance heating of a conductive mesh between the components or by inductive heating of the reinforcement fibres (Hansmann, 2003). Hansmann also reports that successful bonding can be achieved by placing a film of plastic with a lower melting temperature between the parts being bonded. The entire part is then heated with the bonded areas placed under pressure. This is obviously only possible with certain combinations of polymers.

2.6 Processing Considerations

2.6.1 Isothermal vs. Non-isothermal Processing

Isothermal processing entails the heating of the laminate to the polymer melting temperature and then holding it there, under pressure, until the required consolidation has taken place before cooling it.

Non-isothermal processing involves heating the laminate to the polymer melting temperature outside the mould. The laminate is then swiftly transferred to the mould where pressure is applied to enable consolidation (Tufail, 2007). The mould is often heated to below melting temperature of the polymer to slow down the cooling of the matrix.

Pressure has to be maintained during cooling to prevent fibre misalignment (waviness) and consequent reduction in mechanical properties (McDonnell et al, 2001).

2.6.2 Laminate Placement Techniques

Lystrup (2006) reported that shrinking the inner layers of a commingled laminate for a concave curvature allows the laminate to form better to the mould. Polymer fibres shrink when heat is applied which then crinkles the reinforcing fibres in the commingled roving. A hot-air blower can be used to shrink the fabric locally wherever it may be needed.

Hansmann (2003) suggests that the first ply can be held to the mould using an adhesive tape and then each subsequent ply can be tacked to the layer below it. A blunt soldering iron, heated well above the plastic's T_g, can be used for the tacking process. Light pressure is applied with the tip which melts the polymer and fuses two or more plies together locally.

2.6.3 Other Considerations

Lystrup (2006) reported that most thermoplastic materials have to be completely dry with no absorbed water before melting as water reacts with the polymer during heating. He suggests the addition of a drying step in the process to remove any water present. Ten Cate (2006) also recommend drying the material as they report their prepreg laminates delaminating after heating if too much water is present.

The crystallinity of semi-crystalline TPs results in their solvent resistance and high temperature properties (Hansmann, 2003). The crystallinity also affects the fracture

toughness of these materials. It is therefore important to have the correct cooling rates for semi-crystalline materials if these properties are required (Ijaz et al, 2007).

2.7   Consolidation Mechanics

Consolidation is the process in which the thermoplastic matrix melts and wets the reinforcing fibres. The process starts with the fibre yarns moving closer to each other when pressure is applied. As the temperature reaches the melting temperature, T_m, of the thermoplastic, the matrix fibres melt. The molten polymer then flows amongst the fibres with the aid of applied pressure until all the fibres are melt-impregnated (Bourban et al, 2001).

Impregnation is governed by Darcy's law which is valid for laminar flow of fluids through a homogeneous porous media (Svensson et al, 1998 and Bourban et al, 2001). Darcy's law is described by:

$$\frac{dx}{dt} = \frac{S}{\eta} \times \frac{dp}{dx} \qquad (1)$$

where x is the depth of melt penetration, t is the time, S is the permeability, p is the driving pressure and η is the viscosity of the molten polymer. In words, it states that the rate of fluid flow is proportional to the permeability of the fibre bed and the applied pressure gradient and inversely proportional to the viscosity of the molten polymer.

Several models have been developed to describe the impregnation of thermoplastics in reinforcing fibres during processing (Svensson et al, 1998 and Bourban et al, 2001). These mathematically describe the nature of the flow between the fibres for various preforms. They also relate impregnation time to processing parameters of temperature and pressure as well as powder particle/fibre diameter and matrix mixing quality. These models also predict void content which allows process time optimisation for certain maximum void requirements.

Experiments and the above-mentioned models have shown that temperature and pressure have the greatest influence on laminate quality. However, McDonnell et al (2001) reported that temperature had a greater influence on laminate mechanical properties than pressure.

An interesting study performed by Hagstrand et al (2005) showed that increased void content in a unidirectional commingled glass/polypropylene caused by inadequate time at pressure in a non-isothermal moulding process caused a slight increase in beam stiffness and strength. This was due to the voids causing thicker laminates and therefore increased cross-sectional moment of inertia. This indicates that even though voids, which weaken a laminate's mechanical properties, can actually increase structural properties. This also implies that processing time can be decreased in certain cases and therefore result in decreased manufacturing costs.

Ijaz et al (2006) described the consolidation behaviour of vacuum processed commingled material as a two-stage process. They used semi-crystalline polyethylene terephthalate (PET) and amorphous PET (LPET) in their studies. The first stage occurs around the glass-transition temperature where solid-state compaction occurs. The second stage occurs when the polymer melts and thereby impregnates the reinforcing fibres. The first stage was found to be much more pronounced for the LPET samples, accounting for about 70 % of consolidation as opposed to the 40 % for the semi-crystalline samples.

It was suggested that the first stage consolidation effect can be used in certain cases by 'pre-consolidating' the laminate to reduce the final volume change. This could improve moulding accuracy and reduce the chance of vacuum bag rupture. The above-mentioned two-stage process is unique to vacuum processing. The more common press moulding process usually involves melting the polymer prior to placing it in the mould and therefore is not affected.

3 MANUFACTURING EXPERIMENTS

3.1 Introduction

Experimenting in commingled CFRTP moulding started by using materials and equipment that were easily available. The aim was to gain an understanding of the process and necessary parameters needed to create parts of acceptable quality.

Processing then progressed to more advanced methods with complex moulds, external pressure applied in a high temperature autoclave and varied material lay-ups. This chapter describes the experiments performed and the methods used to establish a sound processing method of commingled CFRTP material.

These methods were used to manufacture the case study backrests that are described in Chapter 7.

3.2 Initial Experimental Findings

Processing was initially performed in an oven in Stellenbosch University's Mechanical and Mechatronic Engineering Department's composites laboratory. These experiments were performed with the help of Pieter Reuvers, a final year mechanical engineering student. Flat panels were made on an aluminium plate with various vacuum-bagging materials until successful panels were produced. Commingled material from Hiform was used in these early experiments.

It was realised here how critical it is to use the correct vacuum bagging consumables, viz., vacuum bag, sealant tape, release film and breather/bleeder cloth. Several experiments were performed with easily obtainable materials. For example, wax paper and aluminium foil were used for release film whilst silicone gasket maker was substituted for sealant. These were impractical and often unable to handle the necessary temperatures. Figure 2 shows the results of these early attempts where either consolidation was inadequate or the consumables damaged the lay-up.

Figure 2: Results of early processing attempts

Some success was eventually reached showing that commingled CFRTPs can be processed with an oven and standard vacuum pump. It was shown that complete consolidation can be achieved with high quality surface finishes and relatively thick laminates. Figure 3 shows a

fully consolidated laminate with a high quality surface finish obtained by processing the material between two polished steel plates. A prototype hydrofoil (Figure 5) was also made by placing the commingled material between two aluminium plates - one curved and one flat - as shown in Figure 4. The thickest part of the hydrofoil was 10 mm showing that relatively thick laminates can be processed with this technique. Dimensional accuracy would not be ideal with this method as the thin plates easily warp. A suggestion to improve the process would be to have solid machined moulds. This was, however, not the focus of the research and therefore not pursued further.
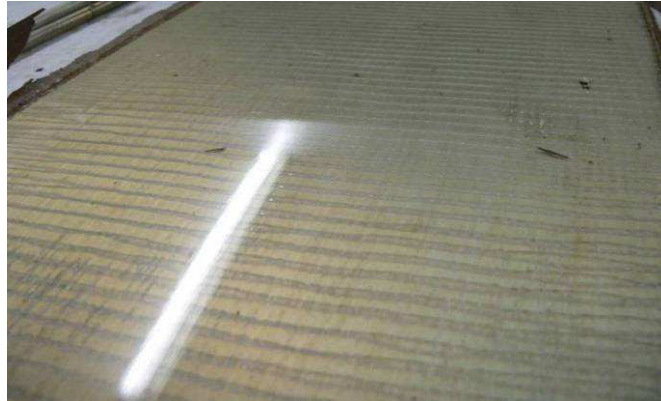
Figure 3: High quality surface finish obtained in a simple oven process

Figure 4: Hydrofoil mould and lay-up

(left: mould plates; right: commingled material in mould)

Figure 5: Untrimmed consolidated hydrofoil manufactured from commingled Hiform LPET/GF material

3.3 Autoclave Processing – Flat Panels

AAT Composites (Strand, South Africa) made an autoclave available to perform further manufacturing experiments. It is capable of temperatures up to 400 °C and pressures of 6 bar allowing experiments to be performed on virtually any thermoplastic composite material.

Flat panel experiments were performed again to establish the viability of autoclave processing. These were successful and panels were produced with various commingled materials such as PP/GF, LPET/GF and PPS/CF. All these materials were processed in a similar manner using vacuum bagging consumables that were rated to the correct temperatures, applying vacuum, heating to the materials' processing temperature, holding it there for a period of time and then cooling. Figure 6 shows examples of these materials.

Figure 6: Examples of CFRTP panels produced in an autoclave

(left: PP, right: PPS)

It was also shown that pre-consolidated materials, such as PPS/GF supplied by Ten Cate, can be reprocessed using an autoclave vacuum bag technique. This was done by stacking several panels of Ten Cate's PPS/GF with Carr Reinforcement's commingled PPS/CF. Figure 7 shows how the materials were stacked and Figure 8 shows the successfully consolidated material. The discolouration is believed to be from the either the release film or sealant tape although this was not confirmed.

The consumables for the high temperature processing of the PPS consumables proved to be quite unreliable. The sealant tape was difficult to work with as it is very soft and messy and the vacuum bagging was quite stiff. Vacuum loss was difficult to prevent and this showed that great care is needed when processing high temperature CFRTPs.
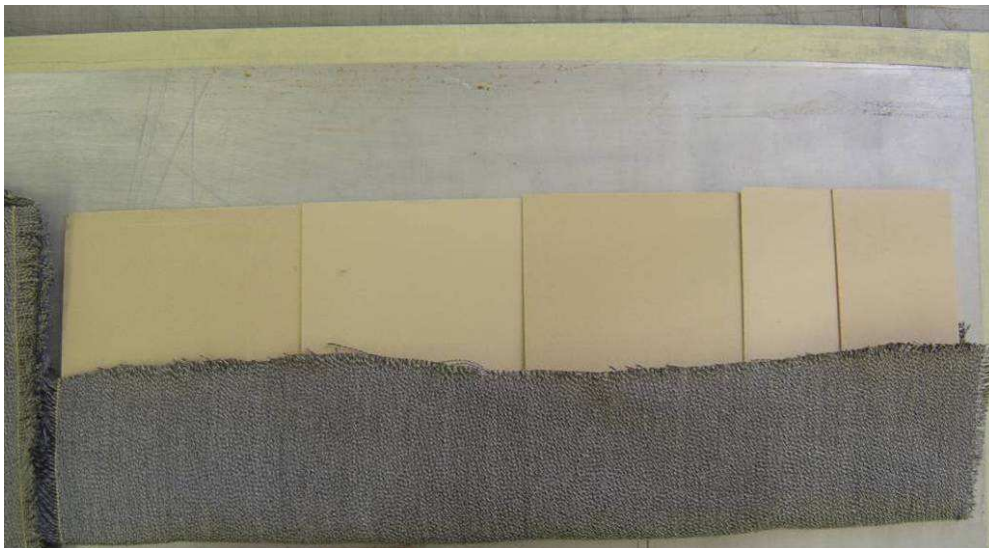
Figure 7: Stacked consolidated and unconsolidated PPS composites

Figure 8: Consolidated Ten Cate and Carr Reinforcement materials

3.4 Autoclave Processing – Complex Geometry

3.4.1 Initial Experiments

Processing of parts with more complex geometry began after success with flat panels was reached. A small mould was designed by Terblanche (2007) which included certain geometrical features that could typically occur in real-life parts. A CAD drawing of the mould is shown in Figure 9.
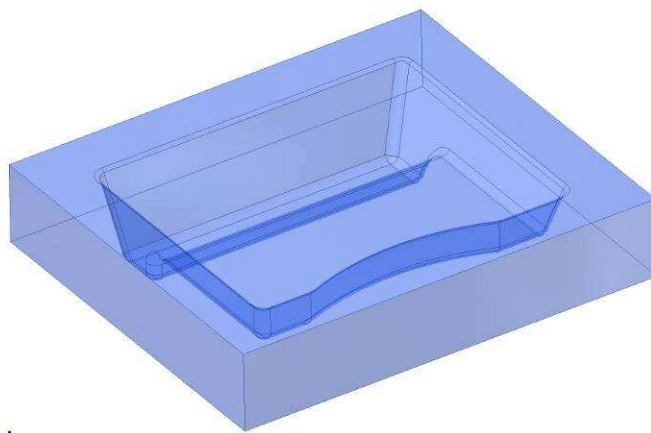
Figure 9: CAD drawing of experimental mould

The aim of these experiments was to determine the ability of commingled materials to be moulded into a relatively complex shape using an autoclave process. This involved a trial-and-error process of changing parameters such as process time and autoclave pressure. Each part was visually inspected and changes in the process were decided on for the next part.

Material placement techniques were also investigated here. The first method was to use an adhesive spray (Airtac 2) to bond the material layers to the mould and to each other. This was found to be quite successful but the effect of the spray on the material properties is unknown and should be investigated further. The other placement method was to use a

soldering iron and melt layers together at certain points/seams. This method is slightly more time-consuming than the adhesive spray but it is believed to be more effective as it allows more movement in the laminate during processing which limits the amount of bridging.

An example of a poorly consolidated part is shown in Figure 10 where bridging is evident in corners and poor consolidation can be seen over most of the part. The bridging was caused by insufficient slack in the vacuum bag preventing adequate pressure in the corners. The poor consolidation was caused by the processing time being too short to allow the mould to reach an acceptable temperature.

Figure 10: Poorly consolidated experimental part (LPET/GF – autoclave processing)

These experiments showed the importance of correct lay-up techniques and process parameters. Sound processing techniques were established which resulted in parts such as the one shown in Figure 11 being successfully consolidated. It can be seen that there is no bridging in the corners of the part and complete consolidation was achieved. The whitened areas on this part are from damage caused during demoulding.
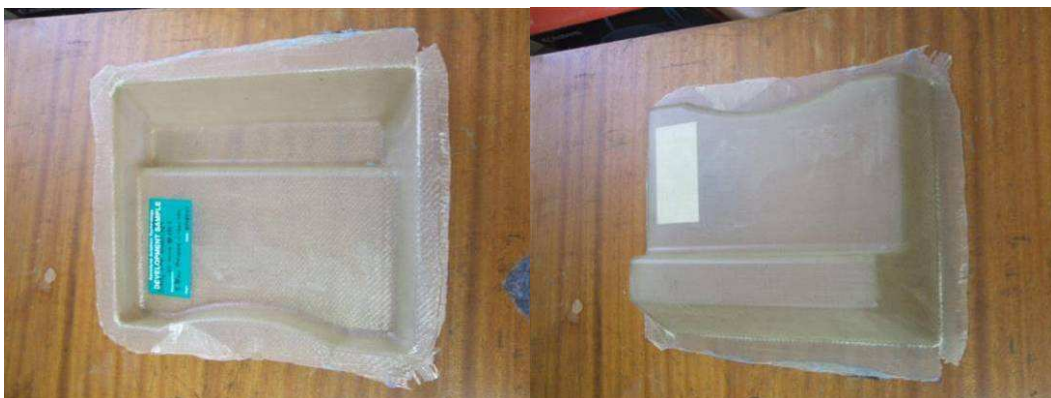
Figure 11: Top and bottom view of successfully consolidated part.

3.5 Detailed Autoclave Processing Description

This section describes the procedure, established by the above-mentioned experiments, to produce parts with complex geometry with a vacuum bagging technique in an autoclave. These procedures were used in the manufacture of the case study backrests that are described in Chapter 7.

3.5.1 Moulding Preparation and Set-up

Figure 12 shows the layout sequence of the materials and consumables on the mould. Here it can be seen that the commingled materials are placed directly on the mould surface followed by the release film, bleeder and vacuum bag. Sealant tape is used to seal the vacuum bag to the mould. Vacuum can be applied to the bag via a nozzle either through the bag or the mould itself. The experiments showed that a permanent nozzle in the mould is more reliable than one placed in the bag.

The use of a temporary tacking aid such as a spray-on adhesive can help the placement of the commingled materials in the mould. However, the use of adhesives should be carefully considered as it could limit the shifting of the material necessary to prevent bridging.
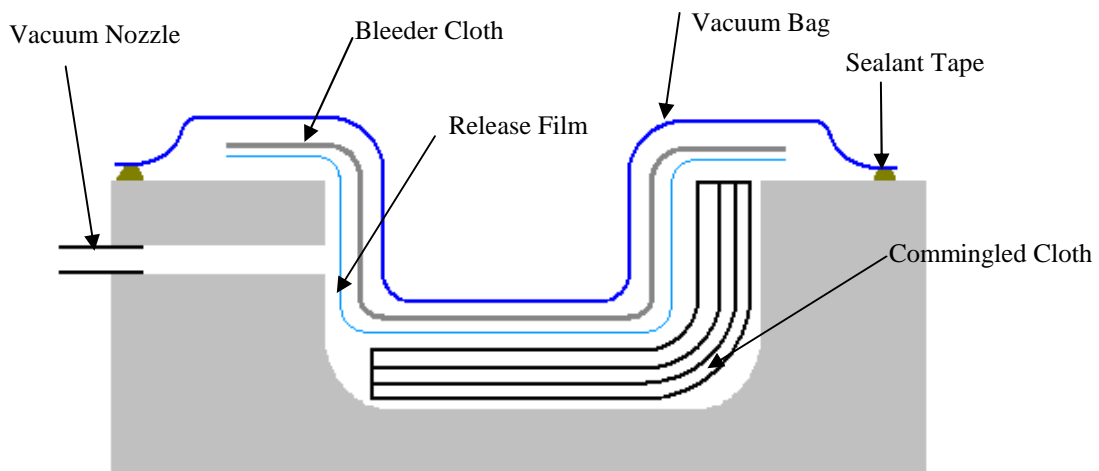
Figure 12: Schematic of materials and consumables placement for autoclave processing

The consumables best matched to a specific material must always be used where possible. Consumables with a temperature rating that is too low will obviously prevent successful part consolidation. Consumables with a rating that is too high will be too expensive as the price increases rapidly with temperature rating.

3.5.2 Mould Preparation

Aluminium moulds (as used in the experiment) should have a smooth surface finish and sharp edges should be avoided. Hard anodising is advisable as it makes the mould easier to clean and resistant to scratching. A release agent should be applied to the mould correctly.

The release agent should be re-applied after moulding of each part especially when demoulding has required scraping on the mould surface.

3.5.3 Vacuum Bagging

The vacuum bagging of commingled CFRTP materials is similar to that of TSCs. The most relevant guidelines are described in this section according to the author's experience in vacuum bag processing.

The vacuum bag should always have excess slack. This lets the bag press into the mould corners completely and allows for shifting and settling of the laminae during processing. This settling or compaction of commingled composites during processing was described in detail by Ijaz et al (2007).

Even if enough slack has been provided in the vacuum bag it is still important to check that the laminate is being firmly pressed into all the corners of the mould once the vacuum has been applied. If it is not then the vacuum should be released slightly and the bag should be adjusted accordingly. Pushing the laminate into tight corners with a blunt plastic 'pusher' (flat bar) helps seat it properly in the mould. These steps prevent bridging of the vacuum bag and laminate and ensure proper consolidation in the corners.

The vacuum bag should be checked thoroughly for any leaks before placing the mould in the autoclave. The easiest way to check for a leak is to remove the vacuum pipe (if there is a one-way valve on the mould), wait for a few minutes and then see if the bag has loosened at all in that time. Leaks often occur where the bag is not making a complete seal with the sealant tape. Checking for folds and pressing this area with one's fingers helps to remove these leaks.

3.5.4 Processing Temperature

Processing temperature is dependent on the matrix material and the limitations of the consumables being used. It is desirable to have the temperature as high as possible to decrease the viscosity of the molten matrix. However, having the temperature too high can cause degradation of the matrix and failure of the vacuum consumables.

A rule of thumb is to process at the highest processing temperature recommended by the material supplier and 10 °C below the maximum temperature tolerated by the consumables. This safety margin allows for possible overshooting of autoclave temperature.

The time at processing temperature should be increased if a solid metal mould is being used. This allows for the thermal lag of the mould. The temperature cycle that was used for the curved parts is shown in Figure 13. It includes the extra time at maximum temperature for the mould to reach processing temperature. It also takes into account the slow heating and cooling times of the autoclave itself.
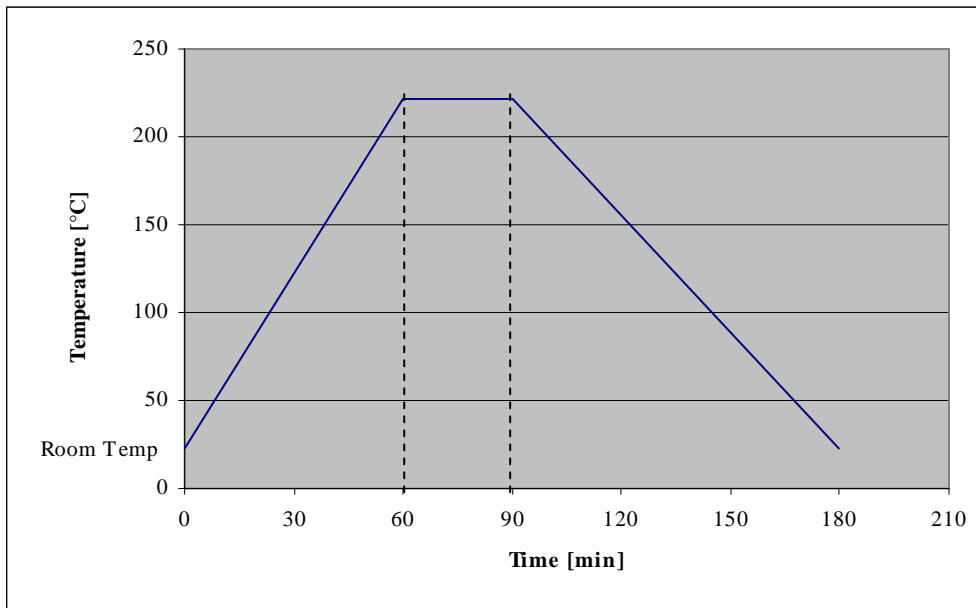
Figure 13: Autoclave temperature cycle for LPET

3.5.5 Processing Pressure

Applying pressure in addition to vacuum is only necessary with parts with complex geometry and sharp curves. Pressure application also speeds up consolidation (Ijaz et al, 2006) which makes it desirable to use if available. The successful parts produced in the manufacturing experiments had 5 bar of pressure applied in the autoclave.

Pressure should be applied until the matrix material has cooled below its melting temperature, if semi-crystalline, or glass transition temperature, if amorphous.

3.5.6 Demoulding

Demoulding a part from an aluminium mould can be particularly difficult when cold. There is a large difference in the coefficient of thermal expansion between aluminium and consolidated CFRTPs (about 20 µm/m°C) and the mould therefore squeezes the part after the matrix has solidified while cooling. It is therefore preferable to remove a part from the mould while it is as hot as possible but still solid and safe enough to handle. It is also advisable to design the mould without steep release angles to prevent this from being a problem.

3.6 Conclusion

The experiments described in this chapter provided the knowledge to successfully produce flat sheets and complex parts with commingled CFRTP material. The importance of the correct mould preparation, consumables and processing parameters was realised. It was also seen that high temperature vacuum consumables, such as those for PPS CFRTPs are difficult to work with and vulnerable to vacuum loss. This could limit the viability of vacuum processing the materials applicable to the aerospace industry.

4 FLEXURAL MATERIAL TESTING

4.1 Introduction

This chapter describes the flexural tests performed on a wide variety of CFRTP materials and discusses their results and conclusions.

The aim of the tests was to create a better understanding of the behaviour of laminated thermoplastic composites and make a comparison between materials with different fibres, matrices and weave styles. Commingled CFRTPs, pre-consolidated CFRTPs and TSCs were tested to make a comparison between these types of composites too.

Flexural testing was chosen as many parts made out of the materials used undergo flexural loading in their use. It is also a good test to assess the overall performance of a material as it combines tension and compression. Flexural test specimens are smaller and easier to prepare than for other tests (e.g. tensile testing) and therefore more suitable for the large number of materials that needed testing.

4.2 Experiment Description

4.2.1 Equipment

The equipment used in the experiment is listed in Table 2.

Table 2: Experiment equipment used in flexural testing

Testing Machine	Instron 1026 Universal Tensile Tester (Serial No. H1367)
Load Cell	HBM Type U2B 2 kN Force Transducer (Serial No. H23415 2)
LVDT	HBM Type WA/20 mm (Serial No. 052310184)
Bridge Amplifier	HBM Spider 8 4.8 kHz/DC. Compatible with inductive and resistive transducers
Software	Catman Easy – Supplied by HBM for use with the Spider 8 Bridge Amplifier

Both the LVDT and load cell were calibrated by correlating output voltages with known displacements and masses, respectively. These were then verified with several known masses and displacements within the calibration range.

The testing standard used was ASTM D790-03 "Standard Test Methods for Flexural Properties of Unreinforced and Reinforced Plastics and Electrical Insulating Materials" (ASTM D790-03, 2003). The formulae below were referenced from this standard.

Sample sizes of 12.7 mm x 50.8 mm were cut according to the standard.

A minimum of 5 samples were tested per material, per direction (0° and 90°).

The samples were unconditioned (as supplied/manufactured) and were tested at room temperature.

The crosshead speed of the tester was set to 5 mm/min.

A test jig was made to be mounted in the testing machine with variable span. The thin samples (< 1.6 mm) had a span of 25.4 mm. Thicker samples (> 1.6 mm) had a span determined by the formula *16d* where *d* is the specimen thickness. Figure 14 shows the test set-up.

Figure 14: Flexural testing jig

4.2.2   Calculations

Maximum forces were measured at the breaking point for brittle failures and at the yield point, where the force-deflection curve became non-linear, for yielding failures.

The flexural modulus was calculated with the formula

$$E_B = L^3 m / 4bd^3 \qquad\qquad\qquad (2)$$

Where:
E_B = modulus of elasticity in bending [MPa],
L = support span [mm],
b = width of beam tested [mm],
d = depth of beam tested [mm] and
m = slope of the tangent of the initial straight-line portion of the load-deflection curve [N/mm].

The flexural strength was calculated using the formula for span-to-depth ratios larger than 16 to 1:

$$\sigma_f = (3PL/2bd^2)[1 + 6(D/L)^2 - 4(d/L)(D/L)] \qquad (3)$$

where:
σ_f = stress in the outer fibres at midpoint [MPa]
P = load at a given point on the load-deflection curve [N],
L = support span [mm],
b = width of beam tested [mm] and
d = depth of beam tested [mm].

Figure 15 and Figure 16 show typical force-deflection curves for a brittle and ductile failure, respectively. F_{max} is the force used to calculate the flexural strength of the samples and D_{max} is the deflection used to calculate the strain at failure. (Failure-strain is not discussed in this report.)
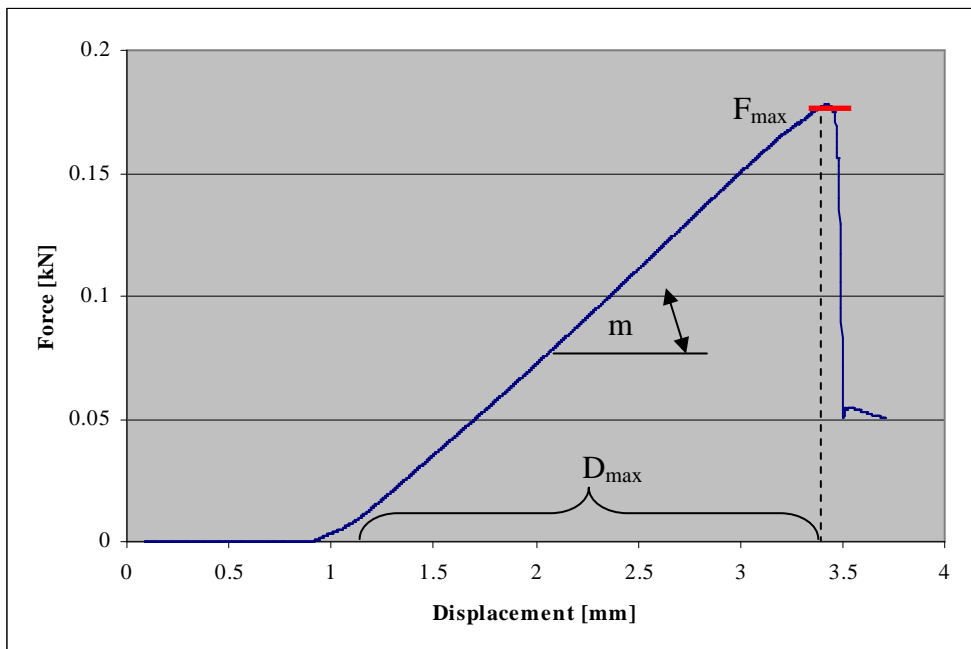
Figure 15: Typical brittle failure
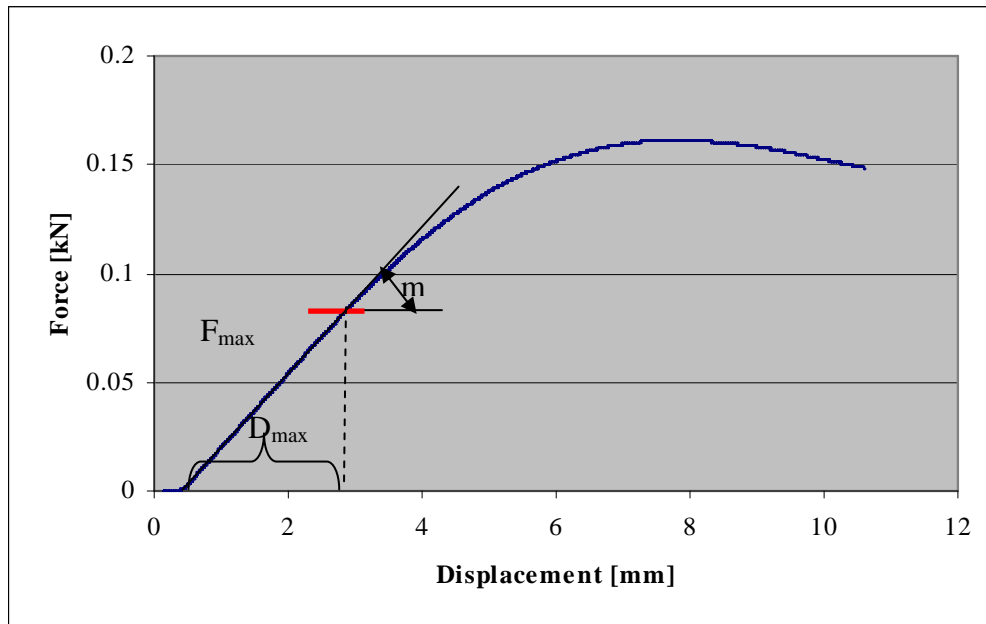
Figure 16: Typical ductile failure

4.2.3 Tested Materials

Materials were chosen with the comparative goal of the tests in mind. Thus some materials were chosen that can perform the same task or have similar weave styles but different matrices. Other materials were chosen for the comparison between commingled thermoplastic composites, pre-consolidated thermoplastic composites or thermosetting prepregs. Some materials were also chosen to investigate the effect of oxidation and the inclusion of a bronze mesh. The materials tested are listed in Table 16 in Appendix A.1. The process parameters and consumables used for the selected materials are listed in Table 19 in Appendix A.3.

The fibre volume fractions of the fibre-reinforced materials in Table 16 are shown in Figure 17. These were either obtained from data sheets or calculated from fibre weight contents and densities listed in the figure. Table 3 shows the fibre volume fraction that was measured for certain materials using Thermo-Gravimetric Analysis (TGA) tests.
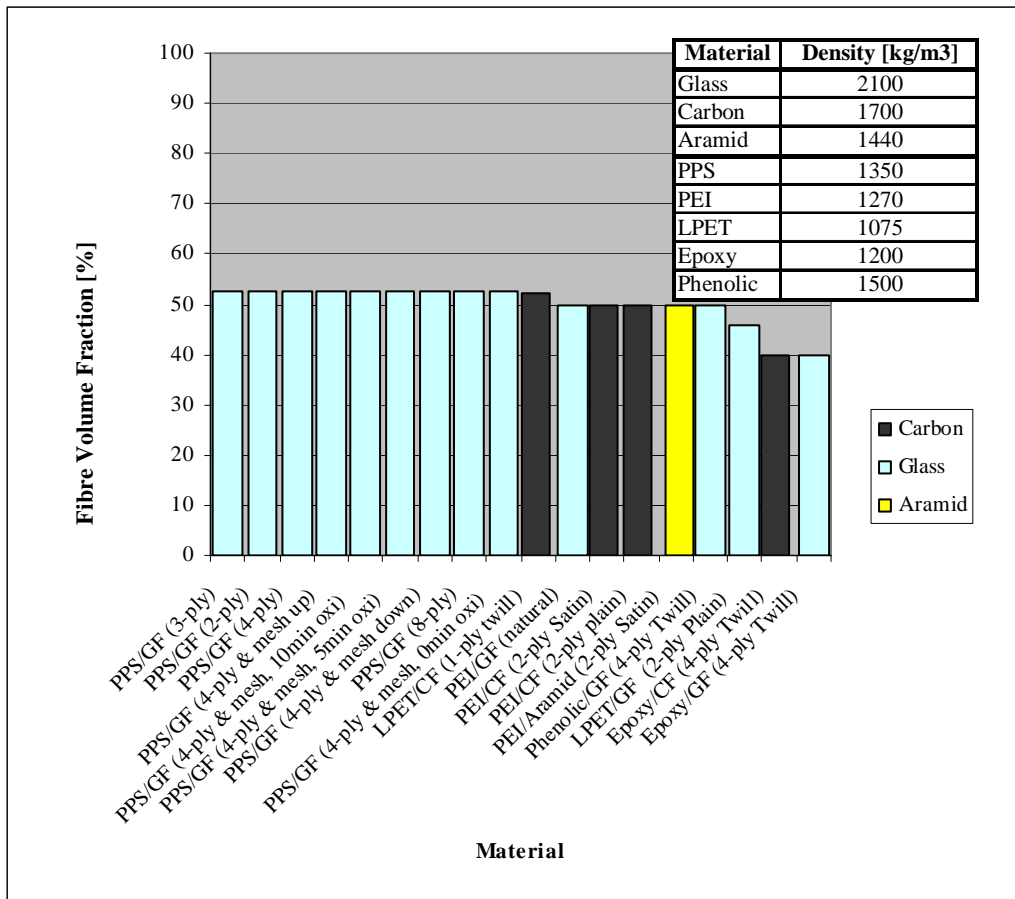
Figure 17: Calculated fibre volume fraction of tested materials

Table 3: Measured fibre fraction from TGA tests

Material	V_m [v%]
PPS/GF (8H Satin weave, 4-ply)	42
PPS/GF (8H Satin weave, 4-ply with bronze mesh)	42
PPS/CF (Satin weave, 4-ply)	57[+]
LPET/GF (Plain, 2-ply)	54
LPET/CF (Twill, 1-ply)	55[+]

4.3 Results

The results are sub-divided into sections where specific trends are apparent and conclusions are made. A table of results for all the materials is given in Appendix A.3.

Fibre directions referred to in this report correlate to warp and weft i.e. 0° direction refers to warp and 90° direction refers to weft as defined by the manufacturers.

4.3.1 Flexural Modulus

Figure 18 shows the flexural modulus values for the tested materials as an average of the 0° and 90° directions. The first and most obvious conclusion to make is that unreinforced materials (Radel's PPSU) have a significantly lower modulus than fibre reinforced materials. It can be seen here that even the low-performance composites (LPET/CF and LPET/GF) have greater stiffness compared to the Radel material. This underlines the potential of composite materials.
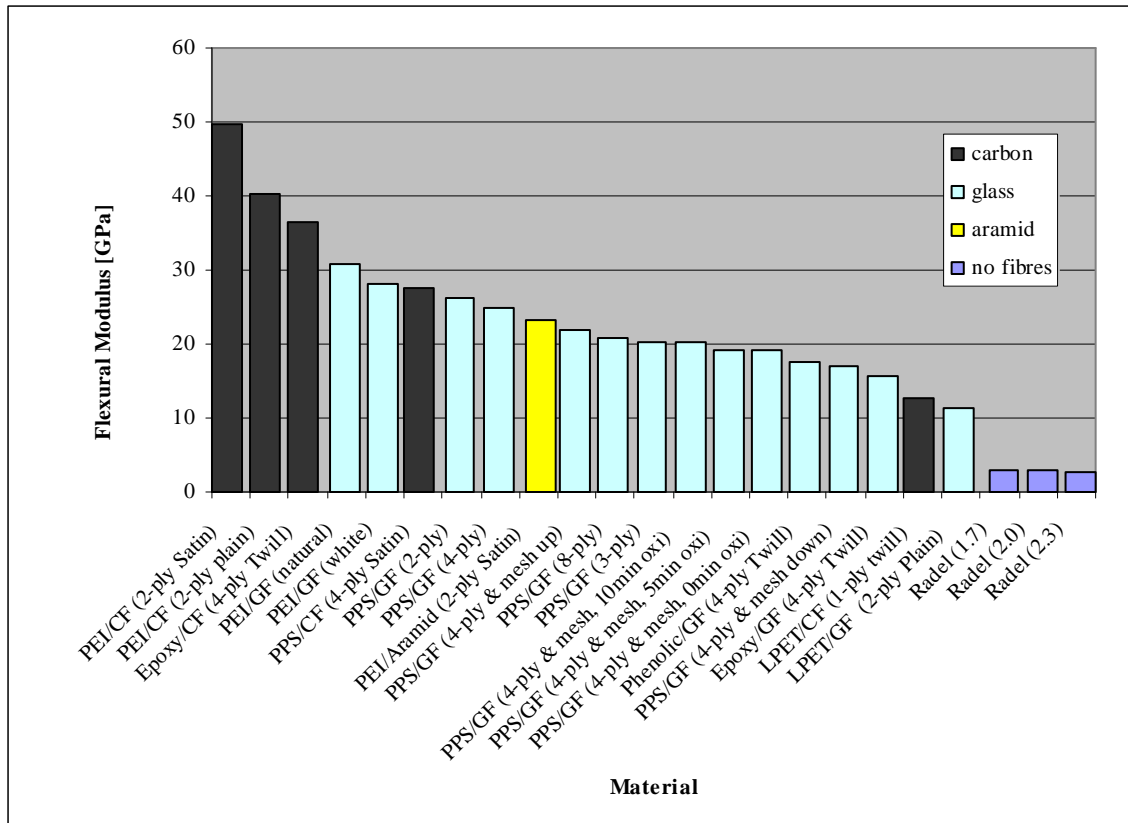
Figure 18: Average flexural modulus of tested materials

It can also be seen that the carbon composites showed higher stiffness values than those of the glass composites.

The matrix providing the highest moduli for a specific fibre type is PEI, with its carbon fibre samples showing the highest values of all the test samples. The PPS samples showed the next highest values after PEI.

The commingled materials showed poor mechanical properties compared to the other materials. The LPET/CF modulus was particularly low. It is believed that this is due not only to the low modulus of LPET but also the coarse weave of this material. The coarser the weave the larger the bends in the fibres, which results in the properties being influenced more by the matrix than the reinforcement.

Figure 19 shows the difference in weave coarseness between certain materials. 'Coarseness' refers to the thickness and waviness of the fibre tows – the more fibres per

tow, the coarser the weave. The materials in the figure are, clockwise from top left: LPET/CF, PPS/GF, Epoxy/CF and PEI/CF. The LPET is actually coarser than the Epoxy as it has only one layer to make up about 1 mm total thickness whereas the Epoxy material has 4 layers to make a 1 mm laminate. Thus, the Epoxy's carbon fibres are straighter than those of the LPET laminate. Figure 20 shows the difference between the two carbon fibre commingled materials. The PPS/CF material also has four layers in the laminate of about 1 mm thick.

Figure 19: Different weave styles and coarsenesses

(Clockwise from top right, LPET/CF, PPS/GF, PEI/CF and Epoxy/CF. Top right enhanced for clarity, but still to scale)

Figure 20: Difference between commingled PPS/CF and LPET/CF weaves

(PPS/CF (top), LPET/CF (bottom))

Another reason for the commingled materials' lower stiffness is that precise fibre alignment is difficult to obtain when processing. This effect gets exaggerated with larger fibre bundles in the weave and with unidirectional fabrics. It can be seen that the

commingled PPS/CF from Carr Reinforcements has a modulus that is not far off from the other carbon fibre materials and this is probably due to its finer weave.

One can see that the TSCs have comparable properties to the thermoplastic composites, in spite of the fact that the TSCs have a lower fibre volume content (see Figure 17).

4.3.2   Flexural Strength

The flexural strengths show similar trends to the flexural moduli (Figure 22). Like the modulus values, the carbon composites generally have higher strength values than the glass composites. The strength of the PEI/Aramid is very low compared to the other materials. The reason for this is the low compressive strength of Aramid fibres causing the compression side of the samples to fail first. Figure 21 shows PEI/Aramid samples that failed in compression.
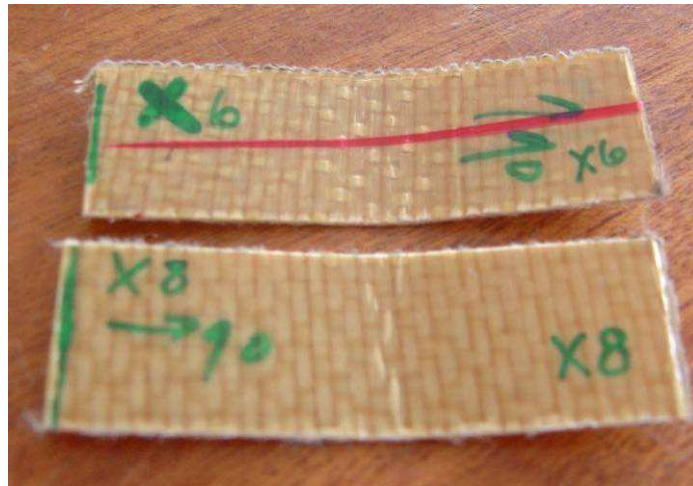
Figure 21: PEI/Aramid samples showing compressive failure

LPET/CF showed poor performance again and this is also due to it having a coarse weave in a low-performance matrix.

Again, the thermoplastic composites have comparable properties with the TSCs even though the TSCs have a lower fibre volume content.
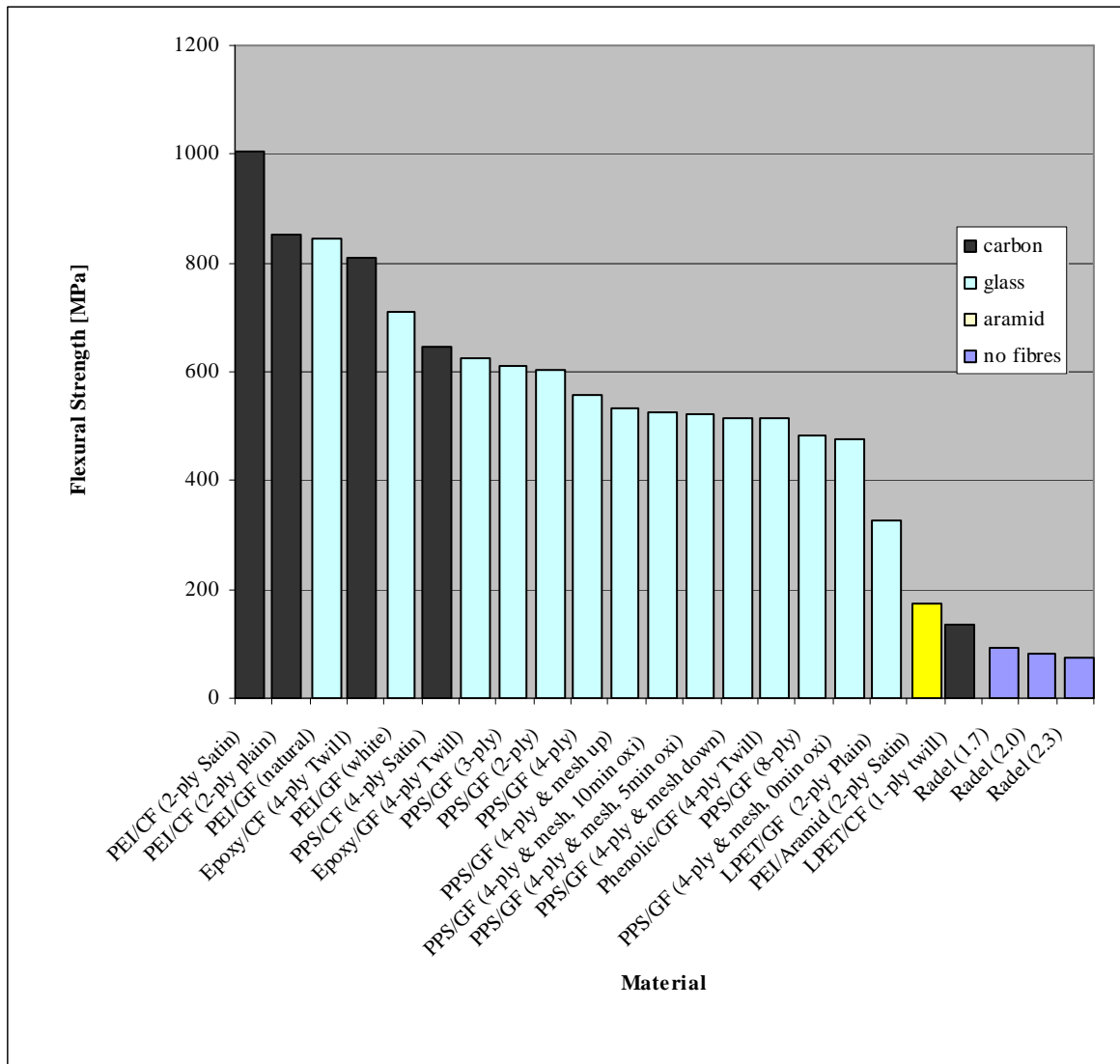
Figure 22: Average flexural strength of tested materials

4.3.3   Weave Style Effects

Weave styles have a significant effect on the difference in flexural strength and modulus in the two dominant weave directions. Figure 23 shows the normalized difference in modulus between the 0° and 90° directions for each material. The value for each material was calculated by taking the difference in the two modulus values and dividing it by the average of the two values. It must be noted that the effects of weave styles discussed here are specific to the bending behaviour of the materials.

It is quite apparent that asymmetrical weaves, specifically satin weaves, cause a significant difference in directional properties. The PEI/CF samples show a clear example of this trend where the satin weave has an 86 % normalized stiffness difference and the plain weave only has a difference of 13 %. The difference between the two weave styles can be seen in Figure 24. Here it can be seen how the satin weave behaves like two layers of perpendicularly stacked unidirectional fabric. This has further implications that are

discussed in other sections of this report. However, this effect of asymmetrical weave patterns averages out with thicker laminates (more plies) as can be seen in Figure 23.

Although this effect of the asymmetry may seem obvious, it is mentioned in this report because of its relevance to thermoplastic composites. Their processing methods, specifically of pre-consolidated sheets, dictate the need for drapable reinforcement fabrics which makes the satin weave most appropriate. This must therefore be considered when designing with these materials.

A similar trend was noticed in the strength results.
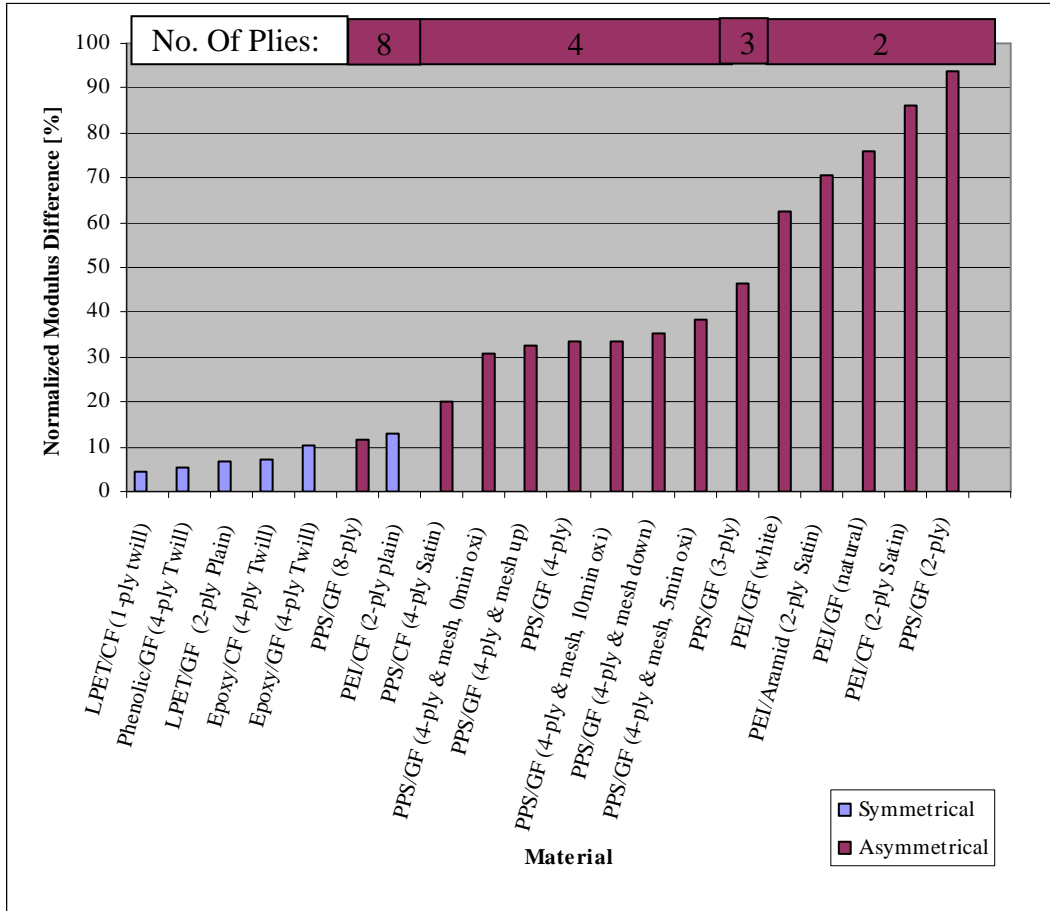
Figure 23: Normalized 0-90 flexural modulus difference of tested materials

Figure 24: Satin weave and plain weave

Further testing was performed in the effects of asymmetrical weave styles, specifically lay-up sequence. PPS/GF (2-ply, 8H satin weave) was used to perform these tests. Four variations were used, each with its own stacking sequence. The stacking sequences are explained in Figure 25 where each layer of fibres is depicted as two UD layers.
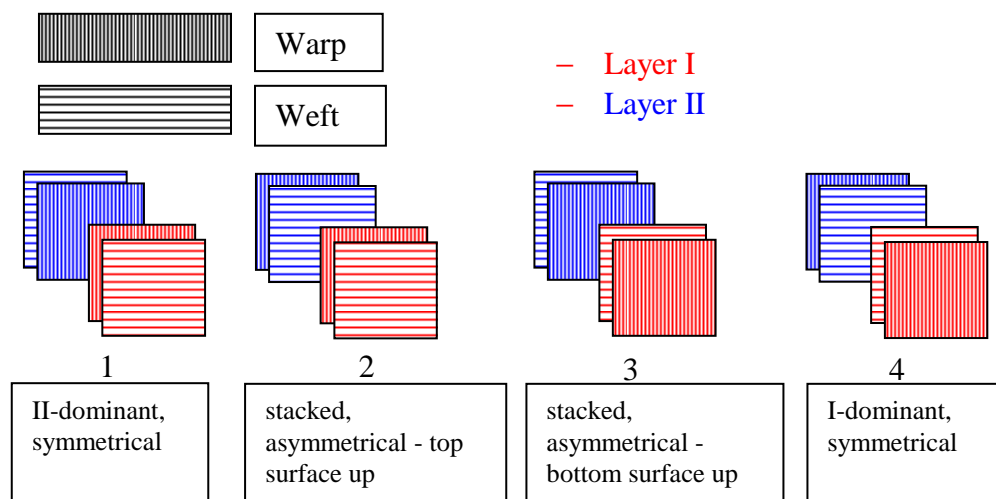
Figure 25: Various lay-up sequences of 2-ply PPS/GF satin weaves

Figure 26 shows the flexural modulus values for the samples with various stacking sequences. It can be seen here that the symmetrical lay-ups have larger differences between their 0° and 90° directions than the asymmetrical lay-ups. The asymmetrical lay-ups showed virtually the same stiffness values, only in opposite directions.

Asymmetrical lay-ups appear beneficial compared with symmetrical lay-ups because of their more isotropic bending properties. A disadvantage is that the asymmetry causes warping of parts made of these materials. Metal meshes, used as electromagnetic shielding, also cause warping; so it may be possible to design a lay-up where these warping effects minimise each other.

Figure 27 shows how asymmetrical lay-ups warp whereas symmetrical lay-ups do not.
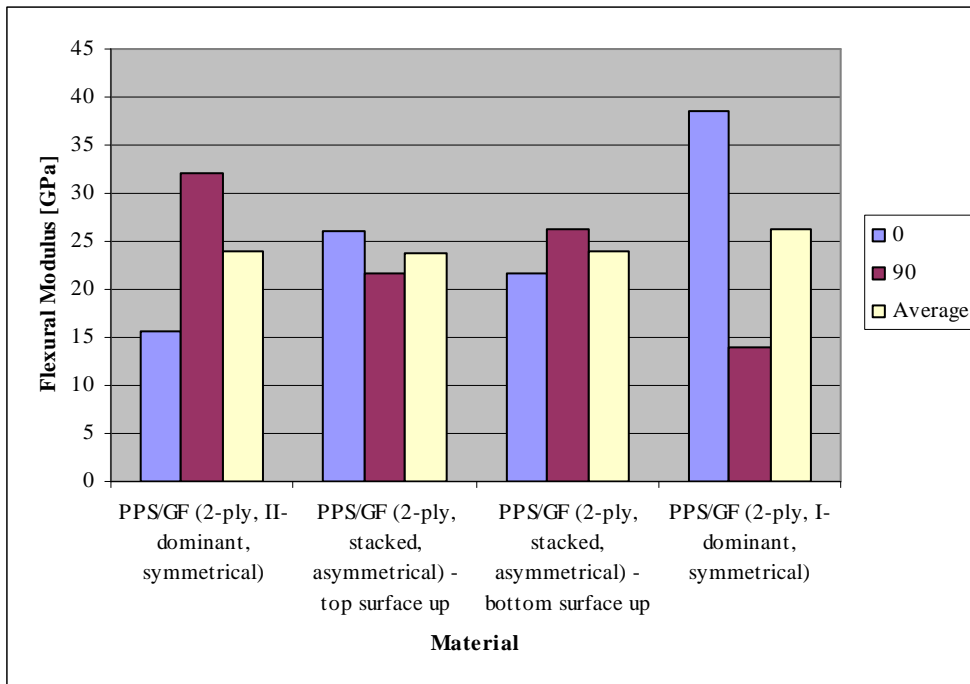
Figure 26: Flexural modulus results of stacking sequence tests

Figure 27: Warped asymmetrical laminates and flat symmetrical laminate

4.3.4   Failure Modes

This section discusses the variations in modulus between the various materials and the correlation between failure modes and modulus. Figure 28 shows the flexural modulus of the tested materials with their corresponding failure mode. The description of the failure modes refer to which side of the sample that failure first occurred and in which manner it

occurred. For example, 'tension abrupt' means it failed on the side of the sample experiencing tensile stress and it failed suddenly without signs of yielding first.

It was observed that the failure mode was linked to the local fibre orientation of the materials.

Yielding occurred when the matrix dominated properties applied. This occurred with the unreinforced plastics and the thin laminates with asymmetrical weave styles. The satin weave creates a pseudo-unidirectional layer on the outside of the laminate, which has matrix-dominated properties in one direction and fibre-dominated properties in the other direction. Yielding failure also occurred in the PEI/Aramid where failure occurred in the compression side of the samples. This can also be seen as matrix dominated behaviour as the weak the fibres buckle in compression which transfers the load to the matrix.

Conversely, brittle (abrupt) failure occurred when samples were loaded in their fibre-dominated directions. This contrast can be seen with the PEI/CF (satin weave) samples where the modulus in the fibre-dominant direction is more than double that of the matrix-dominant direction.
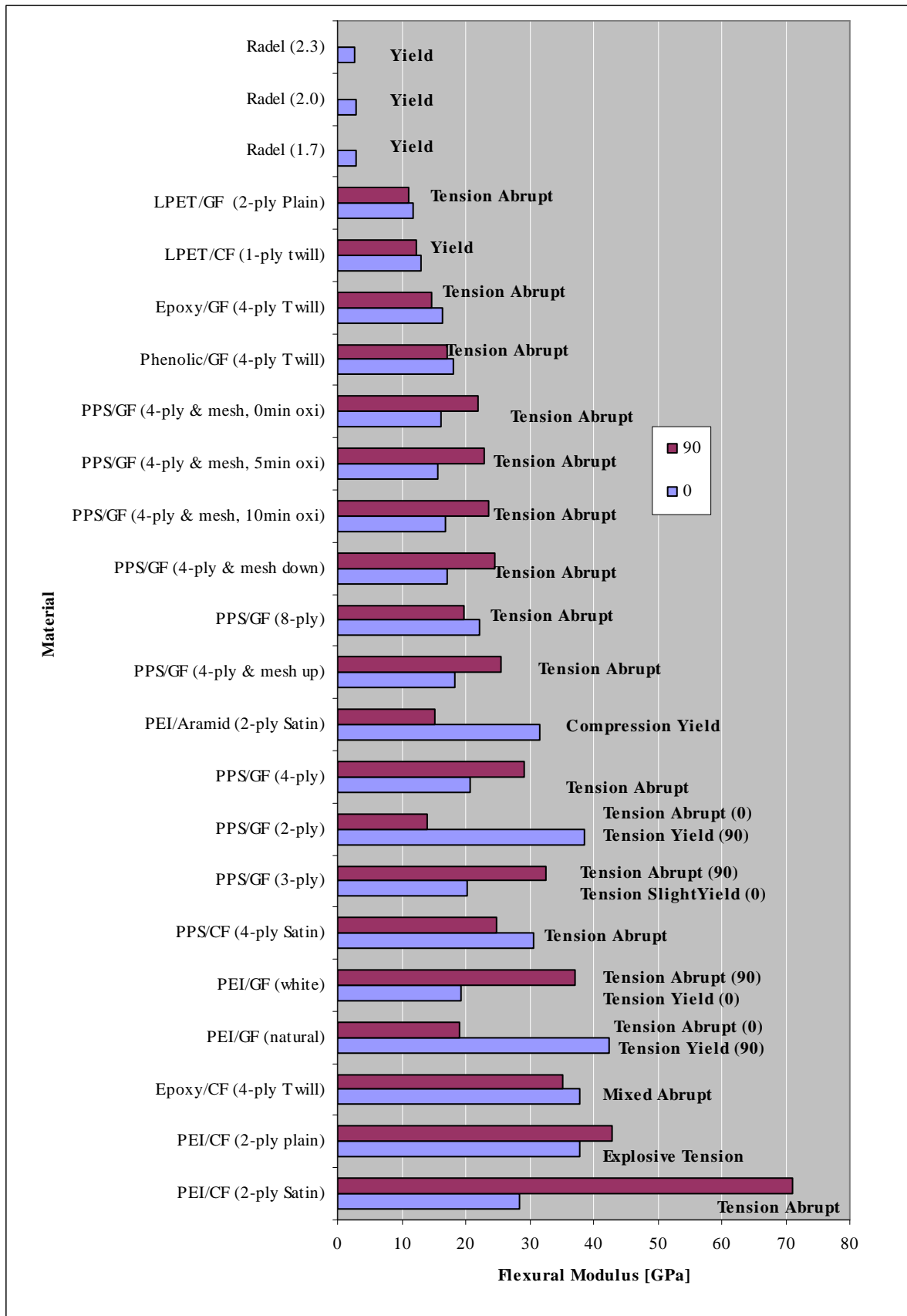
Figure 28: Flexural modulus of materials with corresponding failure modes

4.3.5   Property Variation

Figure 29 shows the relative standard deviation for each material's flexural modulus. The values are relative to the materials' average moduli.

It is clear from the figure that commingled materials have a larger variation. This is due to the coarser weave styles and the processing method. Commingled materials processed by hand have a greater chance of misaligned fibres which causes variable strength and stiffness properties. It must be noted that the materials were processed by inexperienced people (the author and co-workers).

The Epoxy/CF samples also showed a large deviation in stiffness and this is also due to a coarse weave. Improved test values could be obtained by using larger samples for the materials with coarser weaves.

It is also clear from Figure 29 that the pre-consolidated thermoplastic materials and the Radel unreinforced plastic had very little variation in stiffness. This can probably be attributed to controlled processes and quality control allowed during initial processing.

The PEI/Aramid samples had a noticeably higher relative standard deviation in one direction than the other. A closer look revealed that some samples were not completely consolidated causing this variation (see Figure 30). Removing these samples values from the group caused this standard deviation to decrease.
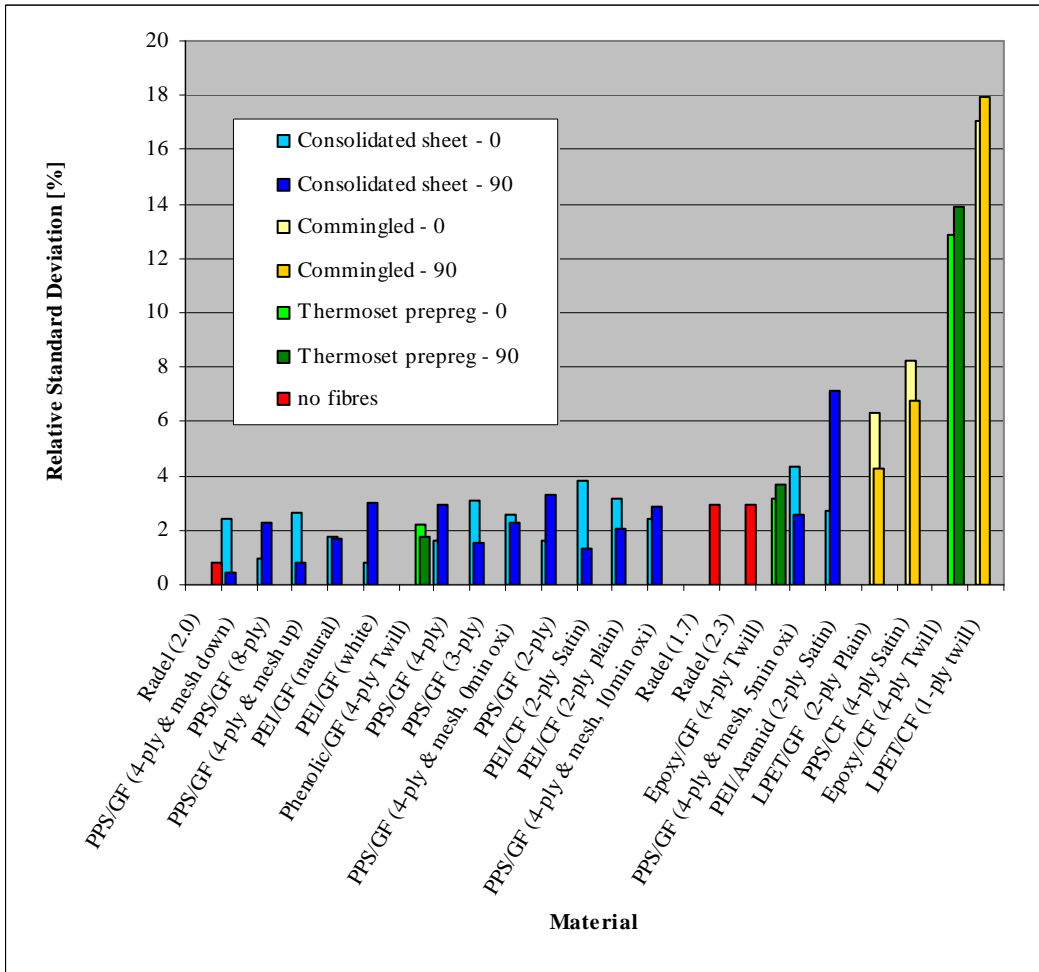
Figure 29: Relative standard deviation of flexural modulus of tested samples
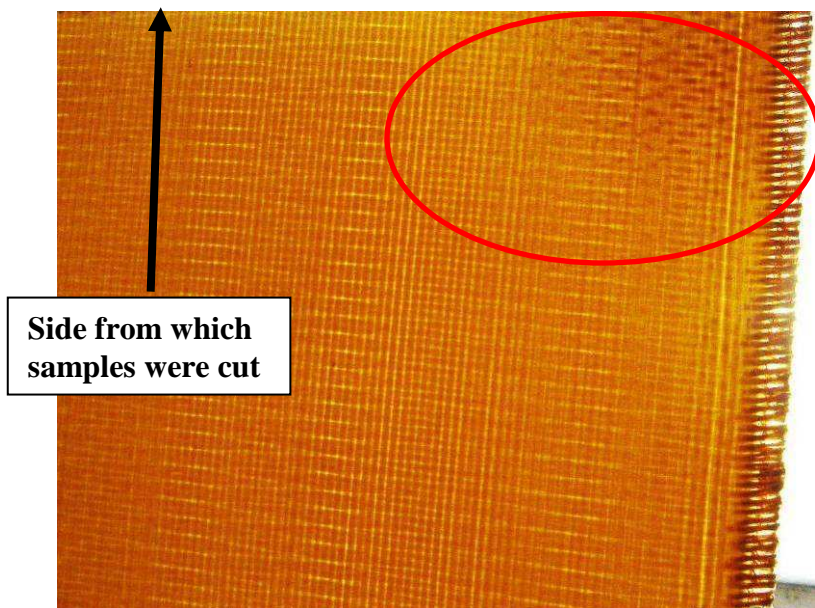
Figure 30: PEI/Aramid with poorly consolidated region

36

It can be seen in Figure 31 that the variation of the strength in the tests of each material was higher than that of the variation in the modulus. This can be attributed to the small sample size allowing imperfections in the materials to have a significant effect.

Another significant trend was the higher deviations in strength with the carbon samples. Even the pre-consolidated PEI/CF samples showed this and this could be because of the relatively coarser weave of these materials compared to the pre-consolidated glass fibre samples. Another reason for the deviation could be because carbon composites tend to be more brittle and thus more susceptible to flaws which vary between samples.

Again, the commingled materials showed high deviations when compared to the other materials.
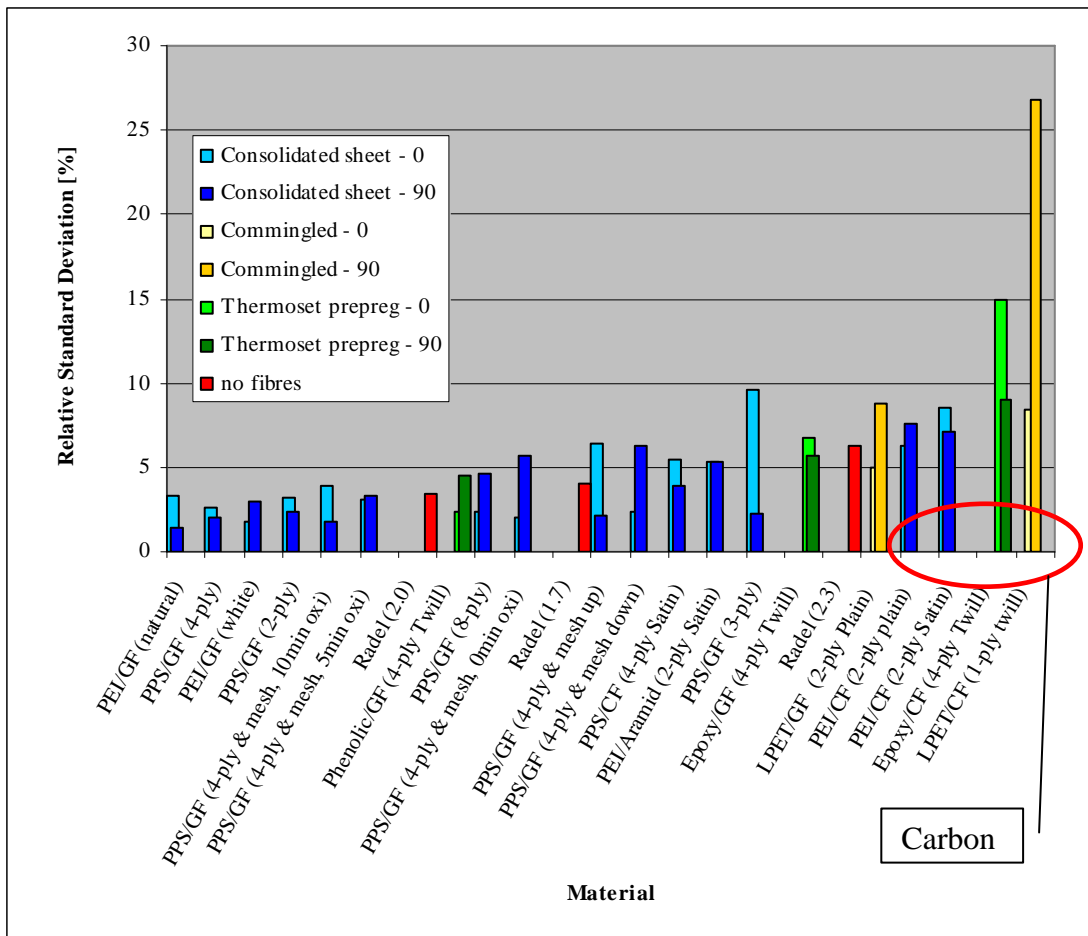
Figure 31: Relative standard deviation of flexural strength of tested materials

4.3.6 Oxidation Effects

It was decided to investigate the effects of oxidation on PPS/GF as oxidation of the polymer was observed during processing where the laminate is heated in air. PPS/GF samples from Ten Cate with bronze mesh on one side were prepared by heating samples for 0, 5 or 10 minutes at processing temperature in air. The samples were then reprocessed

simultaneously in an autoclave cycle under pressure (with the material exposed to vacuum/no air) to ensure consolidation was maintained.

It can be seen in Figure 32 that oxidation for this amount of time has very little effect on the laminate properties. In fact the oxidation of the material slightly increases the mechanical properties.
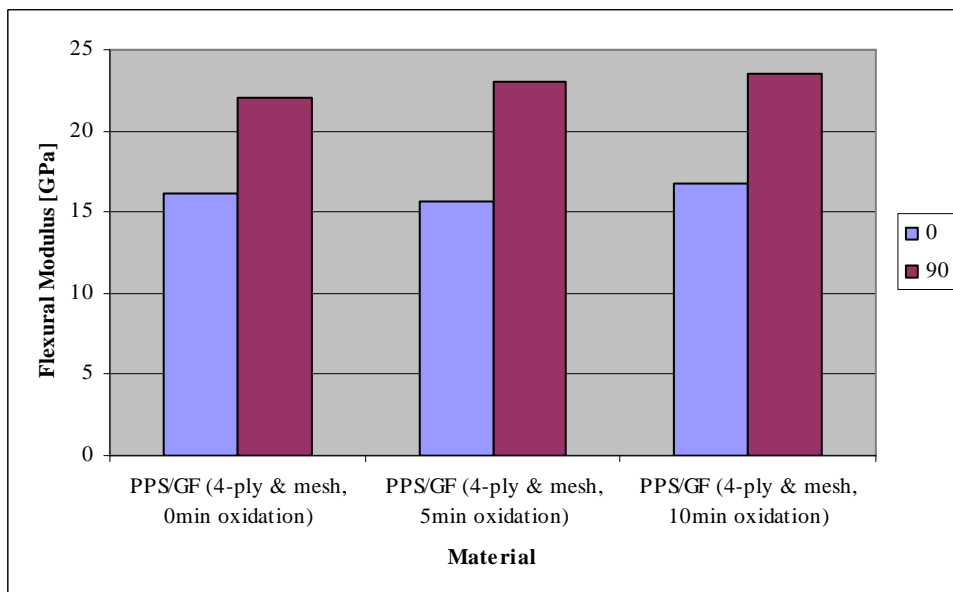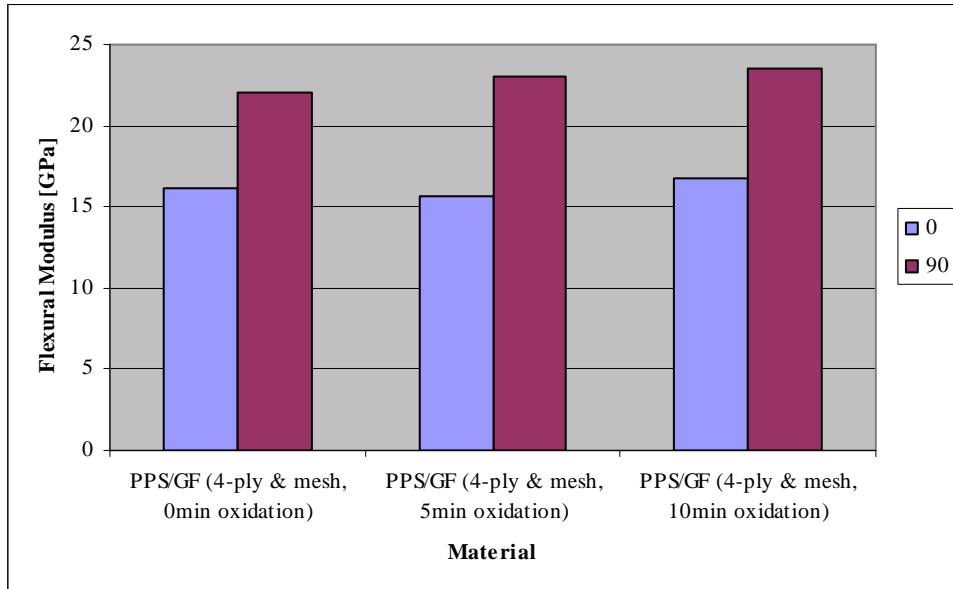
Figure 32: Oxidation effects on mechanical properties of PPS/GF

(Modulus (top) and strength (bottom))

4.3.7 Effect of Metal Mesh

A metal mesh is often a requirement for materials used in aircraft to provide electro-magnetic (EMI) shielding. Tests were performed on the meshed PPS/GF to see what the effects of this mesh are on the laminate.

It can be seen in Figure 33 and Figure 34 that the stiffness and strength of the material is not significantly decreased by the mesh, whether it is on top or bottom. In fact, the specific bending stiffness values (*EI/SG*) are within 5 % of each other. (SG is the specific gravity of the material)

Although the effect of the mesh is minimal, it is advisable to design for the mesh to be on the compression side of a shell, where possible, as the tests showed that this resulted in more stiffness and strength.
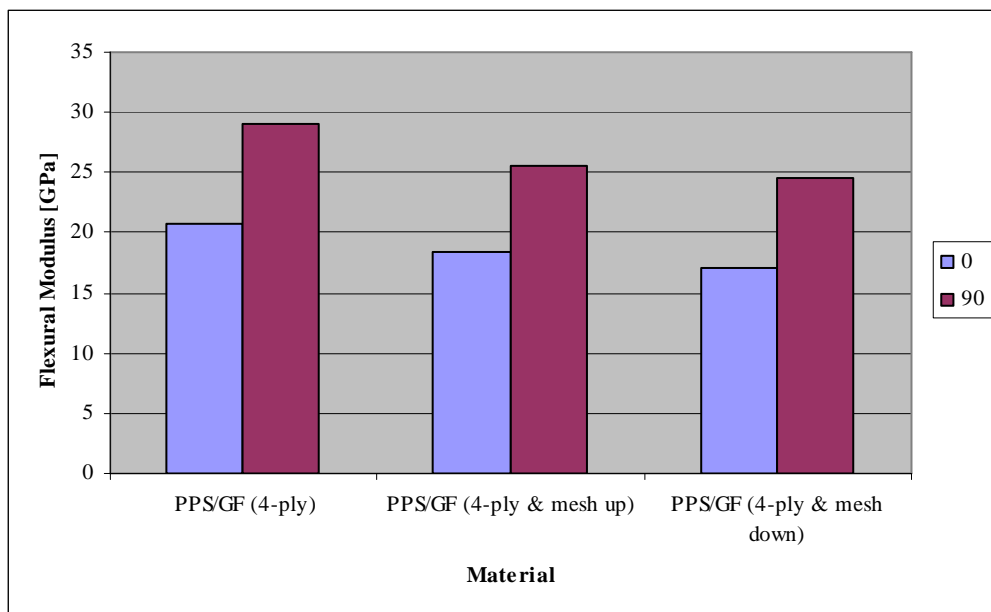
Figure 33: Flexural modulus comparison of unmeshed and EMI-shielded (meshed) PPS/GF
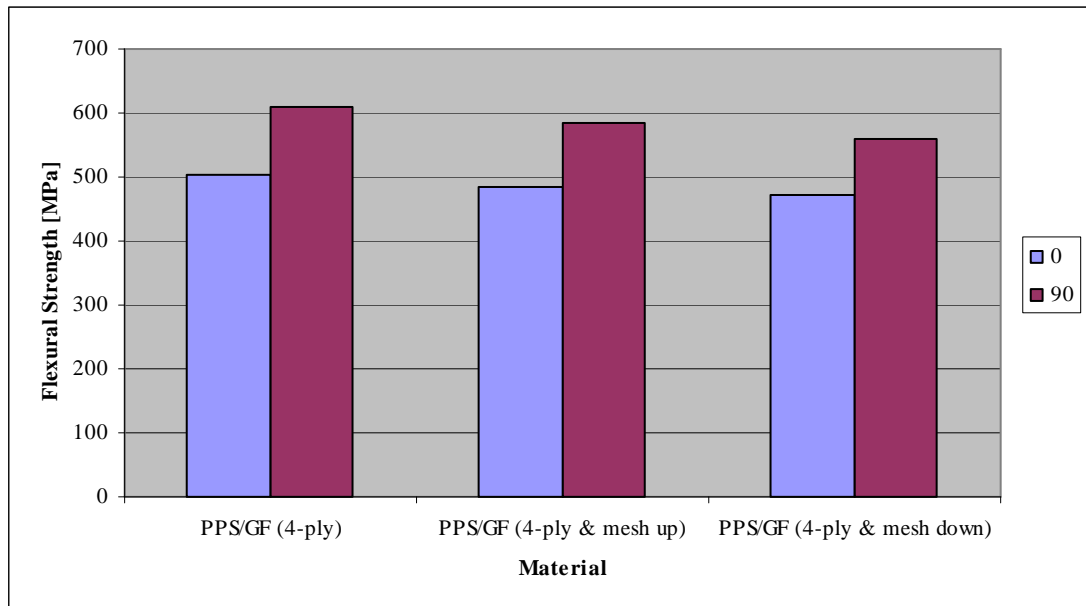
**Figure 34: Flexural strength comparison of unmeshed and
EMI-shielded (meshed) PPS/GF**

4.3.8   Effect of Annealing

As PPS is a semi-crystalline material, tests were performed to investigate the effects of annealing on the strength and stiffness of the composite. 4-ply PPS/Glass sheets from Ten Cate were used in this investigation. The samples were annealed at 150 °C for 3 weeks or 200 °C for 24 hours.

Unreinforced PPS products (no fibres) are commonly annealed to reduce internal stresses and to boost crystallinity in order to get a higher modulus and abrasion resistance. In the case of composites, a higher matrix modulus should increase the modulus of the entire composite. Measurement of the crystallinity by Differential Scanning Calorimetry (DSC) as indirect proof of a rise in modulus was however inconclusive because very few tests were conducted.

The modulus and strength of PPS composites unexpectedly decreased after annealing as can be seen in Figure 35 and Figure 36. There could be a correlation between the decrease in properties and the decrease in mass that occurred during annealing as shown in Figure 37. Another possible reason for the decrease in properties could be oxidation that occurred during annealing. This can be seen in Figure 38 where the samples have increasing discolouration with increasing time in the oven. Further investigation is however necessary to draw a solid conclusion.
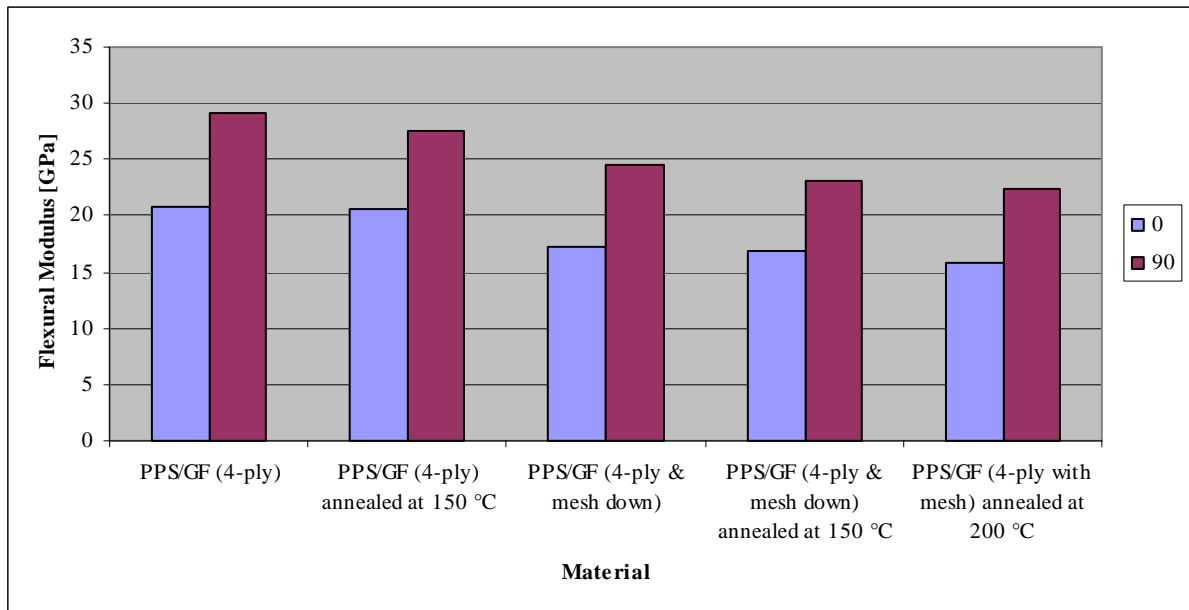
Figure 35: Comparison of modulus of annealed and as-purchased PPS composites
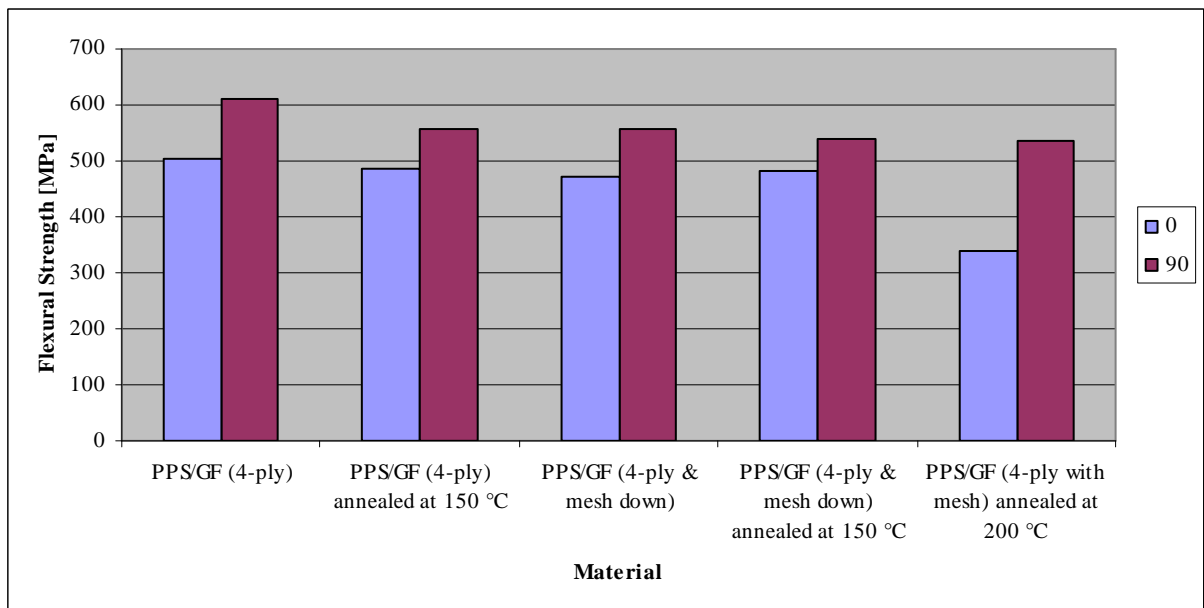
Figure 36: Comparison of strength of annealed and as-purchased PPS composites
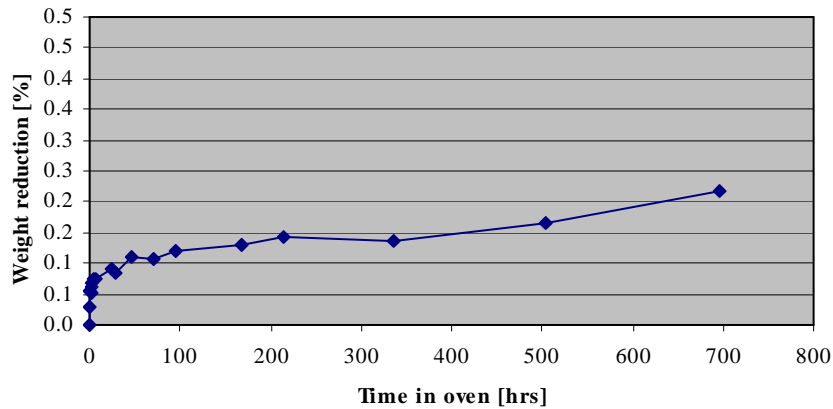
Figure 37: Weight reduction of PPS composites during annealing

Figure 38: Oxidation caused during annealing of PPS composites.

(The darker colour indicates more oxidation has occurred.)

4.4 Conclusions

A broad range of composite materials were tested to get a comprehensive, comparative set of test results. Flexural testing was chosen as the samples are easier to prepare and require less material to prepare than tensile testing samples for example. Flexural tests also provide a good understanding of the materials' behaviour, specifically in bending applications.

Several conclusions were made in the previous section and will be summarised here. Firstly, it can be seen that the pre-consolidated materials generally have better, and more consistent, properties than commingled materials.

With the materials that were tested, the properties of the TSCs and CFRTPs were comparable. Thus, when the manufacturing processes of thermoplastics get established, thermoplastics will be a viable option as a production material.

Finally, the use of high-performance plastics like Radel's PPSU is virtually unnecessary as long as parts can be made from continuous fibre composites. Composites offer increased stiffness and strength with decreased mass.

5 IMPACT TESTING

5.1 Introduction

This chapter describes the impact testing on a wide variety of CFRTP materials and discusses their results and conclusions.

As with the flexural testing as described in Chapter 4, the aim of these tests was to allow a better understanding of the behaviour of laminated composites and make a comparison between different fibres, matrices and weave styles. Again, commingled CFRTPs, pre-consolidated CFRTPs and TSCs were tested to make a comparison between these types of composites too.

Impact testing provides an indication of the toughness of certain materials and thus reveals their damage tolerance. It is also a relatively easy and economical test to evaluate and compare materials.

5.2 Experiment Description

5.2.1 Equipment

The testing was performed at the University of Cape Town using their impact-testing machine. The machine was designed and constructed by one of their MScEng students, Cartmel (1999). The apparatus can be seen in Figure 39.

Figure 39: Impact-testing apparatus

The apparatus is based on a conventional drop tower tester. The crosshead has an integrated load cell, and drop-height and mass can be varied to allow adjustment of impact kinetic energy. The penetrator can also be interchanged to simulate the effects of different projectile shapes.

Force measurement begins when the crosshead passes a velocimeter located just above the test sample. The force-time history is then recorded on a computer with a software package that was written specifically for the apparatus. The software then filters the data, finds the force peak of the first impact and calculates a velocity, displacement and energy history by means of numerical integration. The results can then be saved to a file for further analysis. Figure 40 shows typical data recorded by the apparatus and software. The top left graph is the only graph with purely measured data. The rest of the graphs contain calculated values.
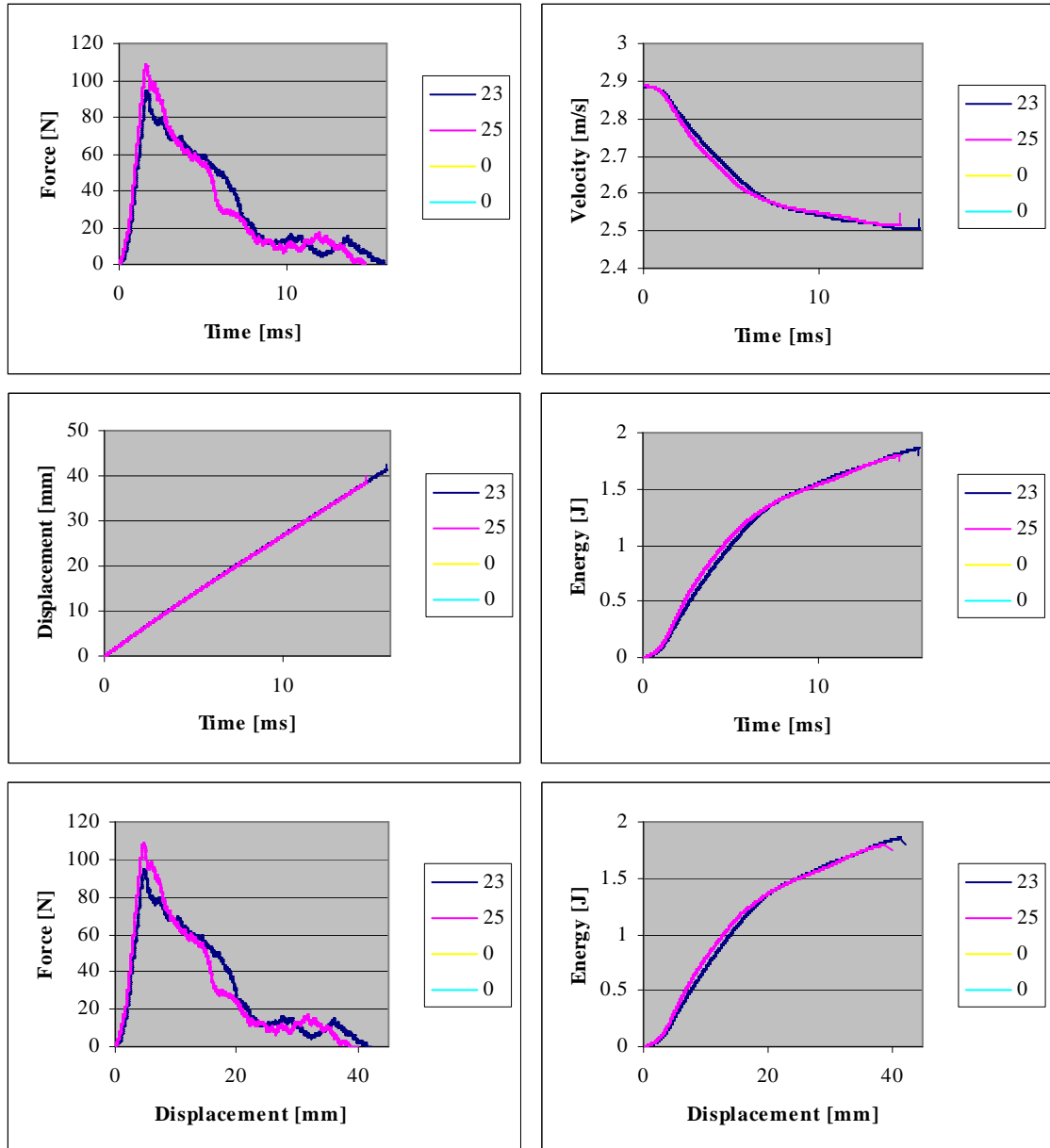
Figure 40: Typical data obtained from impact testing apparatus software

The calibration of the load cell was incorporated into the software.

It was decided to follow the test standard "Measuring the Damage Resistance of a Fiber-Reinforced Polymer Matrix Composite to a Drop-Weight Impact Event" (ASTM D 7136/D 7136M,ASTM International, 2005). Certain minor changes were applied to accommodate the difference in testing apparatus.

Sample sizes of 100 mm × 100 mm were tested.

The samples were unconditioned (as supplied/manufactured) and were tested at room temperature.

The impactor mass was set at 1.3 kg.

A minimum of 5 samples per material were tested. Unfortunately, valid results were not obtained for all samples which resulted in some materials having less sample data. This was due to inadequate clamping conditions causing faulty readings.

The drop height of the impactor was calculated so that all samples received the same impact energy per laminate thickness (6.7 J/mm) as specified in the ASTM standard. Calculations for drop height are shown in the next section.

5.2.2 Calculations

Impact energy is:

$$E = C_E h \tag{4}$$

where:
E = potential energy of impactor prior to drop [J]
C_E = specific energy to thickness ratio of impactor prior to drop, 6.7 J/mm
h = nominal thickness of specimen [mm]

The drop height was calculated with the following formula:

$$H = \frac{E}{m_d g} \tag{5}$$

where :
E = potential energy of impactor prior to drop [J]
H = drop height [m]
m_d = mass of impactor for drop height calculation [kg]
g = acceleration due to gravity, 9.81 m/s^2

The values calculated from the above equations were used to set the impact tester. The rest of the impact information was received from the impact tester's software and stored in Excel files. The data obtained included time [ms] force [N], absorbed energy [J], displacement [mm] and velocity [m/s]. As mentioned in the previous section, only force, initial velocity and time were recorded. Velocity, displacement and energy were calculated by the software as follows:

Acceleration:

$$a(t) = F(t) / m_d \tag{6}$$

$F(t)$ is the force measured by the load cell.

Velocity:

$$v(t) = \int_0^t a(t)dt + v(0)$$

$$\approx \sum_0^t (a(t) * \Delta t) + v(0)$$

(7)

where $v(0)$ is the initial velocity measured by the tester's velocimeter.

Displacement:

$$x(t) = \int_0^t v(t)dt$$

(8)

Energy absorbed by the plate is calculated by combining potential and kinetic energy formulae to get:

$$E_a(t) = \frac{m}{2}\left(v_{impact}^2 - v(t)^2\right) + mgx(t)$$

(9)

The energy absorbed by a specimen was then divided by its thickness to get a thickness-specific energy absorption value.

It was decided to look at the results only up until failure point to see how much energy the materials can absorb before failure. This was deemed relevant for the materials that were tested as they will probably not be used specifically for impact protection. Thus it is only necessary to know how much energy it takes to damage them. The failure point was taken to be the point at which the maximum force was exerted on the test sample (Figure 41). This was adequate as all the fibre-reinforced materials showed brittle behaviour.
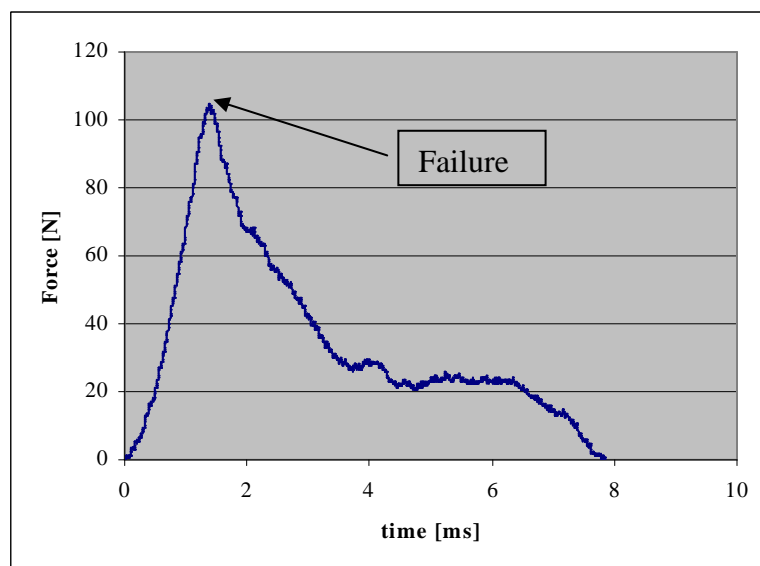
Figure 41: Determination of failure point in impact test force graph

47

5.2.3   Tested Materials

Materials were chosen with the comparative goal of the tests in mind. Thus some materials were chosen that can perform the same task or have similar weave styles but different matrices.   Other materials were chosen for the comparison between commingled thermoplastic composites, pre-consolidated thermoplastic composites or thermosetting prepregs. Some materials were also chosen to investigate the effect of oxidation and the inclusion of a bronze mesh. The materials tested were the same as those listed and used in Chapter 4 within the addition of those listed in Table 24 in Appendix A.6. The process parameters and consumables used for the selected materials are listed in Appendix A.3.

5.3   Results

The results are sub-divided into sections where specific trends are apparent and conclusions are made. A table of results for all the materials is given in Appendix A.7.

Fibre directions referred to in this report correlate to warp and weft i.e. 0° direction refers to warp and 90° direction refers to weft as defined by the manufacturers.

5.3.1   Energy Absorption at Failure – General Comparison

Figure 42 shows the energy that each material absorbed at failure. The values are an average for all the samples per material. 'Impact resistance', in this chapter, refers to the amount of energy a sample can absorb before failure.
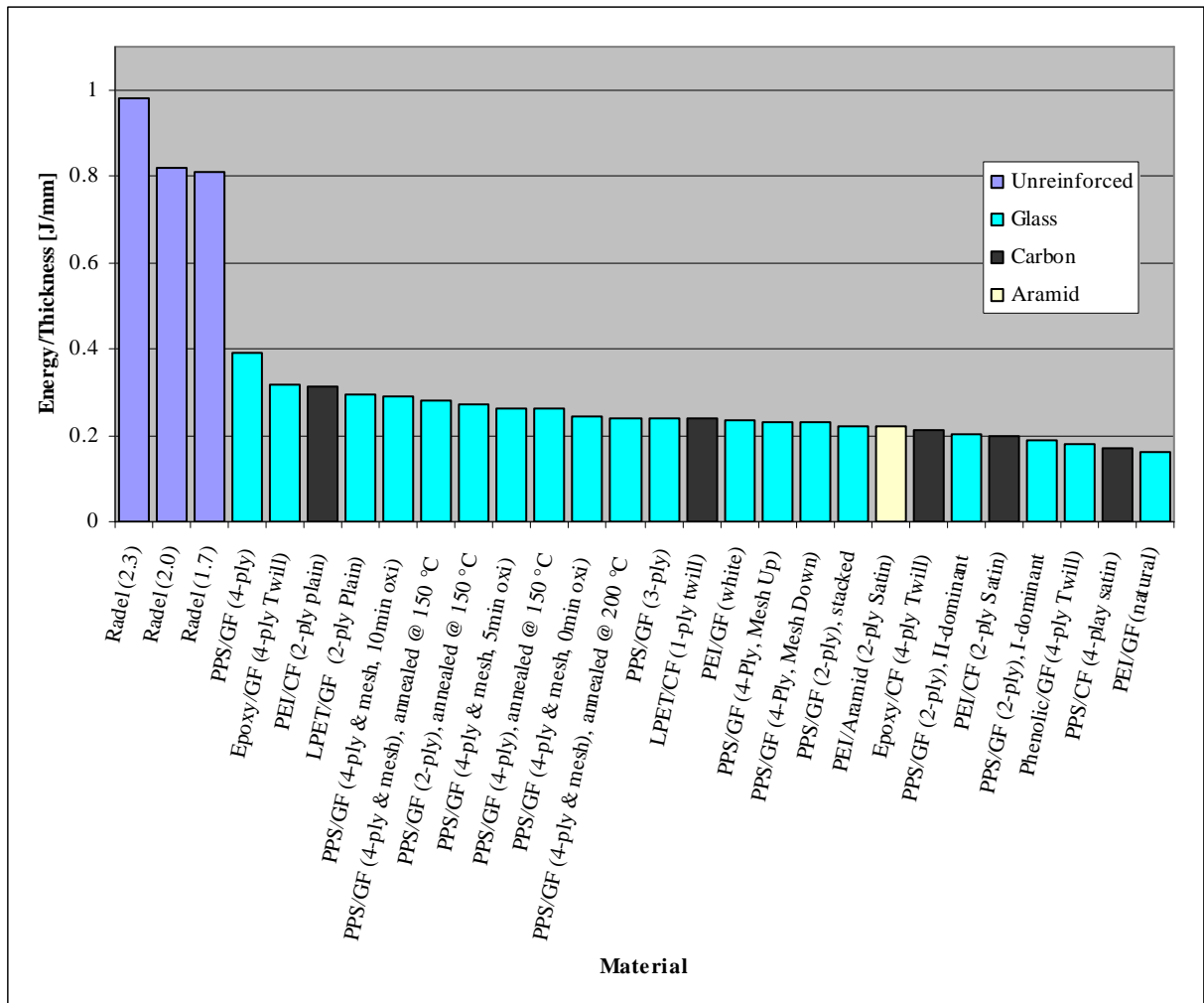
Figure 42: Specific energy absorbed by materials up to failure during impact testing

It can be seen that the unreinforced materials have a much higher impact resistance than the reinforced materials. This is probably due to the lower stiffness and plastic behaviour allowing more displacement before failure.

It was also noted that specific impact resistance was not related to the thickness of the materials. There was also no notable difference between thermosetting- and thermoplastic matrices. This is notable as thermoplastics are supposed to be more impact resistant.

5.3.2   Fibre Comparison

It is not clear from Figure 42 how the type of fibre alone affects impact resistance. The following figures (Figure 43 to Figure 46) show the effect of fibre type for each matrix material. It is clear from these figures that glass fibres allow a better impact resistance than carbon fibres. The only exception is with the PEI composites where it is difficult to draw a conclusion from the results. It can be assumed that the result is caused by the large difference in weave styles among the PEI materials. An unexpected finding is the difference between the natural- and white coloured PEI/GF materials. A reason for this has not been found yet.
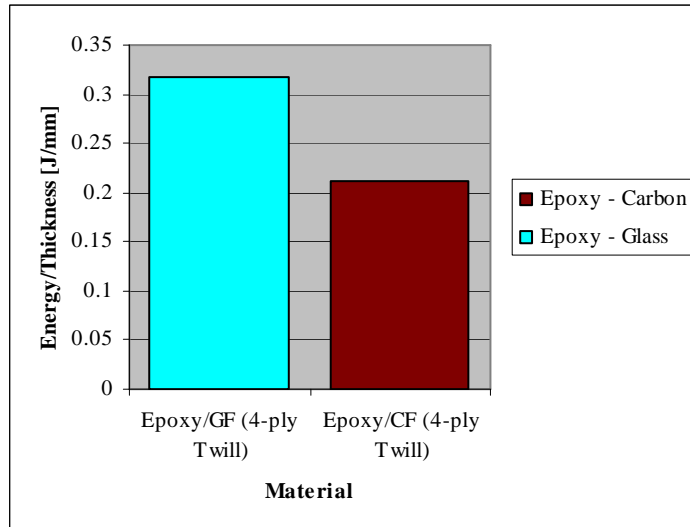
Figure 43: Specific energy absorption of Epoxy composites during impact testing
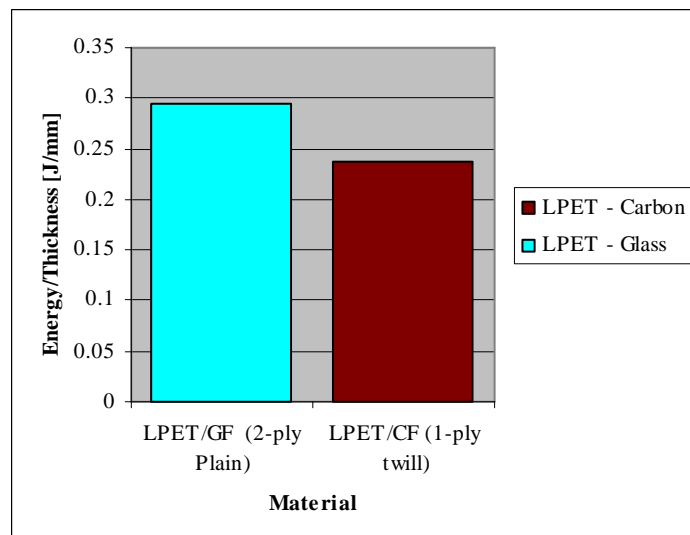
Figure 44: Specific energy absorption of LPET composites during impact testing
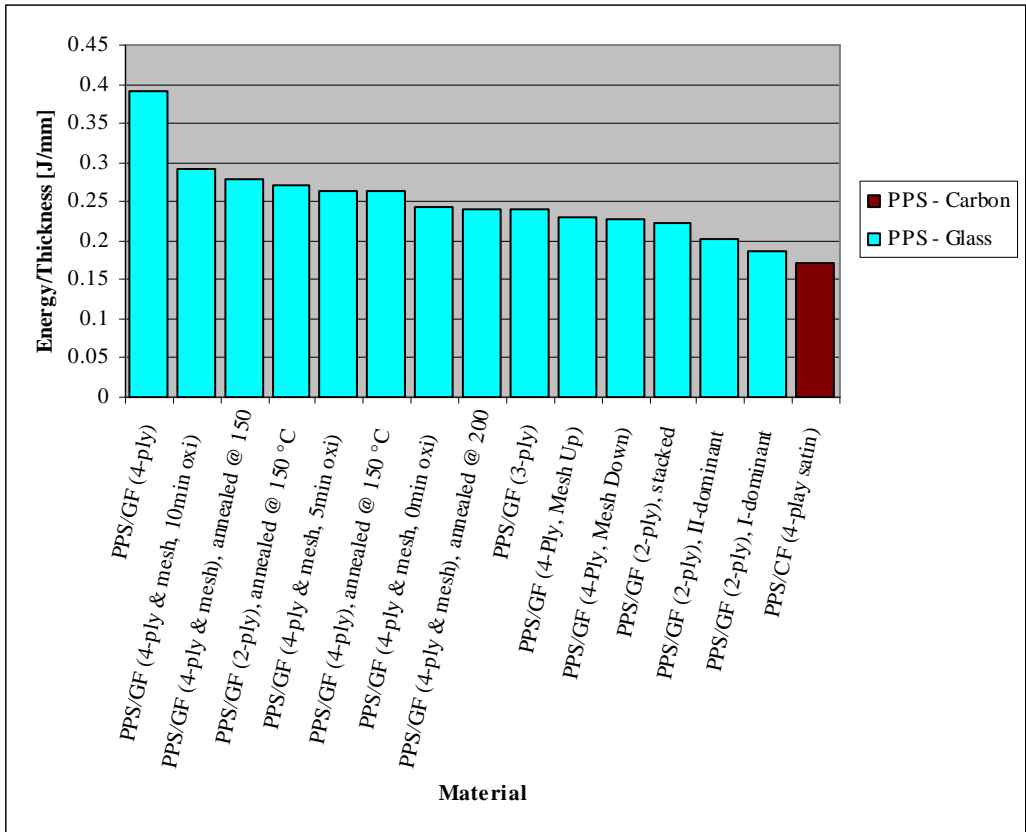
Figure 45: Specific energy absorption of PPS composites during impact testing
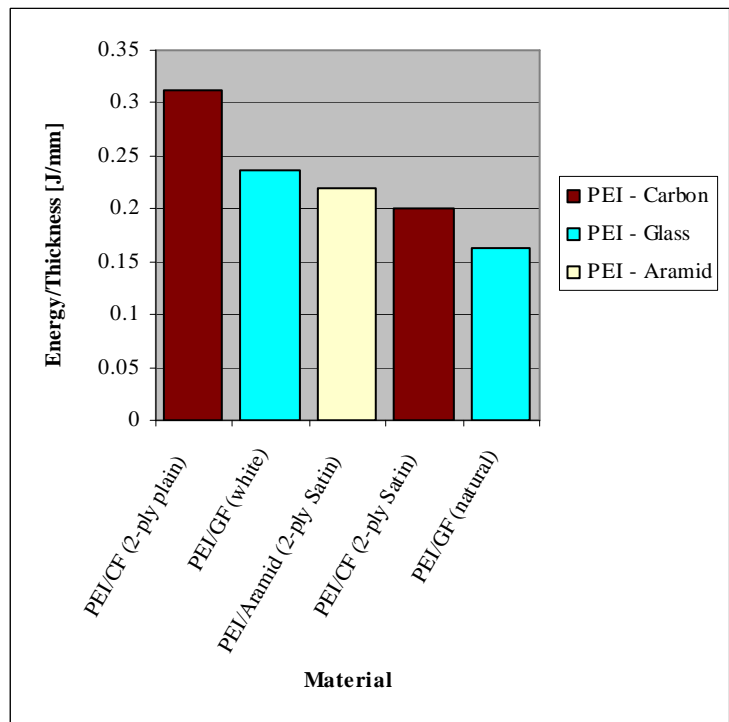
Figure 46: Specific energy absorption of PEI composites during impact testing

51

5.3.3 Damage Area

The damage area resulting from impact was measured for each material and averaged over the samples. The value was determined by multiplying the length and breadth of the damaged area (Figure 47). This is a measure of area that loses strength after impact as the fibres through this area are damaged and/or broken.
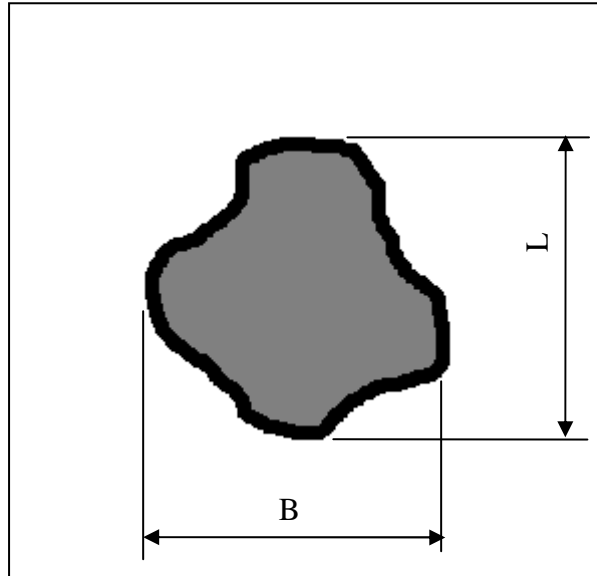
Figure 47: Damage area determination after impact testing

Figure 48 shows the damage areas of the 1 mm thick samples. The 0.5 mm samples were omitted from this graph as many samples had excess damage caused by the impactor mounting hitting the samples instead of just the impactor. It can be seen here that damage area is not necessarily fibre- or matrix-related. The graph shows that Epoxy/CF has a greater damage area than Epoxy/GF but the reverse is true for LPET. Varying damage area could result from different weave styles and fibre-matrix bonding. There is also no clear correlation between damage area and impact energy at failure. This is shown in Figure 49.
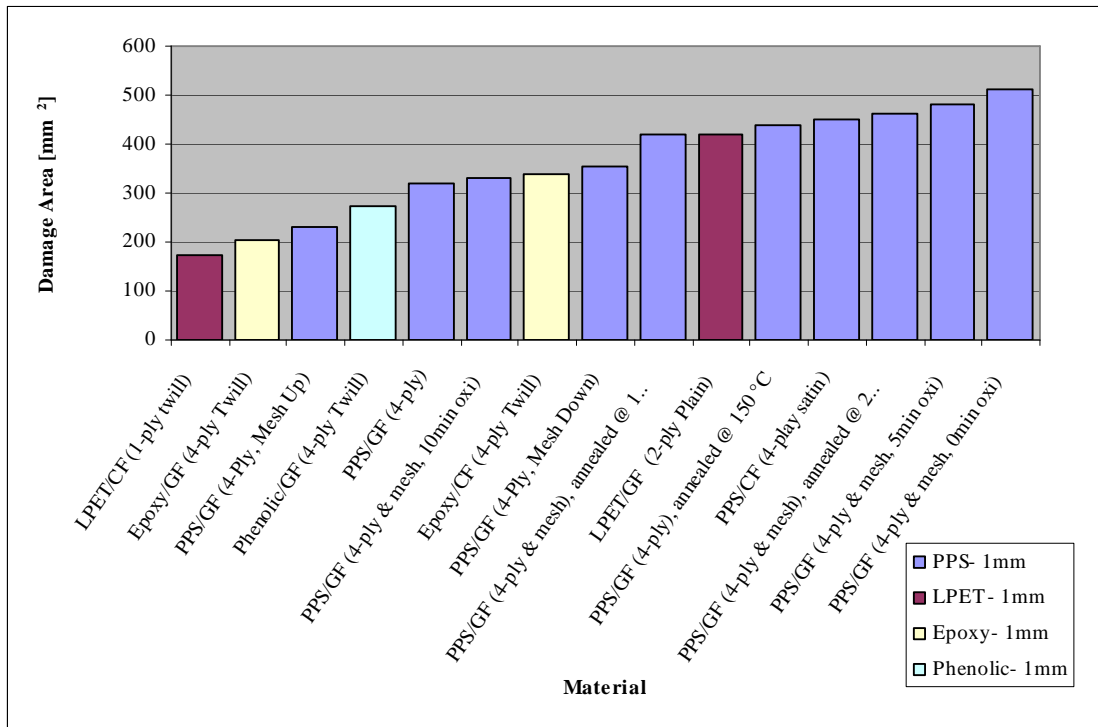
Figure 48: Impact damage area after impact testing
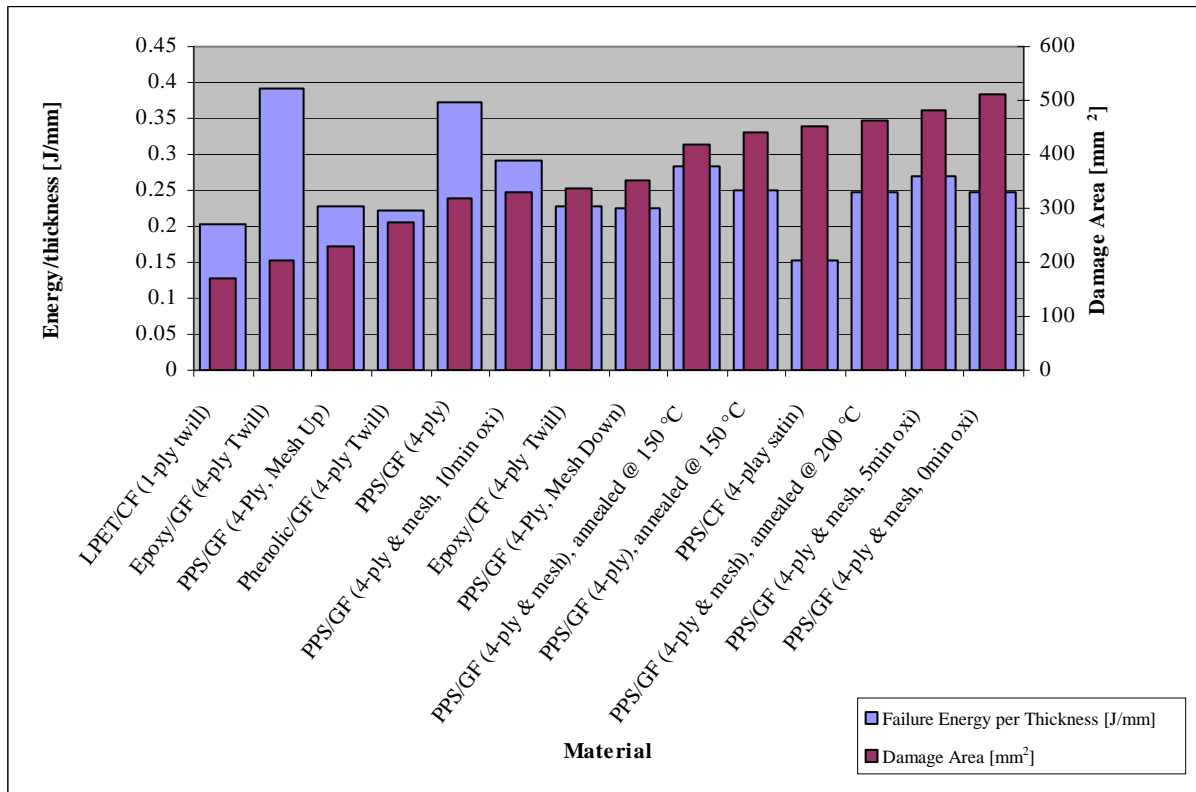
Figure 49: Specific failure energy vs. damage area in impact tested materials

5.3.4 PPS/GF Composites

Several variations of the PPS/GF composites were tested for impact properties. Variations included an added mesh, annealing conditions and oxidation levels. The same material variations were used in the flexural tests and more information on the sample preparation, along with TGA and DSC results, can be seen in Appendices A.4 and A.5.

5.3.4.1 Effect of Metal Mesh

It can be seen from Figure 50 that the addition of a metal mesh decreases the specific impact resistance of the material. There is still a significant difference between meshed and unmeshed samples when looking at the total energy absorbed at failure instead of the specific energy absorbed per thickness [J/mm]. This indicates that a mesh is disadvantageous for impact properties.

It appears that there is not a connection between impact resistance and damage area when the presence of a mesh is considered. It can however be seen that having a mesh on the impact side of the sample results in smaller damage area than having it on the opposite side or having no mesh at all.
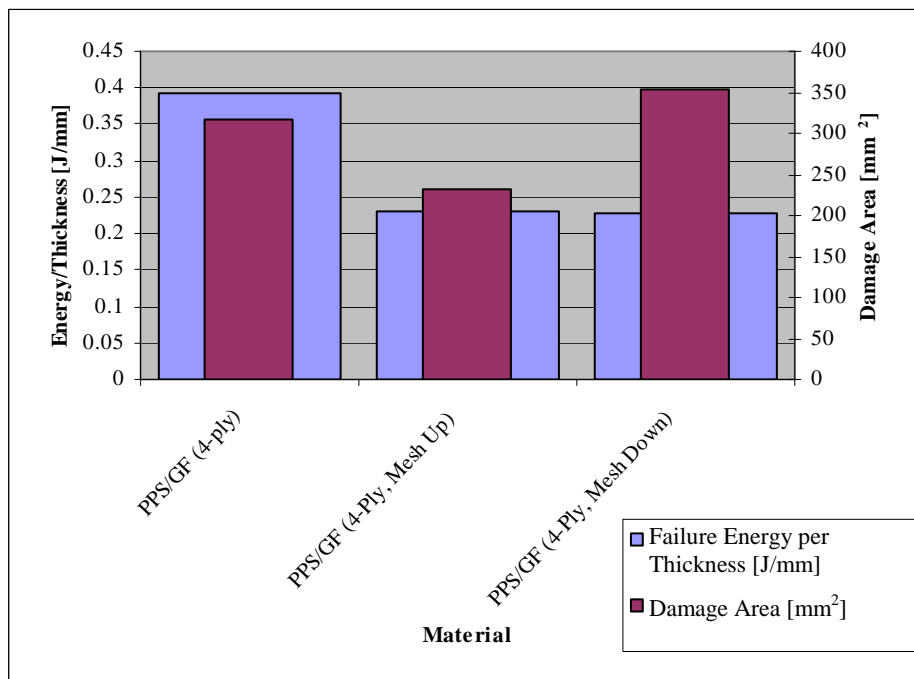
Figure 50: EMI shielding mesh in PPS/GF samples – effect on impact resistance

5.3.4.2 Effect of Annealing

The effects of annealing can be seen in Figure 51. The results show that a meshed sheet gains impact resistance with annealing and this is more noticeable with the samples annealed at 150 °C than those annealed at 200 °C. The opposite is true for a sheet without mesh which loses impact resistance with annealing. The reason for this is currently

unknown. Processing differences have been ruled out as the samples were all processed together.

Figure 51 also shows that annealed samples have larger damage areas with both meshed and unmeshed samples.
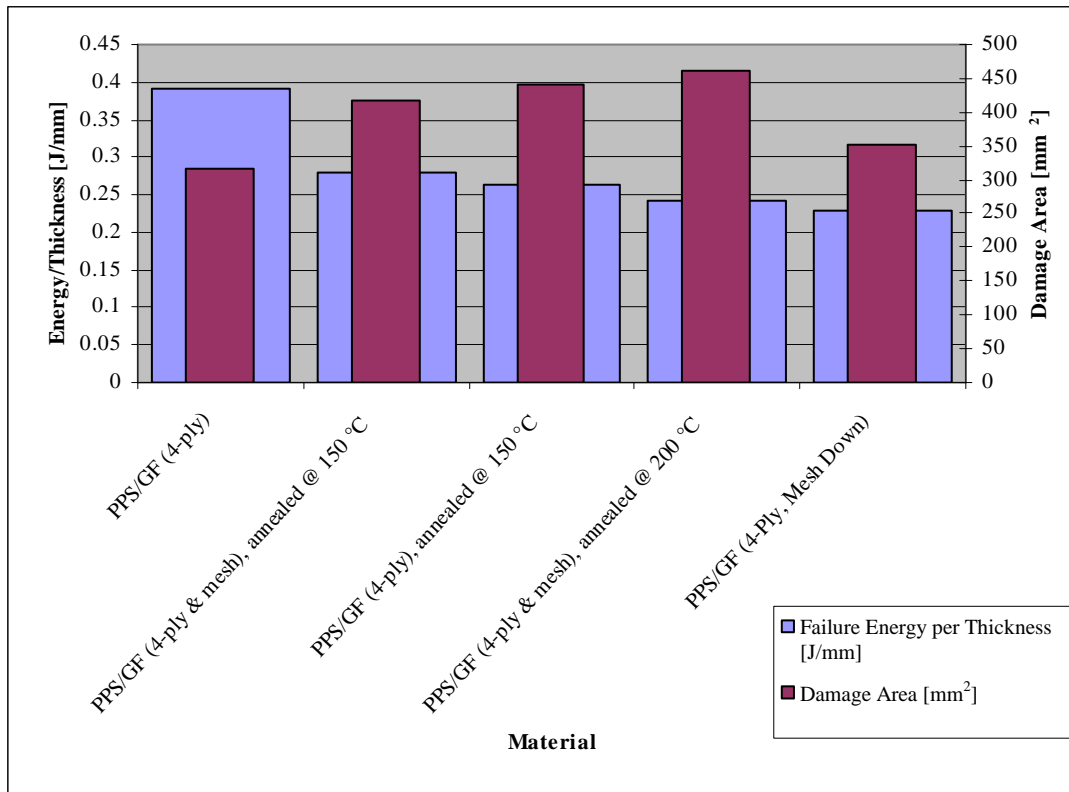
Figure 51: PPS/GF annealing – effect on impact resistance

5.3.4.3   Effect of Oxidation

Figure 52 shows the effects of oxidation on PPS/GF samples. Here it can be seen that the impact resistance increases with oxidation and the damage area decreases with oxidation. This indicates that oxidation that often occurs during processing is advantageous.
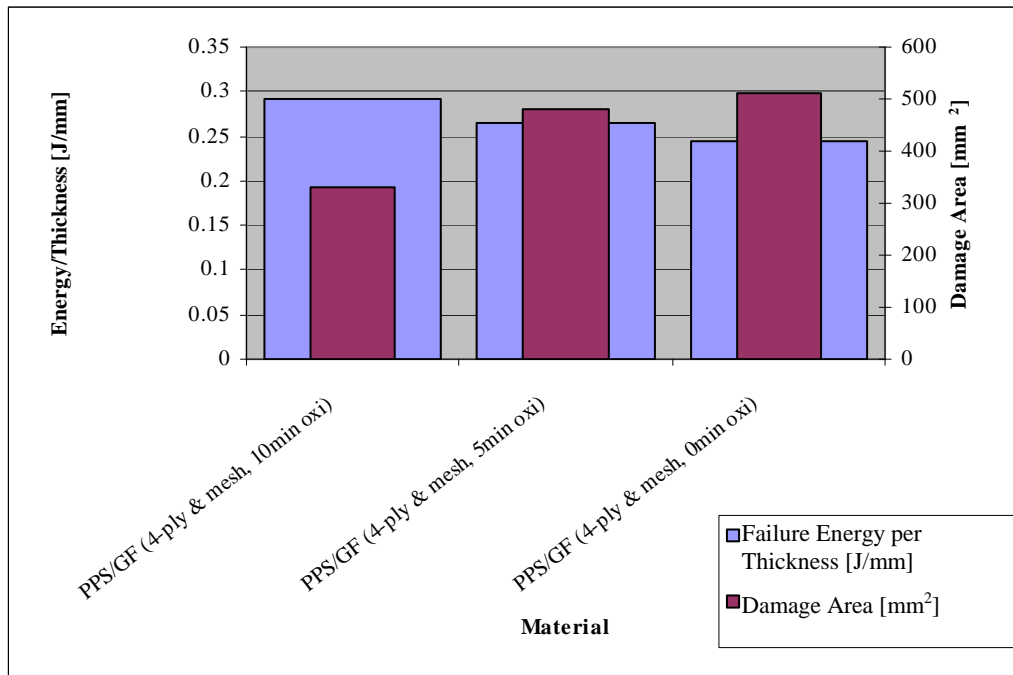
Figure 52: PPS/GF oxidation – effect on impact resistance

5.3.5 Stacking Sequence

It was realised in flexural testing (Chapter 4) that the asymmetry of the satin weave used in the PPS/GF causes variations in material properties depending on the stacking sequence. Figure 25 describes the various stacking sequences that were tested. Figure 53 shows that an asymmetrical stacking sequence results in a better impact resistance than a symmetrical stacking sequence. An asymmetrical weave, however, has a larger damage area. This indicates that the better impact resistance results from the impact force being distributed more widely than with a symmetrical stacking sequence.
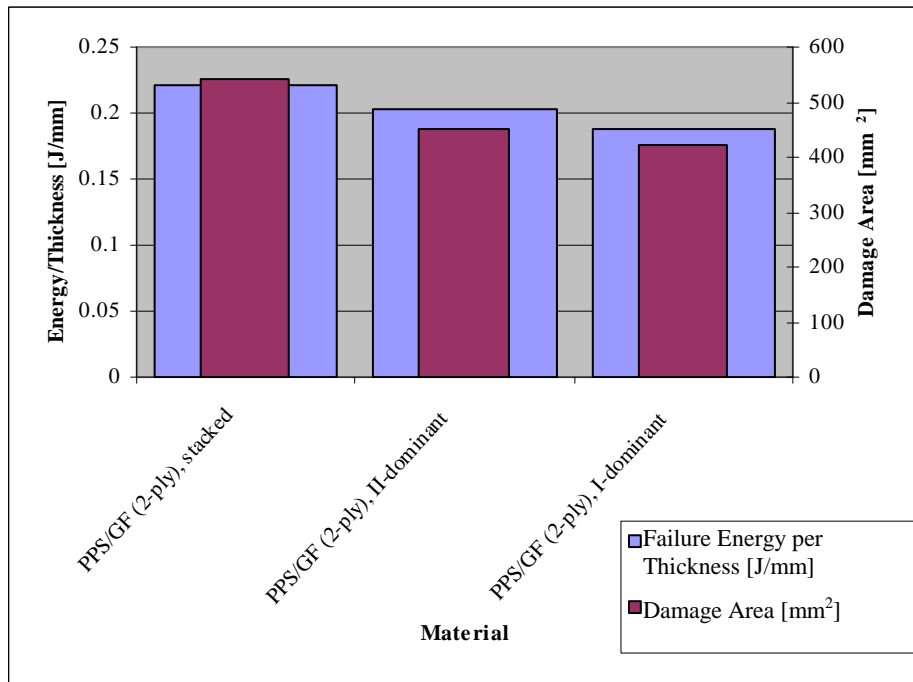
Figure 53: PPS/GF stacking sequence – effect on impact resistance

5.3.6   Failure Modes

Figure 54 shows the failure mode of each material with its corresponding specific impact energy.   It can be seen that lower impact values were observed when the impactor punctured the samples. Thus, the material could not absorb enough impact before failure to stop the impactor from penetrating. The impacted samples can be seen in Appendix A.8. The failure modes in Figure 54 describe the damage to the samples. For example, 'indented cross' means that the impactor did not puncture the sample and left a dent in the shape of cross. 'Closed' or 'open' refer to the holes in punctured samples after the impactor was removed. 'Composite fractions' means that the material delaminated and cracked severely.

A similar graph was created to show the failure mode of each material with its corresponding damage area. A trend could not be seen here i.e. there was no relation between failure mode and damage area.
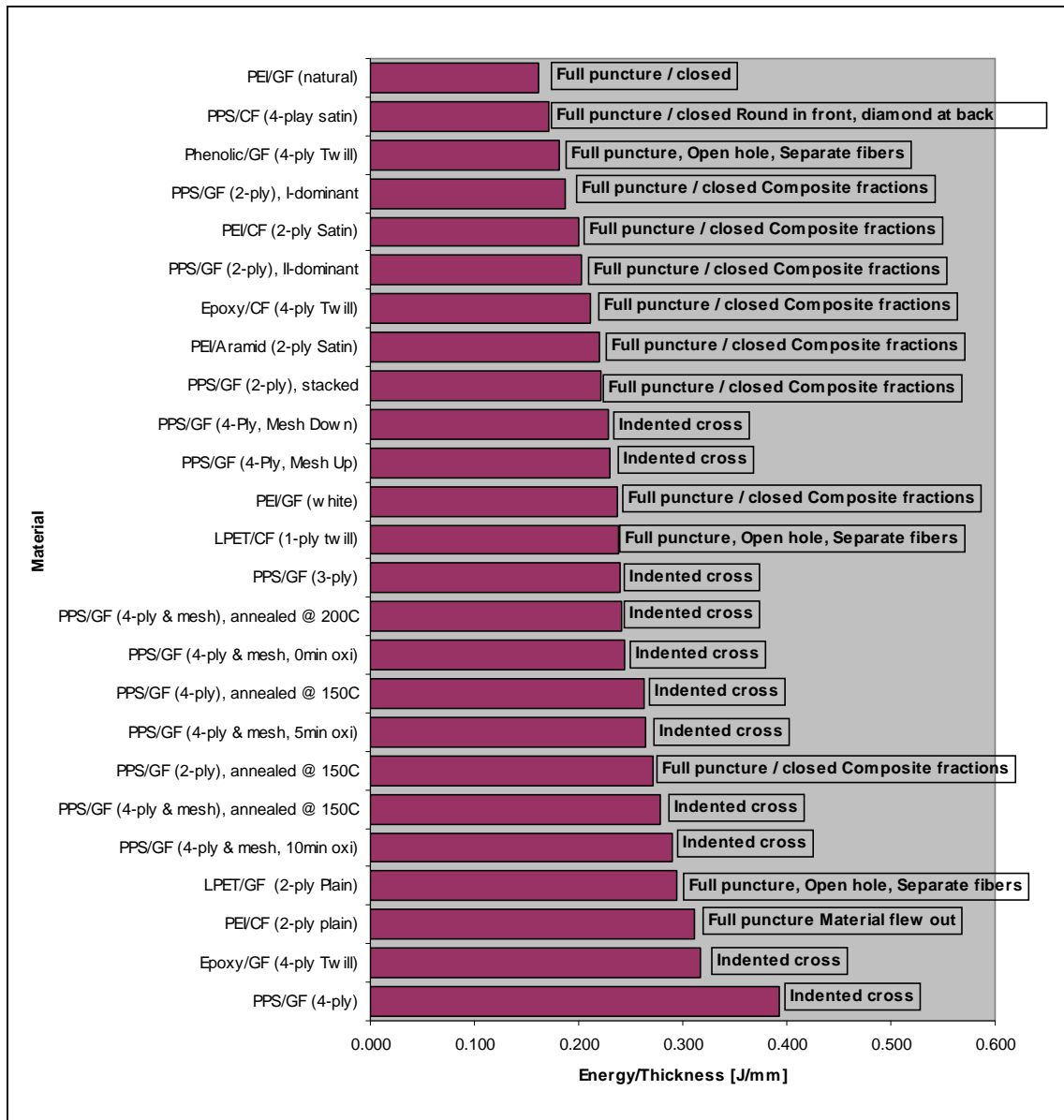
Figure 54: Failure modes in relation to specific impact energy

5.4 Conclusions

A broad range of composite materials were tested to get a comprehensive, comparative set of tests. The impact tests provided an indication of the materials' damage tolerance.

Sample amounts per material were reduced in several cases but repeatability of the valid measurements was deemed adequate.

Glass fibre reinforced composites yielded better impact resistance than carbon fibre reinforced composites for most matrix materials.

Useful conclusions were made with PPS/GF laminates regarding the effect of annealing, mesh attributes and oxidation levels.

Finally, although reinforced composites provide several advantages, unreinforced plastics have better impact resistance. This will need to be considered when designing certain parts.

These impact tests did not reveal the tested CFRTPs to have better impact resistance than the TSCs. This could be because the test was not suited to the current application. Perhaps a better test would be to use the impact of large objects on composite parts to simulate passenger head impacts during aeroplane crashes.

6   AIRCRAFT SEAT BACKREST FINITE ELEMENT MODEL

6.1   Introduction

The case study of this thesis is an airline seat backrest. This was chosen because it has certain strict requirements and provided certain challenges to be met. Airline backrests have to be strong enough to withstand frequent loads (typically people pulling on them when standing up) and they have to be light enough to not overburden the aeroplane. There have also been stringent fire, smoke, toxicity and heat release regulations that favour the use of TPs. The geometry of the particular backrest in this study is also sufficiently complex to demonstrate the use of commingled CFRTPs.

A finite element (FE) model of the experimental backrest was created. The first purpose of the model was to aid in the lay-up design to ensure the backrest would have adequate strength for the design loads. The model was also used to compare the stiffness and strength properties of a backrest made of reinforced LPET with one made of reinforced Epoxy material.

The model predicts that there will be no failure in the structure of the backrest under a limit load (LL) of 890 N applied in the aft direction at the top corner of the backrest. The stress results are presented for this load case with the maximum stresses and their locations indicated.

Although PPS was recommended as the most suitable matrix material in Chapter 2.3, LPET was used as the matrix polymer for the CFRTP backrests as it was more easily obtainable.

6.2   Description of Model

6.2.1   Software and Geometry

The model was first created by AAT Composites as a 3D CAD surface model in *ProEngineer* drawing package. An *IGES* file of each part (front skin, back skin and pivots) was then created and imported into *MSC Patran*, a FE pre- and postprocessor package. The displacement and stress results were calculated with *NASTRAN* and the results were displayed with *Patran.*

6.2.2   Meshing and Element Types

Meshing involves defining finite elements of the model i.e. breaking it up into smaller pieces that are connected to each other by nodes.

The meshing of shell elements was done using *Patran*'s *Advanced Surface Mesher (ASM)*. This module first creates a pseudo mesh of triangular elements which is then converted into a quad-element mesh. ASM aids in correcting geometry that has been altered slightly in the importing process. It allows the user to stitch, merge and alter surfaces relatively easily. Figure 55 shows the front- and back-view of the meshed model.

The elements that were used for the backrest skin were linear quad (4-node) elements and triangular (3-node) elements. The triangular elements were only created by ASM to prevent excessively skew quad elements.

The element edge length was chosen to be 7.5 mm on the relatively flat surfaces and 2-3 mm around the fillets where several elements were needed to sufficiently follow sharp curves. This resulted in 21 400 surface elements in the backrest skins.

It was decided that one layer of elements should be used where the front and back skin are bonded together as this would simplify the model. The other option would be to link the two layers of elements with rigid links but this carries a risk of interfering with the true stiffness of the part. The single layer can be seen in Figure 56 (marked in red).

The shell elements were defined as laminate elements. These are 2D elements that have membrane, bending and transverse stiffness. The properties of the laminate elements were assigned by specifying the number of layers, their thickness, material properties and material/fibre orientation (relative to a global coordinate axis). Each lamina has a predefined isotropic or 2D orthotropic property assigned to it. The stress results for these elements are then calculated for each layer relative to their longitudinal and transverse directions defined by their fibre orientation.

The elements' material orientation was defined by a vector projected onto the plane of an element. Most of the elements had their orientation defined by the global z-axis. This did not work for the elements perpendicular to the z-axis. For these, a coordinate system was defined so that its x-axis lies between the z- and x-axis of the global coordinate system. The material orientation for the remaining elements was then defined by this new x-axis.

The normals of the shell elements were adjusted so that all the normals around the hollow section face inwards and those of the inner surface face backwards. Element normals are indicated in Figure 56 by the black arrows. This allowed the definition of the composite lay-up sequence, from bottom to top, to be consistent for all elements.
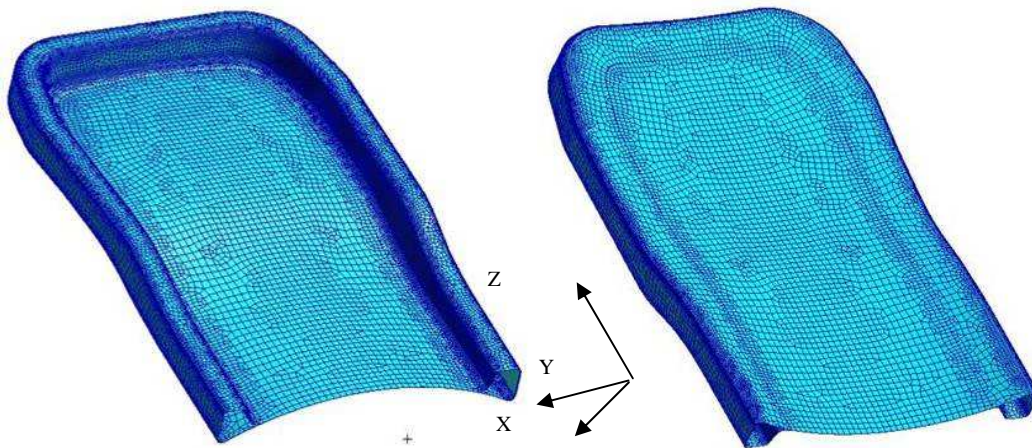
Figure 55: Front and back view of meshed backrest skins
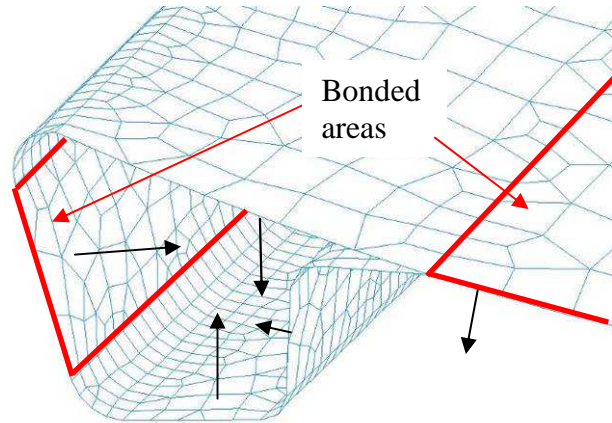
Figure 56: Display of element normals and bonded areas

The aluminium pivots of the backrest were meshed into 10-node tetrahedral elements using Patran's paver mesh function. Paver mesh is used to mesh objects that have irregular geometry. The tetrahedral elements were used as they are the simplest to mesh with. For both pivots, 14 428 tetrahedral elements were used.

The pivots were attached to the surface-section of the model with MPCs (multi-point constraints) where the pivots and composite skin would be bonded. MPCs define the displacement of a dependent node by a function of the displacement of an independent node and are also known as 'rigid links'. The chosen parameters of the MPCs in this model were to match the dependent nodes' displacement to the displacement of the independent nodes. The independent nodes were all on the pivots and the dependent nodes were on the skin.

All the nodes on the inside of each pivot hole were linked to a central node using MPCs. These central nodes were used to define the displacement boundary conditions of the model. This is shown in Figure 57.
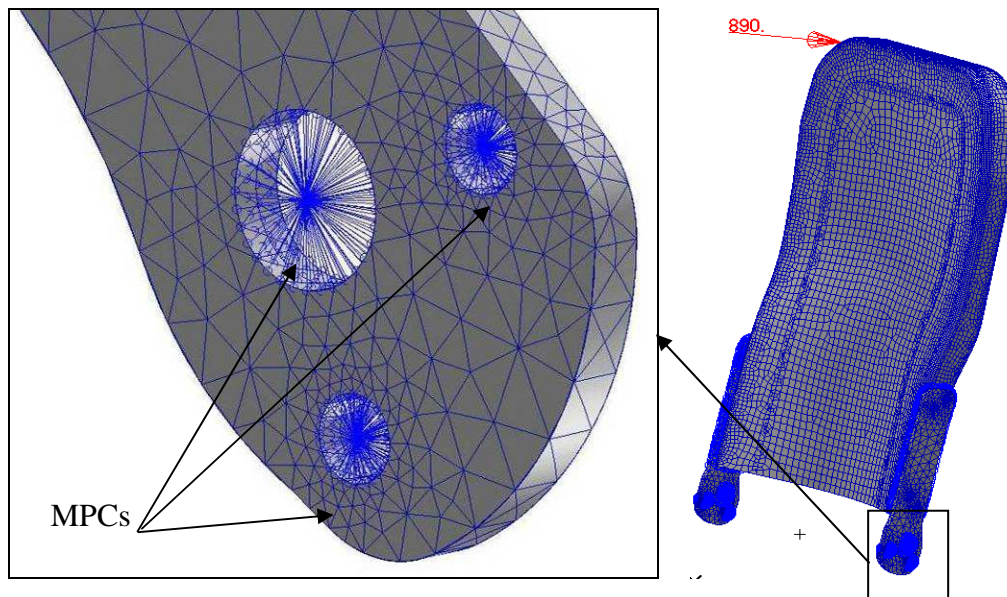
Figure 57: Pivot connections

6.2.3 Material Properties

Orthotropic stiffness properties for the composite materials were based on material tests performed by two final year students (Reuvers, 2006 and Terblanche, 2007), information from the supplier (Bak, Comfil ApS) and textbook average values. All the LPET materials were supplied by Comfil ApS and the Epoxy materials by SGL epo GmbH. The stiffness properties are listed in Table 4 and the strength properties are listed in Table 5.

The stitched ±45° LPET/CF was modelled as two layers of UD material, hence the same properties listed for both materials. The properties of the warp (0°) and weft (90°) directions for the woven LPET/GF was assumed to be the same. Transverse properties for the LPET/CF UD and stitched material were assumed to be similar to that of the LPET/GF UD tested by Terblanche (2007). This is because the transverse properties of UD composites are matrix dominated and fibre volume ratios are similar between the two materials.

Table 4: LPET and Epoxy composite stiffness properties

Material Name	ρ [kg/m^3]	E_L [GN/m^2]	E_T [GN/m^2]	G_{LT} [GN/m^2]	G_{Lz} [GN/m^2]	G_{Tz} [GN/m^2]	ν_{LT} [-]
LPET/GF 2/2 twill weave (30001-3)	1875 *	11 **	11 **	3.5 ***	3.5 ***	3.5 ***	0.05 ***
LPET/CF stitched ±45° 30023-6 and LPET/CF UD 30012-6	1530 *	112 *	6.4 **	5 ***	5 ***	3? ***	0.3 ***
Epoxy/GF PR FB1304 280/1270 FT1021 38	1808 *	21 **	21 **	3.5 ***	3.5 ***	3.5 ***	0.05 ***
Epoxy/CF PR UD CST 200/600 FT 102 40 (2 layers)	1600 ***	135 *	10 ***	5 ***	5 ***	3 ***	0.3 ***

(* Information from supplier, ** Tested value, *** Textbook average value)

The orthotropic strength properties were obtained from the same sources as the stiffness properties. The compression strength properties were assumed to be of the same magnitude as the tensile properties. This is a conservative assumption, because the transverse compression strength of UD layers is normally higher than the transverse tensile strength. The assumptions used in the stiffness properties were also used for the strength values.

Table 5: LPET and Epoxy composite strength properties

Material Name	σ_L^+ [MPa]	σ_L^- [MPa]	σ_T^+ [MPa]	σ_T^- [MPa]	τ_{LT} [MPa]
LPET/GF 2/2 twill weave (30001-3)	173**	173**	173**	173**	60***
LPET/CF stitched ±45° 30023-6 and LPET/CF UD 30012-6	1290*	1290*	20.9**	20.9**	60***
Epoxy/GF PR FB1304 280/1270 FT1021 38	200***	200***	200***	200***	60***
Epoxy/CF PR UD CST 200/600 FT 102 40 (2 layers)	1800**	1800**	30***	30***	60***

(* Information from supplier, ** Tested value, *** Textbook average value)

The thicknesses used for the orthotropic materials in the FE model are listed in Table 6. The actual Epoxy composite materials are half the thickness of that in the model but two layers were modelled as one for simplicity.

Table 6: Orthotropic material layer thickness

Material Name	Thickness [mm]
LPET/GF 2/2 twill weave (30001-3)	0.4
LPET/CF stitched ±45° 30023-6	0.4
LPET/CF UD 30012-6	0.45
Epoxy/GF PR FB1304 280/1270 FT1021 38	0.5
Epoxy/CF PR UD CST 200/600 FT 102 40 (2 layers)	0.4

The Epoxy adhesive used to bond the composite skins together and to the aluminium pivots were modelled using the isotropic properties listed in Table 7. These values were also obtained from either the supplier or textbook average values. The shear stiffness value for any isotropic material is calculated by *NASTRAN* using the Young's Modulus (*E*) and Poisson's Ratio (*v*) if a value is not specified.

Table 7: Isotropic material properties

Material Name	ρ [kg/m]^3	E [GN/m^2]	ν [-]	σ_y [MPa]	τ_{ut} [MPa]
Epoxy Adhesive	1250***	2.5***	0.35***	n/a	40***
Aluminium 7075 T6	2800***	71***	0.33***	480***	n/a

(* Information from supplier, ** Tested value, *** Textbook average value)

The thickness of the adhesive layer in the FE model was adjusted to comply with the distance between skins as defined by the mould design.

6.2.4   Laminate Definitions

Each material type/lay-up variation had its own group, element property and material definition. The lay-up sequences of the composite skins were defined in *Patran* by specifying the material, thickness and orientation of each lamina.

'Dummy' layers were used in some groups where a certain ply did not span the entire lay-up, typically an UD layer. This was done so that the layer numbers would refer to the same material type and orientation throughout the model except in the inner section (section 5 in Figure 58). The dummy layers had a thickness of 1 µm, a stiffness 1/1000th of the carbon UD lay-up and zero mass. These properties ensured that they did not interfere with the stiffness or mass of the model. It was not possible to match the laminae of the inner section to the rest of the model; therefore the lamina numbering here does not correspond to the rest of the model.

Figure 58 shows the location of the property sets for the skins where each property is indicated in a different colour. Property sets 1, 3 and 5 are where the front and back skins are bonded together. Property sets 2 and 4 are unbonded sections of the front skin and property sets 6 and 7 are unbonded sections of the rear skin.
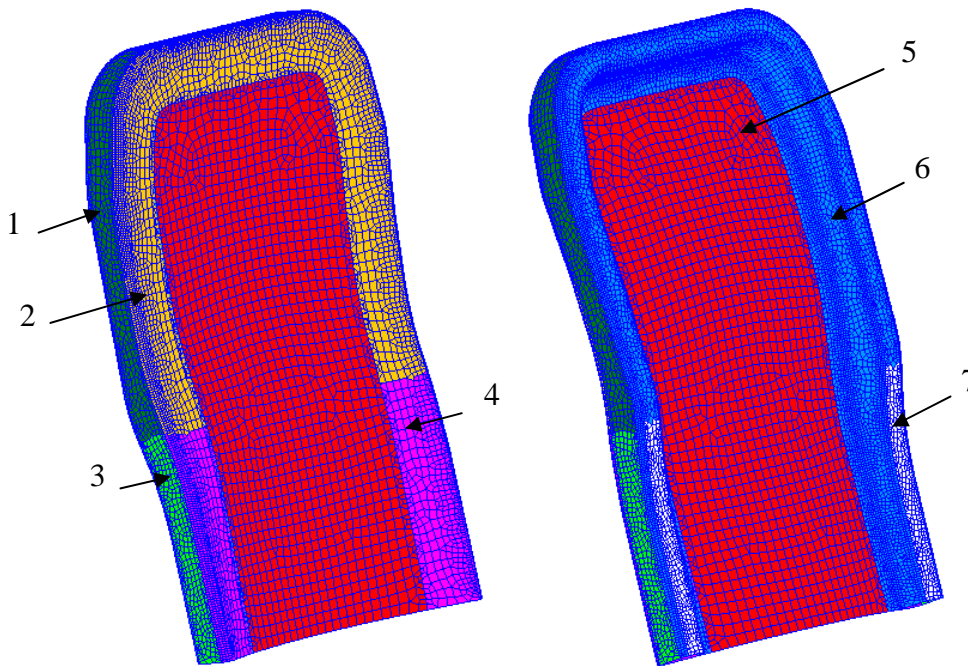
Figure 58: Element property sets

(front view (left) and rear view (right))

The lay-up sequence was determined iteratively by analysing the stresses in the laminates and altering the lay-up until the stresses were adequately below the strengths of the materials. The final lay-up was chosen to be $[+45°_{C,UD}/-45°_{C,UD}/0°-90°_{GW}/-45°_{C,UD}/+45°_{C,UD}]$ for the front skin and $[+45°_{C}/-45°_{C,UD}/0°-90°_{GW}/90°_{GW}/-45°_{C,UD}/+45°_{C,UD}]$ for the back skin. Additional layers of carbon UD were placed on the front skin at sections 3 and 4 (Figure 58) and the back skin at section 7. Thus, the areas where the front and back skin are bonded together are modelled as one laminate with 16 layers including a layer of adhesive.

6.2.5   Model Mass

The masses of the FE model, calculated by Patran using the material densities listed in Section 6.2.3, were 1.98 kg and 2.13 kg for the LPET and the Epoxy backrests, respectively. This includes the composite skins, pivots and adhesive.

6.2.6   Support Boundary Conditions

Support boundary conditions were placed on the pivots in the FE model to represent test mounting conditions.

Both pivot hinge points were fixed in all rotational and translational directions except for the rotation about the Y-axis. All the pivot locking-points were fixed in the X-direction. Refer to Figure 55 for the global coordinate directions.

6.2.7   Load Case

The load case chosen for this study was based on the load specifications of an existing backrest design. This requires the backrest to take an aft 890 N (200 lbf) load at the top corner on the right of the structure. Figure 76 in Appendix B shows the location of the load and boundary conditions. Further load cases can be added to the model should further investigations into structural behaviour be desired.

6.2.8   Buckling Analysis

A buckling analysis was performed on the backrest to ensure that it would not buckle under the required loads. The support boundary conditions were the same as those used in the static analysis, and a force of 1 N was applied at the same node as the limit load described in section 6.2.7. The unit force was used for simplicity because *NASTRAN* calculates the buckling load as a multiple of the applied load.

The first five buckling modes were requested in the analysis.

6.3   Displacement, Stress and Buckling Results

Plots of the displaced structure are shown in Appendix B.2 and plots of the stress results for the laminae and pivots are shown in Appendices B.3 and B.5.

6.3.1   Displacement Results

The maximum allowable displacement results were based on the specifications of an existing backrest made by AAT Composites. These specifications required the backrest to displace no more than 114.3 mm (4.5") under load (load deformation) and 4 mm (0.16") after the load has been removed (residual deformation).

The maximum displacement of the LPET and Epoxy backrests are shown in Table 8. The residual deformation can be determined only through physical testing and is therefore not presented in this report.

The model predicts that the Epoxy backrest will be 21 % stiffer than the LPET backrest.

Table 8: Backrest load displacement

Backrest Material	Load Displacement [mm]
LPET	16.9
Epoxy	13.3

6.3.2   Maximum Stress Results

The maximum stress results for each fibre orientation/reinforcement type are listed in Table 9 and Table 10. Stress distribution plots of the laminae where the highest stresses occur (marked in grey) are shown in Appendix B.3. Nodal averaging was only applied over each property set region which accounts for the discontinuities in some of the plots. The flat

inside section of the backrest was omitted in these plots as the lamina numbering does not match the rest of the model and the stresses here were insignificant.

None of the lamina stresses in the LPET model exceed or even approach the maximum allowable stresses listed in section 6.2.3. Table 26 in Appendix B.4 shows the maximum and minimum stresses in each lamina for both models.

Table 9: Maximum stresses in +45° and -45° carbon UD laminae

Matrix	45º Carbon UD Laminae (3/8/12/16)			-45º Carbon UD Laminae (4/7/13/15)		
	$\sigma\|_L$ [MPa]	σ_T^+ [MPa]	$\tau\|_{LT}$ [MPa]	$\sigma\|_L$ [MPa]	σ_T^+ [MPa]	$\tau\|_{LT}$ [MPa]
LPET	255	19.1	39.2	253	15.4	36.9
Epoxy	267	42.2	25.1	180	10.7	6.63

Table 10: Maximum stresses in 0° carbon UD and glass weave laminae

Matrix	0º Carbon Laminae (1/2/10/11)			0°/90° Glass Weave Laminae (5/6/14)	
	$\sigma\|_L$ [MPa]	σ_T^+ [MPa]	$\tau\|_{LT}$ [MPa]	$\sigma\|_L$ [MPa]	$\tau\|_{LT}$ [MPa]
LPET	192	35.9	11.9	45.7	7.28
Epoxy	185	42.2	7.94	53.8	6.24

The maximum shear stress in the Epoxy adhesive was calculated to be 6.5 MPa in the LPET model and 5.54 MPa for the Epoxy model. These are both lower than the quoted material shear failure stress.

The maximum Von Mises stress calculated for the pivots was 465 MPa for the LPET model and 460 MPa for the Epoxy model. These values are lower than those of the yield stress and, according to the model, only occur in a very small area of the pivot (see A.1).

6.3.3   Buckling Results

The minimum buckling load for the LPET model was calculated to be -2 554.9 N. As this is a negative load, it implies that the structure will not buckle under a load in the direction of the specified load. The magnitude is also too high to be of concern if the load was applied in the opposite direction.

The minimum buckling load for the Epoxy model was calculated to be -4 087.4 N. This buckling load, as with the LPET model, is in the wrong direction and too large to be of concern.

The other four buckling modes for both models had greater magnitudes than the first and were all also negative, thus causing no concern.

6.3.4   Discussion of Results

The LPET model's maximum displacement under the limit load of 890 N is 16.9 mm. The maximum lamina stress in the carbon UD and glass weave is 255 MPa and 45.7 MPa, respectively. These values are too far below the strength of the material to be of any concern.

The Epoxy model's maximum displacement is 13.3 mm under the same load. The maximum lamina stresses for the carbon and glass lamina are 267 MPa and 53.8 MPa, respectively. These are also below the strengths of the materials and therefore of no concern.

It is interesting to note that the stiffer glass material in the Epoxy model results in lower stresses in the carbon laminae and higher stresses in the glass laminae. This also results in the highest stresses occurring in places different to the LPET model.

The fact that the stresses are far below the strengths of the materials indicates that the lay-up can be optimised significantly to save mass and material cost. This was not the main objective of the research and therefore was not focussed on.

6.4   Conclusions

A lay-up for an experimental backrest was chosen which, according to FE results, experiences no failure under the design load. Any failure that does occur will be due to improper processing parameters.

A comparison was made between backrests made of LPET and Epoxy composites to predict differences in performance of the two material types. These results will be compared to the test results of the manufactured backrests to verify the model.

7 AUTOCLAVE PROCESSING OF AIRCRAFT SEAT BACKREST PARTS

7.1 Introduction

The case study backrests were produced with both commingled LPET CFRTPs and Epoxy composites. This chapter describes the manufacture of the backrest skins and the assembly of the complete backrests. The material chosen for the manufacture of the CFRTP backrests was LPET reinforced with glass fibre or carbon fibres. The ideal matrix material would have been PPS but the poor availability of this matrix in commingled material prevented its use.

7.2 Manufacture of LPET Backrests

Production of the experimental backrest shells began once the principles of autoclave processing of commingled CFRTP materials were established (Chapter 3).

The lay-up was determined by the mould geometry and the FE modelling (Chapter 6). The materials used were commingled LPET reinforced with glass and carbon, respectively. The carbon material was a stitched, biaxial cloth (basically two layers of ±45° UD) and the glass was in a 2×2 twill weave. Strips of carbon UD were also used as local reinforcement.

The use of the different material forms and reinforcing fibres showed the ease with which varied lay-ups can be produced. The drapability of the materials, particularly in biaxial form allowed the lay-ups to be performed with minimal amount of cuts in the material. Figure 59 shows the laying up of the backrest's front skin where the material did not need any cutting. There was slight wrinkling of the glass cloth in the corner but this only occurred outside the trim line.

A spray-on adhesive was used for the placement of the UD strips. This prevented the strips from shifting during the rest of the lay-up process. It was felt that the use of this adhesive should be limited thereby allowing the vacuum and applied pressure to squeeze the material into the mould corners.
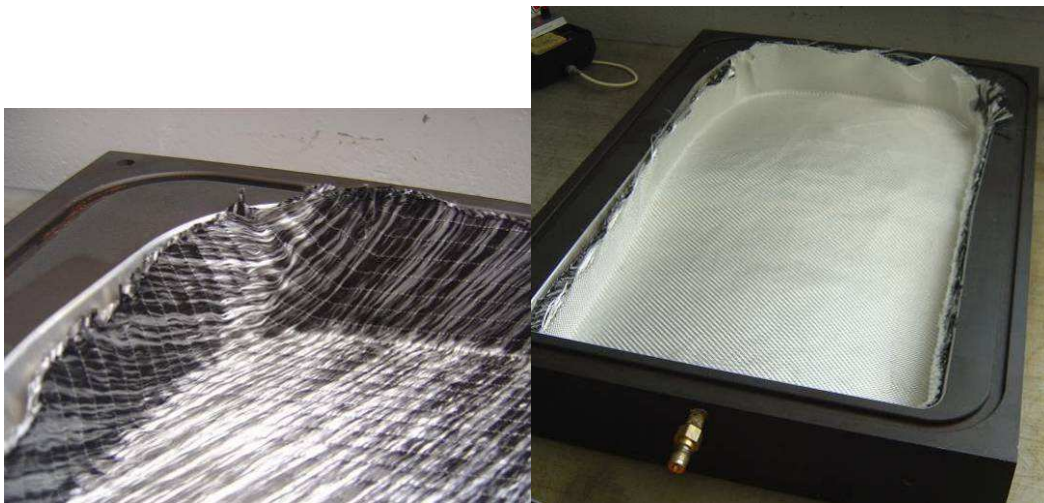
Figure 59: Draping of commingled materials in one of the backrest moulds

Several parts were successfully produced with the autoclave technique. Figure 60 shows a successfully consolidated front- and back skin of the backrest. The only problem that occurred in the manufacturing of these parts was bridging of either the vacuum bag or laminate causing inadequate consolidation in certain areas. This just reinforced the need for careful material placement and vacuum bagging.

Figure 60: Successfully consolidated LPET backrest skins

7.2.1   CFRTP Materials and Consumables Used

The materials used for the backrests were chosen based on physical properties and availability. These materials are listed in Table 11.

Table 11: Backrest CFRTP material specifications

Material	Fibre Content [v%]	Fibre Area Weight [g/m²]	Fibre Lay-out	Supplier
Commingled LPET/Carbon stitched multiaxial	47.3	354	Stitched [±45°] UD	Comfil ApS
Commingled LPET/Carbon UD	47.3	336	UD [90°]	Comfil ApS
Commingled LPET/glass woven cloth	47.3	354	2×2 twill weave	Comfil ApS

The consumables used to produce the backrests are listed in Table 12. They were chosen on the principles discussed in Chapter 3

Table 12: Consumables used for LPET backrest manufacture

Item	Name	Supplier
Vacuum Bag	Capran 526 (Nylon, 232 °C)	Aerovac Systems
Release Film	A6000 (Fluoropolymer ETFE, 260 °C)	Aerovac Systems
Sealant Tape	SM5126	Aerovac Systems
	GS43MR	Aerovac Systems
Bleeder	Woven Glass Fibre	Various
Release Agent	Freekote 700 NC	Airtech Advanced Materials Group
Spray-on Adhesive	Airtac-2	Aerovac Systems

7.2.2   Assembly

Assembly of the backrest involved riveting and bonding the two skins and pivots together. Purpose-made jigs, shown in Figure 61 and Figure 62, were used for the drilling of the rivet holes and bonding of the parts. Bonding was used as it is an established method used for TSCs and the necessary equipment was available for this research. Araldite AV 4076 with Aerosil filler was the adhesive used. The bonding surfaces were roughened with sand paper and cleaned with methanol. Rivets were used for added strength as well as aligning the skins and pivots for bonding.

Figure 61: Drilling jigs for backrest skins

Figure 62: Bonding jig for backrest assembly

7.3 Thermoset (Epoxy) Backrests

Thermoset backrests were made in the same moulds as the thermoplastic backrests. The purpose of these backrests was to compare the thermoplastic backrests with ones made of a material already in use in the airline industry.

The backrests were made using existing processing technology at AAT Composites. This involved laying the epoxy prepreg laminate in the mould, placing the vacuum consumables and then applying heat and pressure for the required curing time of the materials. The processing was performed in a pressclave – a machine where the mould is sealed between two heated plates and the cavity is pressurized.

Epoxy prepreg was chosen as the material to be used and the material lay-up was designed to be comparable with the thermoplastic backrests. The material specifications are listed in Table 13. It was not possible to obtain TSCs with the same fibre volume content as the thermoplastic materials. Therefore testing results will be normalised accordingly – as described in a later chapter.

Table 13: Specification for thermoset material used in backrests

Material	Fibre Content [v%]	Fibre Areal Weight [g/m²]	Fibre Lay-out	Supplier
Epoxy carbon UD prepregs	60	200	UD	SGL epo GmbH
Epoxy glass fabric prepreg	62	280	2×2 twill weave	SGL epo GmbH

7.4 Material Manufacturing Comparison

Each material type's backrests took roughly an hour to lay-up in the moulds. It is believed that the lay-up time for thermoplastic backrests will be shorter than that of the thermoset backrests when performed by skilled and practised operators.

The lay-up of the thermoplastic parts was felt to be easier than that of the thermoset parts. This was because of the drapability of the commingled fabric and the fact that it is not tacky. This allowed easy placement and adjustment of the material in the mould. The only problem with this drapability property would occur with large vertical mould faces where the material would not necessarily stay in place. Here, tack-aids such as a spray-on adhesive would work.

The processing time of a thermoset backrest was much quicker (approximately 1.5 hours) compared to a thermoplastic backrest (approximately 3 hours). The reason for this is that the thermoset parts were processed in a pressclave and the thermoplastic parts were made in an autoclave which has long heat-up times.

The bonding of the backrests took about 20 minutes. The curing time for the Epoxy backrests was 1 hr at 70 °C and the LPET backrests' curing cycle was 2.5 hrs at 50 °C. The reason for the difference in the curing cycle is that LPET has a maximum use temperature of 60 °C and begins to soften and deform at any higher temperature.

7.5 Conclusions and Recommendations

The thermoplastic backrests' processing time looks unattractive from these experiments. However, should the thermoplastic parts be heated and cooled quicker – in a pressclave for instance – then the processing time could be drastically reduced to under an hour. This is because the commingled material only needs about 15 minutes for consolidation at the correct processing conditions.

The bonding of the two skins was a time-consuming, labour intensive process that could be improved upon for the thermoplastic parts. TPCs can be welded (fusion bonded) which involves placing a conductor between two skins and either applying an electric current or an inductive field to heat the conductor and the surrounding material while applying pressure to the joint. The process can take as little as a few seconds to perform (Ahmed et al, 2006) and will probably result in a stronger joint than adhesive bonding. It does however require specialised equipment, but this would become viable for larger production volumes. The only minor downside of this technique is that it requires trimming of the elements where they protrude from the part.

8 BACKREST TESTING

8.1 Introduction

The backrests described in the last two chapters were tested at AAT Composites using their standard test equipment. The purpose of the testing was to evaluate the CFRTP backrests and compare the backrests made of the two materials. Two loads were planned for each backrest: a limit load (maximum design load) and a breaking load. The limit load was the same as that used in the FE model (200 lbf / 890 N) and the breaking load was to be the load at which a backrest failed. The test results were also compared to those of the FE model.

Figure 63 shows a backrest mounted in the test jig.

Figure 63: Backrest mounted in structural test jig

The test set-up consists of a mounting frame in which various backrests can be fastened. It also has a mount for a LVDT (linearly variable displacement transducer) to measure displacement at the point of force application. Force is applied to the backrest by a pneumatic cylinder via a steel cable. A load cell attached to the cable measures the applied force.

A software application was written for the set-up that controls the force applied by the cylinder and records the time [s], force [lb] and deflection [mm] every 0.1 seconds. The data is stored in a .csv (comma-separated variables) file that can be edited in a spreadsheet application such as Microsoft Excel. Air is released from the cylinder once the preset load has been reached so that the backrest returns to rest and data recording is stopped.

AAT Composites regularly uses the test set-up on prototype and production backrests and it is therefore calibrated regularly. The author performed some basic tests to validate the calibration of the equipment.

The masses of the backrests were also measured. The scale is also regularly calibrated and accurate to 1 gram. The mass measurements allowed mass-stiffness comparisons between the backrests made of each material to be made.

8.2 Test Procedure

Each backrest was placed in the jig and fixed with locking pins. These pins fixed the backrest in the way that was simulated in the FE model in Chapter 6. The pulling-cable was mounted on the top left corner of the backrest and pre-tensioned to 22 N. The pre-tension is to take up slack in the cable and the rest of the set-up and is a standard testing procedure at AAT Composites. The LVDT was then placed where the cable was mounted and checked to be horizontal.

The limit load of 890 N (200 lbf) was then applied and data was recorded. The pulling force of the cylinder was then set to maximum and applied to the backrest. Unfortunately the maximum force of the test equipment (~2900 N or 650 lbf) was not enough to break any of the backrests. The maximum-force tests were still performed on all the backrests and the data recorded.

The force-displacement graphs showed a non-linear settling period at the beginning of each test. This was believed to be due to one of two reasons. The first could be the slight play in the backrest mounts and excess slack in the cable that was not taken up by the pre-tension. The other reason for the change in gradient could be load stiffening where the deformation of the backrests under increasing load results in stiffer geometry. This was compensated for in the post processing where the gradient of the linear portion of the graph was used to obtain a zero-displacement point. The calculated 'actual' displacement was then adjusted from this point. This procedure is shown in Figure 64.
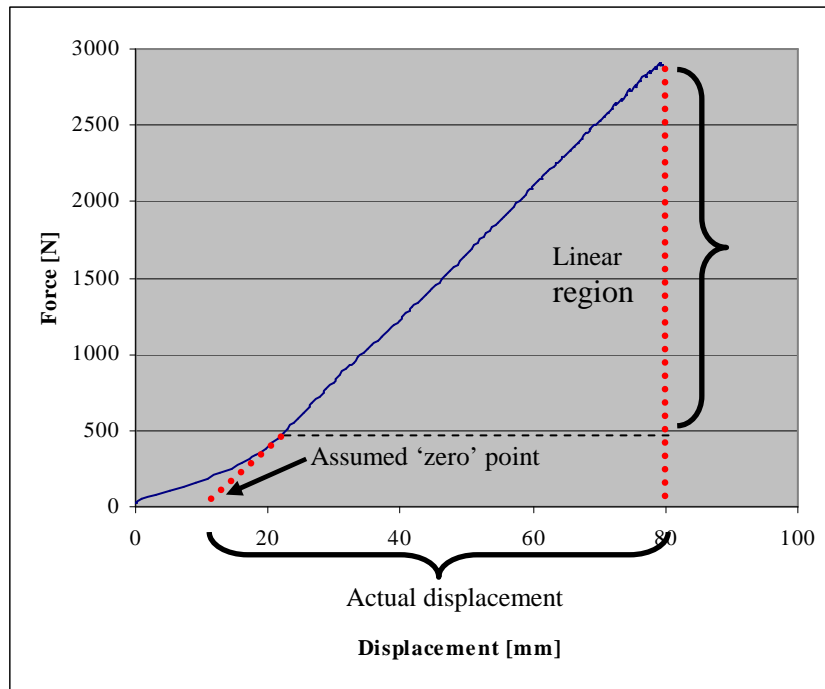
Figure 64: Typical force-displacement graph from backrest tests

8.3 Test Results

Unfortunately, the maximum load of the test equipment (2900 N) was not enough to break the backrests. Certain samples were retested to look for change in stiffness and lack thereof implied that no permanent damage was caused. The LPET backrests had distinctive audible cracking when tested to maximum load but the author believes this was from the adhesive between the centre two skins in the middle (flat) section of the backrest and of no structural consequence.

The average displacement under 890 N load was calculated for the LPET and Epoxy backrests. The results showed that the actual backrests displaced more than predicted by the FE model as shown in Figure 65. It can be seen from the actual backrests that the Epoxy backrests displaced 3.5 % less than the LPET backrests.
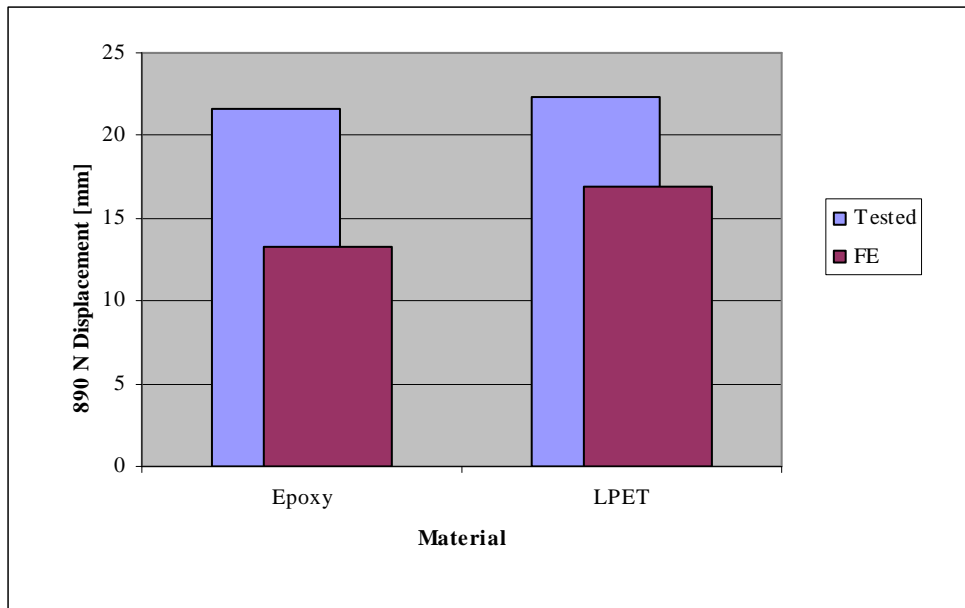
Figure 65: Displacements of tested and FE model backrests at 890 N load

The FEM predicted displacement values were 38.4 % and 24.5 % less than the tested displacements for the Epoxy and LPET backrests, respectively. This is a significant difference that could be due to several factors in the FE model such as material properties and laminae thicknesses. Another reason for this difference could be that the constraints in the FE model were ideal (completely rigid) whereas the actual backrests' mountings could have had some play in them. It is recommended that displacement near the pivot points should be measured in future backrest tests.

The average masses of each material's backrests with their standard deviation are shown in Figure 66. It can be seen that the Epoxy backrests were only 3 % lighter than the LPET backrests but the LPET backrests had a higher standard deviation (100 g vs. 20 g). The higher variation in mass for the LPET backrests was due to the flexibility of the commingled material that can vary the density during lay-up. There is a difference between the calculated and measured masses because the FE model has adhesive over the entire area where the skins touch and the actual backrests did not. Slight differences between model lamina thickness and actual lamina thickness could also have contributed to this discrepancy.
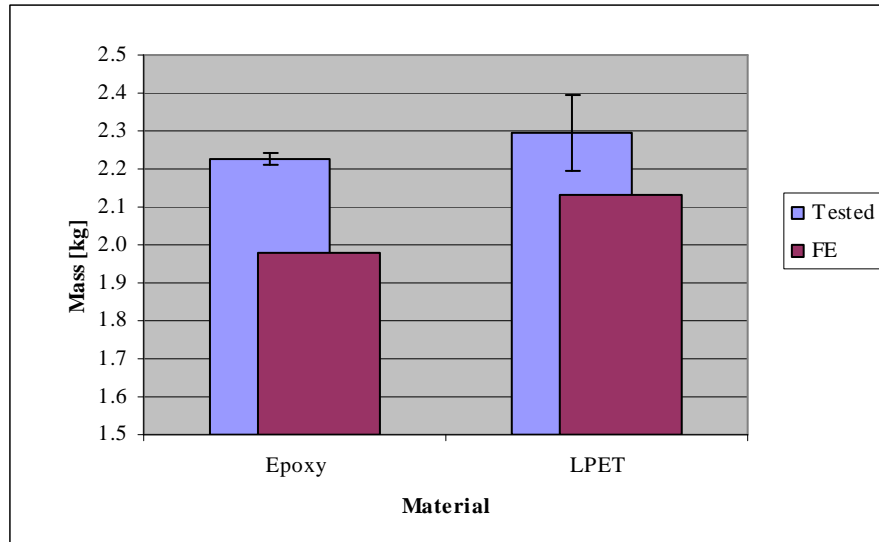
Figure 66: Average backrest masses

Specific stiffness was calculated by dividing the stiffness [N/mm] of the backrests by their mass [kg]. The average value for each material's backrests is shown in Figure 67. It can be seen that the Epoxy backrests had a specific stiffness 4.4 % higher than the LPET backrests. This is not a significant difference especially considering that LPET is not known as a high-performance matrix polymer. This indicates that LPET (and stronger thermoplastics) can compete with thermosets in applications such as these case study backrests.
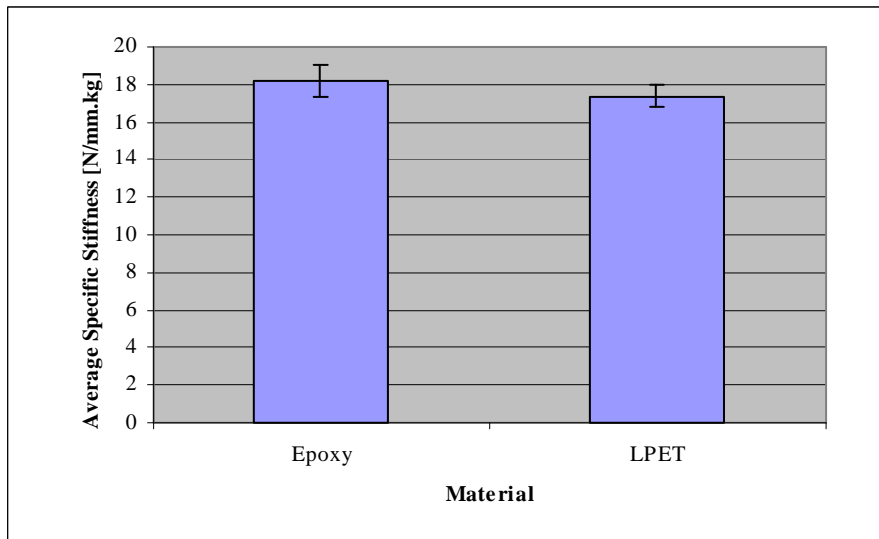
Figure 67: Average backrest specific stiffness (measured)

8.4 Conclusions

Case study CFRTP backrests were tested to compare them with Epoxy composite backrests. The tests revealed that there were significant discrepancies between the tested backrests and the FE model results (Chapter 6). The results did however show that the LPET backrest performed quite similarly to the Epoxy backrests, despite not being ideally bonded. LPET is also not even the best structural matrix material and therefore the use of CFRTP material in similar applications is quite promising.

9 BACKREST COST COMPARISON

This section provides a basic cost comparison between the LPET and Epoxy backrests. It is in no way comprehensive and is only to provide an indication of the costs of making the backrests in this project. Costs of materials were updated by information from the material suppliers during August 2009 and currency exchange rates on 25 August were used to calculate the costs.

The cost of the LPET and Epoxy backrests are listed in Table 14 and Table 15, respectively. The costs involved in the assembly of the backrests were not considered as they were exactly the same for each material's backrests.

Table 14 : LPET backrest cost summary

	Cost/unit		Amount per backrest	R/backrest	
Vac bag	0.90	£/m^2	2	R 22.80	Consumables total
Release Film	2.30	£/ m^2	2	R 58.47	R 128.84
Sealant tape	0.53	£/m	7	R 47.58	
Biax Carbon	24.10	€/ m^2	1.5	R 402.35	Material total
Glass weave	7.97	€/ m^2	1.5	R 133.06	R 535.41
Labour	100.00	R/Hour	1	R 100.00	Processing Total
Autoclave Time	150.00	R/Hour	3	R 450.00	R 550.00

Total	**R 1 214.25**

Table 15: Epoxy backrest cost summary

	Cost/unit		Amount per backrest	R/backrest	
Vac bag	0.55	€/m	2	R 12.24	Consumables total
Release Film	0.30	€/m	2	R 6.68	R 55.67
Sealant tape	5.25	R/m	7	R 36.75	
UD carbon	10.00	€/m	3	R 333.90	Material total
Glass Weave	6.50	€/m	3	R 217.04	R 550.94
Labour	100.00	R/Hour	1	R 100.00	Processing Total
Autoclave Time	150.00	R/Hour	1.5	R 225.00	R 325.00

Total	**R 931.61**

The above tables show that the LPET backrests cost more to produce than the epoxy backrests and this is due to both material costs and processing costs. The total cost of the Epoxy backrests was 23 % lower than the LPET backrests. The combined cost of the LPET raw material is actually less than that of the Epoxy material but the consumables required to process the LPET material increase the cost per backrest.

The higher processing costs of the LPET backrest were due to the longer autoclave times as mentioned in the previous chapter. This value could decrease significantly with improved manufacturing methods.

The price of the CFRTP backrests would have increased if a PPS matrix was used. PPS commingled material is roughly three times more expensive than that of LPET [Thouron, 2009] and the vacuum consumables required to process it are also more expensive. The price of glass commingled material is expected to increase by the same amount. Thus, PPS backrests would only be financially feasible if the rapid processing capability of CFRTPs is utilised. Their excellent FSTH properties could, however, overcome their price when choosing materials.

10 CONCLUSIONS

There is a definite market in the aviation industry for CFRTP seat backrests. The volume of backrests and the strict performance requirements indicate that high performance CFRTPs are suitable materials for the application. Specifically, commingled CFRTPs would be ideal as their drapability allows the manufacture of parts with complex geometry.

A literature study provided background knowledge to CFRTPs regarding processing techniques and mechanics. Different types of thermoplastic matrices used in CFRTPs were also listed and it was decided that PPS would be the ideal material for the case study aircraft backrests.

Processing experiments were performed to establish sound processing techniques of commingled CFRTPs. The experiments began by processing flat panels in a convection oven with vacuum bagging techniques. They then progressed to autoclave processing of parts with complex geometry. It was realised here that the high temperatures required to process the materials require specific processing consumables and tooling.

Flexural tests were performed to gain an understanding of CFRTPs and to quantify their mechanical properties. This testing revealed that CFRTPs have comparable strength and stiffness to the TSCs that were tested. This suggests the viability of replacing TSCs with CFRTPs in many applications. They also revealed that pre-consolidated sheets showed better and more consistent properties than material made from commingled fabric.

The impact testing revealed that the tested CFRTPs and TSCs had similar impact resistance even though thermoplastic composites are supposed to be more impact resistant. This is contrary to what the literature states and further investigation should be performed. The tests also showed that thick unreinforced thermoplastics had much higher impact resistance than the reinforced materials.

A FE model was created to design a material lay-up before the backrests were manufactured. This lay-up was then used to manufacture backrests made of commingled LPET CFRTPs and also Epoxy composites. LPET was chosen as it was more attainable than PPS CFRTPs. The successful manufacture of the backrests was followed by stiffness testing to compare the material types for the case study. The testing revealed that the stiffness and mass of the CFRTP backrests were very similar to the Epoxy backrests. This implies that commingled CFRTPs can replace the use of TSCs in similar applications.

A basic cost comparison was made between the Epoxy backrests and the CFRTP backrests. It showed that the Epoxy TSC backrests cost 23 % less than the LPET commingled CFRTP backrests. This was due to the higher cost of consumables and the longer autoclave cycles. It was concluded that commingled PPS backrests would only be viable if their processing time was reduced drastically. Although they could still cost more, PPS backrests would still be a viable option for their FSTH properties.

It is believed that the work documented here has established knowledge in the properties and application of commingled CFRTPs. Further work is needed to optimise processing time of these materials to make them more competitive with TSCs. The processing time of commingled materials will probably never be as quick as that of press formed pre-consolidated sheets. Their ability to be formed into more complex parts does however make their use advantageous.

11 RECOMMENDATIONS

The mechanical performance of CFRTPs was found to be similar to TSCs in the tests and case study of this project. However, one of the main advantages of CFRTPs – faster processing – was not realised. This is due to the long heating and cooling cycles of the oven and autoclave used in this study. Further projects should be undertaken to speed up the processing of commingled CFRTPs while retaining their ability to produce parts of complex geometry.

The vacuum bag consumables of CFRTPs are expensive and often unreliable and difficult to work with, particularly those for high temperature TPs such as PPS, PEI and PEEK. Further work should be done in the use of re-usable silicon-type vacuum bags to address these issues.

The impact testing performed in this project did not show much difference between the CFRTPs and TSCs that were tested. It is recommended that large projectile impact tests be performed to simulate head impacts during aeroplane crashes. This test is relevant to the aerospace industry and could distinguish certain materials' performance from others.

REFERENCES

1. Ahmed, T.J., Stavrov, D. and Bersee, H.E.N. 2006. An Experimental Investigation into Resistance and Induction Welding for Aerospace Structures: A Comparison. American Institute of Aeronautics and Astronautics - Structures, Structural Dynamics and Materials Conference.

2. ASTM International, 2003, Standard Test Methods for Flexural Properties of Unreinforced and Reinforced Plastics and Electrical Insulating Materials, D790 – 03.

3. ASTM International, 2005, Standard Test Method for Measuring the Damage Resistance of Fiber-Reinforced Polymer Matrix Composite to a Drop-Weight Impact Event, D 7136/D 7136M – 05[ε1].

4. Bak, H. 2007. Managing Director of Comfil ApS, via e-mail: henning.bak@comfil.biz.

5. Bigg, D.M., Hiscock, D.F., Preston, J.R. and Bradbury, E.J. 1988. High Performance Thermoplastic Matrix Composites. *Journal of Thermoplastic Composite Materials*. 1:146.

6. Bourban, P.-E., Bernet, N., Zanetto, J.-E. and Månson, J.-A.E. 2001. Material Phenomena Controlling Rapid Processing of Thermoplastic Composites. *Composites: Part A*. 32:1045-1057.

7. Cartmel, P. 1999. A Laboratory Simlulation of Low Velocity Projectile Impact on Thin Plates. Master of Science in Engineering Thesis, University of Cape Town, Cape Town.

8. Comfil ApS [2006]. Available: http://www.comfil.biz/material-properties/composite-materials/polymer-matrix-types.php. [Referenced on 25 September, 2009].

9. Cramer, D. 2004. A Novel Approach to Improving Cost-Effective Production of Advanced Composite Structures in High Volume. Presented at the 4th Annual Society of Plastics Engineers Automotive Composites Conference, USA.

10. E-Composites, Inc. 2003. Opportunities in Continuous Fibre Reinforced Thermoplastic Composites 2003-2008. Available for purchase: Helpdesk@e-composites.com (e-mail).

11. Hagstrand, P.-O., Bonjour, F. and Månson, J.-A.E. 2005. The influence of void content on the structural flexural performance of unidirectional glass fibre reinforced polypropylene composites. *Composites: Part A*. 36:705-714.

12. Hansmann, H. 2003. Composites Compendium – Thermoplastic Resins. ASM Handbook / extraction. Werkstofftechnologien / Kunststofftechnik. Hochshule Wismar.

13. Ijaz, M., Robinson, M. and Gibson, A.G. 2007. Cooling and Crystallisation Behaviour During Vacuum-Consolidation of Commingled Thermoplastic Composites. *Composites: Part A*. 38:828–842.

14. Ijaz, M., Robinson, M., Wright, P.N.H. and Gibson, A.G. 2006. Vacuum Consolidation of Commingled Thermoplastic Matrix Composites. *Journal of Composite Materials*. 41:243.

15. Kingsley-Jones, M. 2009. Available: http://www.flightglobal.com/articles/2009/06/19/328460/airbus-and-boeing-concur-on-likelihood-of-2010-recovery.html. [Last referenced 20 October 2009].

16. Lystrup, A. 2006. Vacuum Consolidation of Thermoplastic Composites for Wind Turbine Rotor Blades. *Polymer Composite Materials for Wind Power Turbines: Proceedings of the 27th Risø International Symposium on Materials Science*. Risø National Laboratory, Roskilde, Denmark. 231-238.

17. McDonnell, P., McGarvey, K.P., Rochford, L. and Ó Brádaigh, C.M. 2001. Processing and Mechanical Properties Evaluation of a Commingled Carbon-fibre/PA-12 Composite. *Composites: Part A*. 32:925-932.

18. Reuvers, P.P. 2006. Continuous Fibre Reinforced Thermoplastic. Final year mechanical project, Department of Mechanical and Mechatronic Engineering, Stellenbosch University, Stellenbosch.

19. Svensson, N., Shishoo, R. and Gilchrist, M. 1998. Manufacturing of Thermoplastic Composites from Commingled Yarns – A Review. *Journal of Thermoplastic Composite Materials*. 11:22.

20. Ten Cate Advanced Composites. 2006. Press Forming of CETEX® Continuous Fiber Reinforced Thermoplastics.

21. Terblanche, U. 2007. Development of a Manufacturing Process for Commingled Multi-Directionally Curved Continuous Fibre Reinforced Thermoplastic Composite Parts. Final year mechanical project, Department of Mechanical and Mechatronic Engineering, Stellenbosch University, Stellenbosch.

22. Thouron, O. 2009. Schappe Techniques, via e-mail: OThouron@schappe.com

23. Tufail, M. 2007. Processing Investigation and Optimization for Hybrid Thermoplastic Composites. *Journal of University of Science and Technology Beijing*. 14.2:185.

APPENDIX A: MATERIAL TESTING

A.1   Materials Tested

Table 16: Tested materials for flexural and impact tests

Manufacturer	Material	Form Description
Ten Cate	**PPS/GF** (4-ply, 8H Satin)	Pre-consolidated, as supplied
Ten Cate	**PPS/GF** (3-ply, 8H Satin)	Pre-consolidated, as supplied
Ten Cate	**PPS/GF** (2-ply, 8H Satin)	Pre-consolidated, as supplied
Ten Cate	**PPS/GF** (4-ply, 8H Satin & mesh down)	Pre-consolidated, as supplied
Ten Cate	**PPS/GF** (4-ply, 8H Satin & mesh up)	Pre-consolidated, as supplied
Ten Cate	**PPS/GF** (4-ply, 8H Satin & mesh, 0 min oxidation)	Pre-consolidated, as supplied
Ten Cate	**PPS/GF** (4-ply, 8H Satin & mesh, 5 min oxidation)	Heated in air at 320 °C for 5 minutes, reconsolidated in autoclave
Ten Cate	**PPS/GF** (4-ply, 8H Satin & mesh, 10 min oxidation)	Heated in air at 320 °C for 10 minutes, reconsolidated in autoclave
Radel	**PPSU** (1.7 mm)	As supplied
Radel	**PPSU** (2.0 mm)	As supplied
Radel	**PPSU** (2.3 mm)	As supplied
Ten Cate	**PEI/GF** (2-ply, 8H Satin, natural colour)	Pre-consolidated, as supplied
Ten Cate	**PEI/GF** (2-ply, 8H Satin, white pigment)	Pre-consolidated, as supplied
Carr Reinforcements	**PPS/CF** (4-ply, 5H Satin)	Commingled, autoclave processed
Ten Cate	**PEI/CF** (2-ply, 5H Satin)	Pre-consolidated, as supplied
Ten Cate	**PEI/CF** (2-ply, Plain)	Pre-consolidated, as supplied
EPO	**Epoxy/GF** (4-ply, Twill)	Prepreg, processed by AAT Composites
EPO	**Epoxy/CF** (4-ply, Twill)	Prepreg, processed by AAT Composites
Ten Cate	**PPS/GF** (8-ply, 8H Satin)	Pre-consolidated, as supplied
PRIMCO	**Phenolic/GF** (4-ply, Twill)	Prepreg, Processed by AAT Composites
Ten Cate	**PEI/Aramid** (2-ply, 5H Satin)	Pre-consolidated, as supplied
Hiform	**LPET/GF** (2-ply, Plain)	Commingled, autoclave processed
Comfil	**LPET/CF** (1-ply, Twill)	Commingled, autoclave processed

A.2 Complete Flexural Testing Results

Table 17: Flexural test results

			Modulus [GPa]		Strength s-d <16		Strength s-d >16		Average Modulus [GPa]	Average Strength [MPa]	Failure Mode
			0°	90°	0°	90°	0°	90°			
A	Ten Cate	PPS/GF (4-ply 8H Satin)	20.8	29.1	476.8	584.3	503.2	610.3	24.9	556.8	Tension abrupt
B	Ten Cate	PPS/GF (3-ply 8H Satin)	20.2	32.5	472.9	635.8	531.2	690.3	26.4	610.7	Tension abrupt (90°), tension slight yield (0°)
C	Ten Cate	PPS/GF (2-ply 8H Satin)	38.5	13.9	704.8	299.2	826.3	380.0	26.2	603.1	Tension abrupt (0°), tension yield (90°)
D	Ten Cate	PPS/GF (4-ply & mesh down)	17.2	24.5	443.1	533.5	472.1	558.2	20.8	515.1	Tension abrupt
D	Ten Cate	PPS/GF (4-ply & mesh up)	18.4	25.5	458.6	557.5	485.1	583.2	21.9	534.2	Tension abrupt
E	Ten Cate	PPS/GF (4-ply & mesh, 0 min oxi)	16.2	22.0	421.6	483.9	447.9	503.7	19.1	475.8	Tension abrupt
F	Ten Cate	PPS/GF (4-ply & mesh, 5 min oxi)	15.6	23.0	433.4	553.6	460.8	582.3	19.3	521.5	Tension abrupt
G	Ten Cate	PPS/GF (4-ply & mesh, 10 min oxi)	16.8	23.5	441.2	554.2	469.6	582.8	20.2	526.2	Tension abrupt
H	Radel	Radel (1.7 mm)	2.92		88.57		91.00		2.9	91.0	Yield
I	Radel	Radel (2.0 mm)	2.87		79.43		80.70		2.9	80.7	Yield
J	Radel	Radel (2.3 mm)	2.71		72.97		74.26		2.7	74.3	Yield
K	Ten Cate	PEI/GF (2-ply 8H Satin, natural)	42.31	19.05	875.45	396.14	1138.74	552.94	30.7	845.8	Tension abrupt (0°), tension yield (90°)
L	Ten Cate	PEI/GF (2-ply 8H Satin, white)	19.37	36.99	415.33	709.52	578.18	844.44	28.2	711.3	Tension abrupt (90°), tension yield (0°)
M	Carr Reinforcement	PPS/CF (4-ply 5H Satin)	30.48	24.87	589.42	621.96	617.54	671.45	27.7	644.5	Tension abrupt
N	Ten Cate	PEI/CF (2-ply 5H Satin)	28.37	71.20	644.22	1176.26	745.59	1262.10	49.8	1003.8	Tension abrupt
O	Ten Cate	PEI/CF (2-ply Plain)	37.78	42.93	717.73	705.85	883.16	818.93	40.4	851.0	Explosive tension
P	EPO	Epoxy/GF (4-ply Twill)	16.40	14.78	595.97	552.59	648.02	603.08	15.6	625.6	Tension abrupt
R	EPO	Epoxy/CF (4-ply Twill)	37.72	35.09	777.32	769.65	809.94	806.83	36.4	808.4	Mixed abrupt
V	Ten Cate	PPS/GF (8-ply 8H Satin)	22.08	19.65	498.38	467.34	499.23	468.34	20.9	483.8	Tension abrupt
W	PRIMCO	Phenolic/GF (4-ply Twill)	18.04	17.07	502.40	481.51	524.56	504.88	17.6	514.7	Tension abrupt
X	Ten Cate	PEI/Aramid (2-ply 5H Satin)	31.58	15.09	172.88	122.74	175.68	127.28	23.3	151.5	Compression yield
Y	Hiform	LPET/GF (2-ply Plain)	11.72	10.99	301.38	331.79	325.00	376.21	11.4	350.6	Tension abrupt
Z	Comfil	LPET/CF (1-ply Twill)	12.94	12.40	133.16	158.89	134.33	161.61	12.7	148.0	Yield

Table 18: Additional flexural test results

			Modulus [GPa]		Strength (s-d >16)		Modulus [GPa]	Strength (s-d >16)	Failure mode
			0°	90°	0°	90°			
AA	Ten Cate	PPS/GF (2-ply, II-dominant, symmetrical)	15.6	32.1	**0°**	**90°**	23.9	511.6	Tension yield (0°), tension abrupt (90°)
AB	Ten Cate	PPS/GF (2-ply, stacked, asymmetrical) - top surface up	26.0	21.7	310.0	713.1	23.9	671.9	Tension abrupt
AB	Ten Cate	PPS/GF (2-ply, stacked, asymmetrical) - bottom surface up	21.7	26.2	683.5	660.3	24.0	579.8	Tension abrupt (0°), tension yield (90°)
AC	Ten Cate	PPS/GF (4-ply) annealed @ 150 °C	20.7	27.6	676.8	482.8	24.1	522.0	Tension abrupt
AD	Ten Cate	PPS/GF (2-ply, I-dominant) annealed @ 150 °C	38.3	13.1	486.9	557.1	25.7	529.9	Tension abrupt (0°), tension yield (90°)
AE	Ten Cate	PPS/GF (4-ply with mesh) annealed @ 150 °C	16.9	23.1	767.6	292.2	20.0	510.4	Tension abrupt
AF	Ten Cate	PPS/GF (4-ply with mesh) annealed @ 200 °C	15.8	22.4	482.5	538.3	19.1	437.5	Tension abrupt (0°), tension yield (90°)

's-d' refers to span to depth ration of the flexural test samples

A.3 Material Process Parameters and Consumables

This appendix covers the processing parameters for the CFRTP materials used in the flexural testing.

The LPET materials were processed as described in the report AMTS-07-04-M-2: WBS S1.4.2. The PPS materials were processed in a similar manner, only with a different processing temperature and consumables. The processing cycles for the two matrices are shown in Figure 68. Although the flat panels could have been processed without external pressure it was decided to apply extra pressure to be consistent with part processing parameters.

The processing/preparation conditions for all the thermoplastic materials used in the flexural testing, and in previous experiments, are listed in Table 19 and the consumables used are listed in Table 20. The pre-consolidated PPS materials that need reconsolidation were processed under the same conditions as commingled PPS.
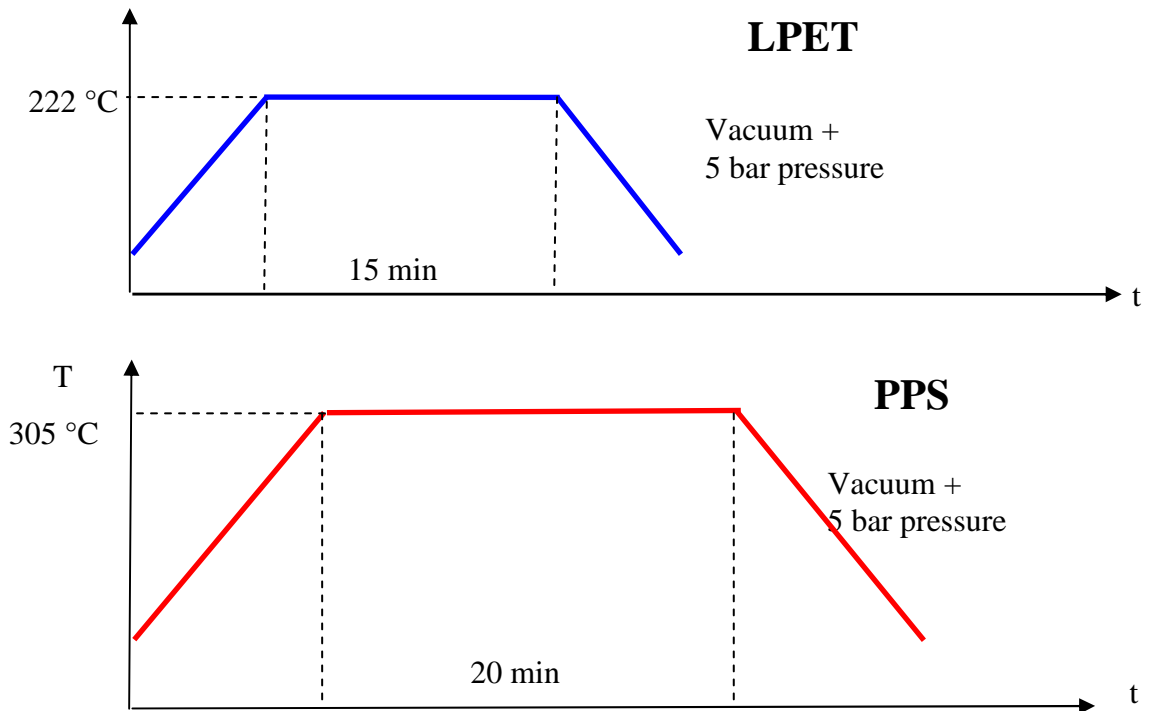
Figure 68: Processing Cycles for LPET and PPS

(Top: LPET, Bottom: PPS)

Table 19: Thermoplastic processing parameters for autoclave

Matrix Material	Temperature	Time at Temperature	Pressure
PPS	305 °C	20 minutes	5 bar
LPET	222 °C	15 minutes	5 bar

Table 20: Consumables used in autoclave of CFRTPs

Material	Item	Name (Material, Maximum. Temp.)	Supplier
LPET and PP	Vacuum Bag	Capran 526 (Nylon, 232 °C)	Aerovac Systems
	Release Film	A6000 (Fluoropolymer ETFE, 260 °C)	Aerovac Systems
	Sealant Tape	SM5126	Aerovac Systems
	Bleeder	Woven Fibre Glass	Various
PPS	Vacuum Bag	VB-3 (PTFE, 315 °C)	Aerovac Systems
	Release Film	MR FILM (PTFE, 315 °C)	Aerovac Systems
	Sealant Tape	SM5160 (371 °C)	Aerovac Systems
	Bleeder	Woven Fibre Glass	Various

A.4 Thermo-Gravimetric Analysis (TGA)

Thermogravimetric Analysis (TGA) is a type of testing that is performed on samples to determine changes in weight in relation to change in temperature. In our case, the TGA is used to determine the fibre weight content of 5 composites by burning off the matrix (see Table 21). Rectangular samples of 2 mm × 2 mm (5-10 mg) were cut from the composite sheets, in such way that the thickness of the samples equalled the thickness of the composite. This way, one can make sure that the measured fibre content is representative of the entire composite, which will also prove to be useful for subsequent DSC analysis (see the next chapter). The instrument used is a Perkin Elmer Pyris TGA 7 as shown in Figure 69. After placing the samples in the micro-balance, the oven was raised and the temperature was increased from 45 °C to 920 °C at 20 °C/min in either a nitrogen or an oxygen atmosphere.
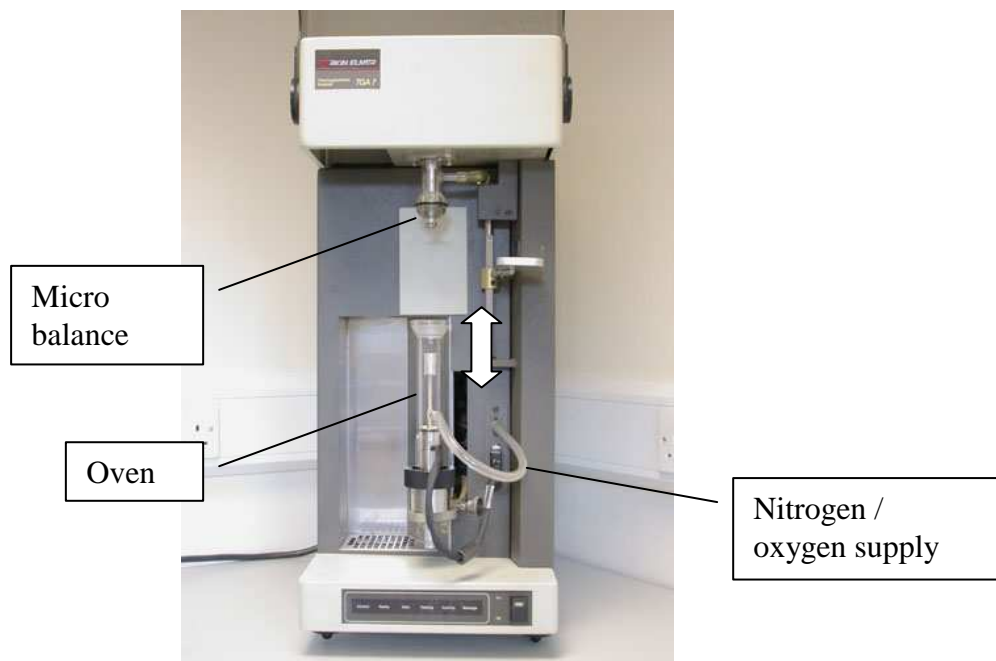
Figure 69: Perkin Elmer Pyris TGA 7

Table 21: Overview of TGA samples

Material	Manufacturer	Fibre content[*] [wt%]
PPS/GF (8H Satin weave, 4-ply)	Ten Cate	63
PPS/GF (8H Satin weave, 4-ply with Bronze mesh)	Ten Cate	-
PPS/CF (Satin weave, 4-ply)	Carr Reinforcement	-
LPET/GF (Plain, 2-ply)	Hiform	60
LPET/CF (Twill, 1-ply)	Comfil	54

[*] Data sheet values

A.4.1   PPS composites

Figure 70 shows the weight loss curves for the three PPS composites, burned off in either a nitrogen or an oxygen environment. It can be seen that PPS starts degrading at approximately 425 °C. For the glass fibre based composites, the fibre contents measured in nitrogen are 12 % higher than when tested in oxygen. The reason for this is that at elevated temperatures cross-linking of the aromatic PPS yields a substance that is hard to burn off in nitrogen atmosphere. The presence of oxygen, however, allows degradation to continue and consequently, in the case of PPS, yields a more accurate (in closer agreement with the datasheet values) value for the fibre content. For the same reason it can be expected that an overestimation of the fibre content is obtained in nitrogen environment for the carbon

based composite. In this case, however, measuring in oxygen does not provide a solution. In oxygen, the carbon fibres degrade at elevated temperatures, hence leaving only 3 % of the original sample mass behind at the end of the analysis. The TGA is not suitable to determine the fibre content of carbon fibre based composites. For the glass-based composites, we can see that approximately 50 % extra PPS is burned off in oxygen. Using this value, we can estimate that the fibre mass content of the carbon-based composites is approximately 50 %.
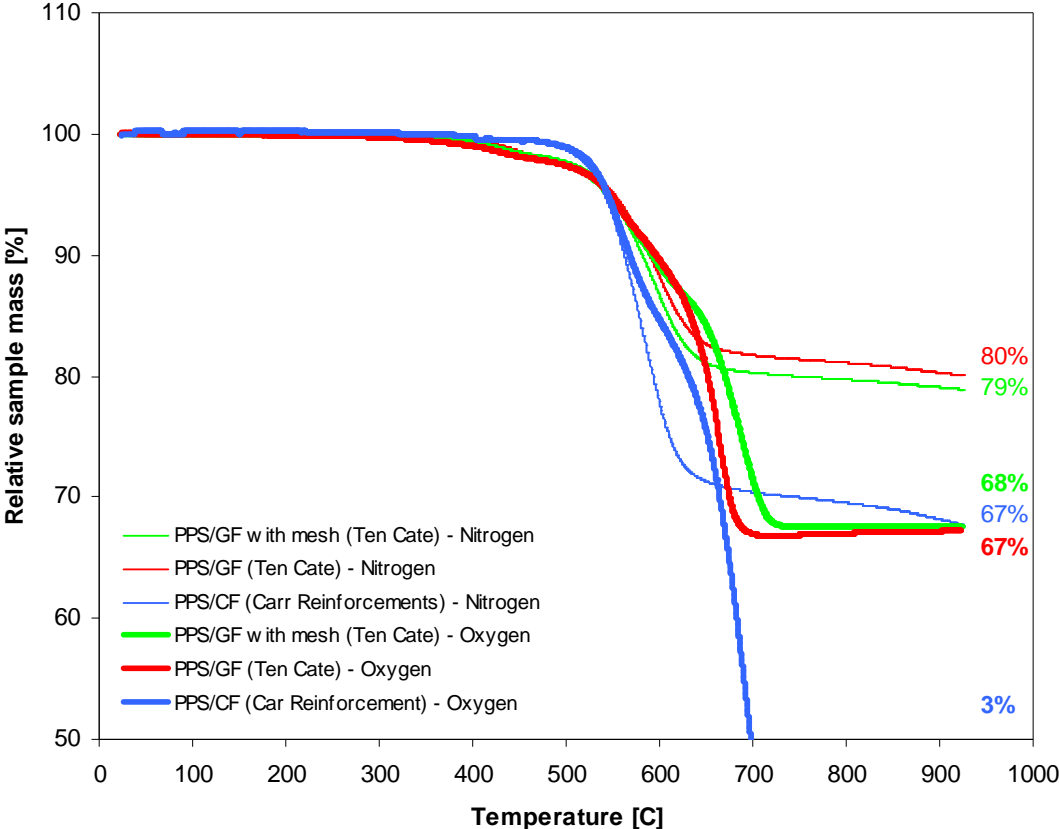
Figure 70: TGA curves of PPS composites analyzed in nitrogen or oxygen

A.4.2 LPET composites

Figure 71 shows the weight loss curves for the two LPET composites, burned off in either nitrogen or oxygen environment. It can be seen that LPET starts degrading at approximately 350 °C. For the glass fibre based composites, the fibre contents measured in nitrogen are 5 % higher than when tested in oxygen. It appears that just as in the case of PPS an oxygen free environment is required to achieve full degradation of the material. The quoted datasheet value is in between both measured values. The carbon composite fully degrades in oxygen environment. From the glass based composites, one can determine that 6 % extra matrix is burned off in an oxygen environment. With this value it is estimated that the fibre content of the carbon composite is approximately 57 wt %.
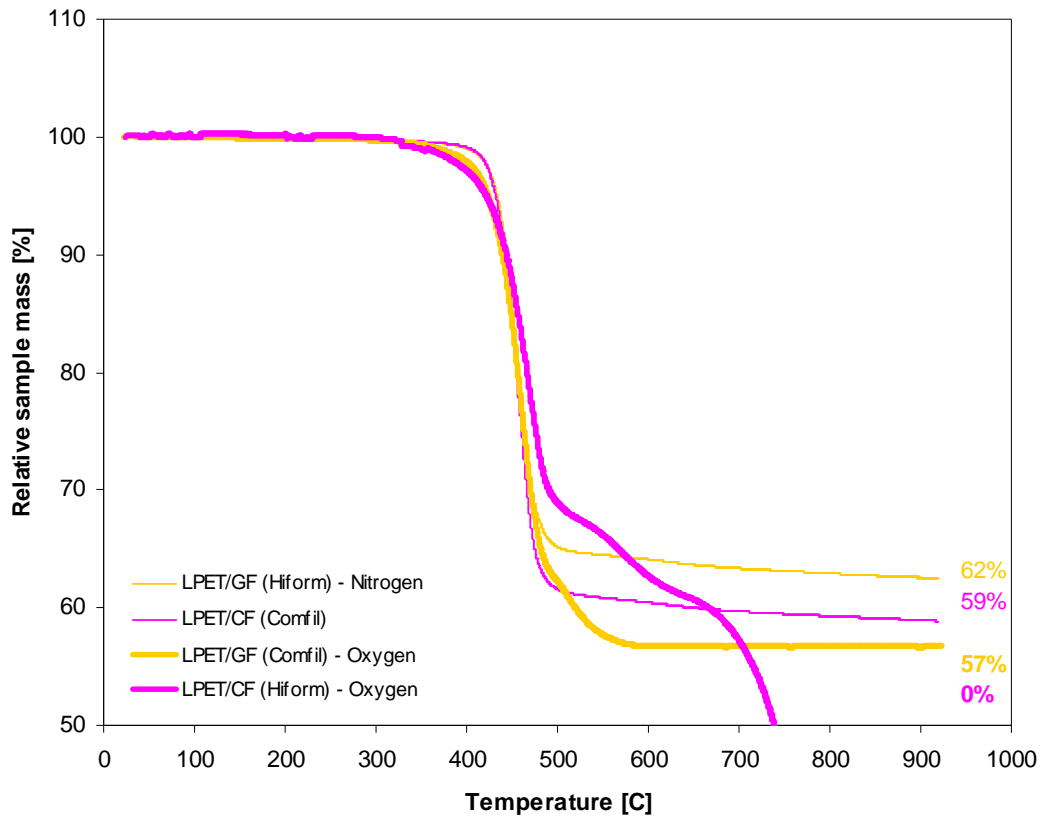
Figure 71: TGA curves of LPET composites analyzed in nitrogen or oxygen

A.4.3   Final results

The measured fibre weight contents (W_f) are summarised in Table 22 and the fibre volume contents (V_f) have been calculated using equation 10 and the densities presented in the same table.

$$V_f = \frac{W_f / \rho_f}{W_f / \rho_f + W_m / \rho_m} \cdot 100\%$$

(10)

Table 22: Composite composition by weight and by volume

Material	W_f [wt%]	W_m	ρ_f^* [kg/m^3]	ρ_m^*	V_f [v%]	V_m
PPS/GF (8H Satin weave, 4-ply)	68	32	2100	1350	58	42
PPS/GF (8H Satin weave, 4-ply with Bronze mesh)	68[**]	32	2100[***]	1350	58	42
PPS/CF (Satin weave, 4-ply)	50[+]	50[+]	1760	1350	43[+]	57[+]
LPET/GF (Plain, 2-ply)	62	38	2100	1100	46	54
LPET/CF (Twill, 1-ply)	57[+]	43[+]	1760	1100	45[+]	55[+]

[*] Source: www.matweb.com
[**] The combined content of fibres and mesh
[***] The effect of the mesh on the average density of the solid content (fibres and mesh) has been neglected.
[+] Estimated values

A.5 Differential Scanning Calorimetry (DSC)

DSC is a method for measuring the amount of energy that is required for a phase transition in a material. In this case, focus was placed on melting of the semi-crystalline polymer PPS in order to determine the degree of crystallinity (X_c) and the melting point (T_m). In short, DSC of composites works as follows: Rectangular samples of 4 mm $\times$ 4 mm (20-25 mg) were cut from the composite sheets, in such way that the thickness of the samples equals the thickness of the composite. This way, one makes sure that the fibre content of the sample is representative for the entire composite, and that the fibre content, as previously determined by TGA is representative for our DSC samples. The sample is sealed in a sample cup and placed in one of two ovens of the DSC (DSC Q100 v9, TA Instruments) as seen in Figure 72. An empty cup is placed in the remaining oven. In the case of PPS composites, both ovens are simultaneously heated from 25 °C to 350 °C at 10 °C/min.

Figure 72: The DSC apparatus and the sealing of a composite sample

(left to right)

The energy input to both ovens is initially the same; however, as our sample starts to melt, the sample-containing oven requires more energy to maintain the required heating rate than the empty oven. The difference in heat flow is recorded and when plotted against the temperature, a graph as shown in Figure 73 is obtained in which the 'valley' corresponds to melting of our polymer. The bottom of the valley corresponds to the polymer melting point, which is 281.93 °C in the case of PPS. The total energy that was used to melt the entire sample is found by integrating the surface inside the valley; divided by the mass of the sample gives us the melting enthalpy (ΔH) in J/g (In this case 23.57 J/g). From this value the degree of crystallinity is calculated according to equation 11.

$$X_c = \frac{\Delta H \cdot m_{sample} \cdot \left(1 - \frac{W_f}{100}\right)}{\Delta H_{100}} \cdot 100\% \tag{11}$$

Where;

m_{sample}	=	mass of the composite sample inserted in the DSC [g]
W_f	=	fibre weight content as determined by TGA [%]
ΔH_{100}	=	theoretical melting enthalpy of 100 % crystalline PPS [J/g]

As equation 11 shows, the measured enthalpy [J/g] of composite is first multiplied by terms containing the sample mass and the fibre content in order to get the enthalpy in [J/g] of polymer. Next, the enthalpy is divided by the theoretical melting enthalpy of 100 % crystalline PPS, which can be found in literature. For their PPS, Ten Cate gives a ΔH_{100} of 150.4 J/g.
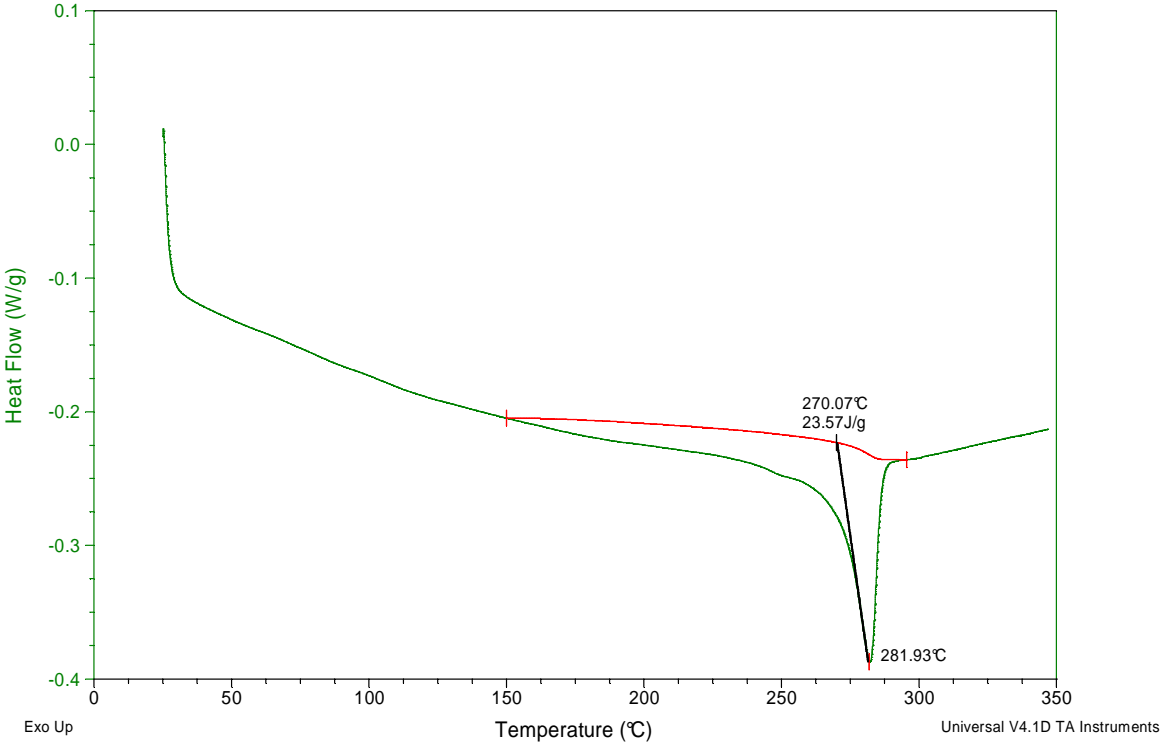
Figure 73: DSC curve for glass fibre reinforced PPS.

The degree of crystallinity and melting point of 6 PPS composites was determined and the results are shown in Table 23. The melting points of all samples range between 281 °C and 283 °C, which is in good agreement with the quoted datasheet values (280 °C). The degree of crystallinity for the PPS composites ranges between 46 % and 54 %. No clear effect of annealing could be found. However as these are preliminary results only, with only a single measurement per material type, it is hard to draw any conclusions. Future research could undertake a thorough analysis of the phenomena that affect the degree of crystallinity, as this is outside the scope of this project.

Table 23: Melting points and degree of crystallinity of various composites determined by DSC

Material	M_{sample} [mg]	T_m [°C]	W_f [%]	ΔH [J/g]	X_c [%]
PPS/GF (4-ply with mesh)					
- as purchased	26.4	282	68	23.6	49
- reconsolidated in autoclave	21.9	283	68	22.2	46
- annealed at 150 °C	25.5	281	68	23.6	49
PPS/GF (4-ply)					
- as purchased	20.6	283	68	25.8	54
- annealed at 150 °C	18	283	68	24.1	50
PPS/CF (4-ply)	20.4	282	50	36.5	49

A.6   Additional Materials Tested in Impact Testing

Table 24 : Additional materials for impact testing

Manufacturer	Material	Form Description
Ten Cate	**PPS/GF** (4-ply, 8H Satin)	Annealed at 150 °C
Ten Cate	**PPS/GF** (4-ply, 8H Satin & mesh down)	Annealed at 150 °C
Ten Cate	**PPS/GF** (2-ply, 8H Satin)	Annealed at 150 °C
Ten Cate	**PPS/GF** (2-ply, 8H Satin, stacked)	Pre-consolidated, as supplied
Ten Cate	**PPS/GF** (2-ply, 8H Satin, II-dominant)	Pre-consolidated, as supplied
Ten Cate	**PPS/GF** (4-ply, 8H Satin & mesh down)	Annealed at 200 °C

A.7 Complete Impact Testing Results

Table 25: Impact test results

			Fmax	E at Fmax	Damage Area	Shape Factor	Dent Depth	Impact Gradient	Failure Energy per Thickness	Ply Thickness
			[N]	[J]	[mm²]		[mm]	[N/mm]	[J/mm]	[mm]
A	Ten Cate	PPS/GF (4-ply, 8H Satin)	107.30	0.373	317.93	0.91	2.10	22.641	0.392	0.950
B	Ten Cate	PPS/GF (3-ply, 8H Satin)	76.38	0.168	457.36	1.05	2.68	-9.740	0.240	0.700
C	Ten Cate	PPS/GF (2-ply), I-dominant	50.20	0.090	420.41	1.17		-25.738	0.188	0.480
D-Up	Ten Cate	PPS/GF (4-ply & mesh up)	95.00	0.228	230.52	0.78	2.00	-19.724	0.230	0.990
D-Down	Ten Cate	PPS/GF (4-ply & mesh down)	101.20	0.226	353.46	0.85	1.73	-12.244	0.229	0.990
E	Ten Cate	PPS/GF (4-ply & mesh, 0 min oxi)	101.55	0.249	512.70	0.92	2.15	-14.110	0.244	1.020
F	Ten Cate	PPS/GF (4-ply & mesh, 5 min oxi)	105.30	0.269	481.45	1.01	2.30	4.218	0.264	1.020
G	Ten Cate	PPS/GF (4-ply & mesh, 10 min oxi)	111.13	0.291	330.03	1.05	1.93	10.720	0.291	1.000
H	Radel	Radel (1.7 mm)	174.50	1.374			3.20	10.552	0.808	1.700
I	Radel	Radel (2.0 mm)	234.40	1.640			2.50	18.251	0.820	2.000
J	Radel	Radel (2.3 mm)	313.70	2.253			2.30	18.785	0.980	2.300
K	Ten Cate	PEI/GF (2-ply, natural)	39.65	0.075	716.65	1.42		-15.925	0.162	0.460
L	Ten Cate	PEI/GF (2-ply, white)	34.00	0.109	730.78	1.58		-3.618	0.237	0.460
M	Carr Reinforcements	PPS/CF (4-ply, 5H Satin)	53.70	0.154	451.27	1.16		-11.887	0.171	0.900
N	Ten Cate	PEI/CF (2-ply 5H Satin)	42.43	0.128	491.31	0.95		-1.069	0.200	0.640
O	Ten Cate	PEI/CF (2-ply Plain)	29.33	0.144	362.94	1.07		2.103	0.312	0.460
P	EPO	Epoxy/GF (4-ply Twill)	155.60	0.393	204.02	1.07	1.00	-23.867	0.317	1.240
R	EPO	Epoxy/CF (4-ply Twill)	112.20	0.227	338.62	0.95		-37.269	0.212	1.070
S	Ten Cate	PEI/Aramid (2-ply, 5H Satin)	39.43	0.105	328.33	1.04		-11.644	0.219	0.480
T	Hiform	LPET/GF (2-ply Plain)	100.83	0.264	420.01	1.09		9.294	0.294	0.900
U	Comfil	LPET/CF (1-ply Twill)	74.28	0.202	171.99	1.15		4.665	0.238	0.850

			Fmax [N]	E at Fmax [J]	Damage Area [mm²]	Shape Factor	Dent Depth [mm]	Impact Gradient [N/mm]	Failure Energy per Thickness [J/mm]	Ply Thickness [mm)
W	PRIMCO	Phenolic/GF (4-ply Twill)	101.20	0.223	273.32	1.02		-18.975	0.181	1.230
X	Ten Cate	PPS/GF (4-ply), annealed @ 150 ℃	94.83	0.250	440.12	1.03	1.77	2.420	0.263	0.950
Y	Ten Cate	PPS/GF (4-ply & mesh), annealed @ 150 ℃	100.75	0.285	418.20	0.99	2.10	20.270	0.279	1.020
Z	Ten Cate	PPS/GF (2-ply), annealed @ 150 ℃	57.47	0.130	369.90	1.20		3.528	0.272	0.480
AA	Ten Cate	PPS/GF (2-ply), stacked	54.10	0.106	542.72	0.96		-11.724	0.222	0.480
AB	Ten Cate	PPS/GF (2-ply), II-dominant	51.80	0.097	451.97	0.94		-7.597	0.203	0.480
AC	Ten Cate	PPS/GF (4-ply & mesh), annealed @ 200 ℃	101.90	0.246	461.96	0.97	2.75	-13.539	0.241	1.020

A.8   Impact Sample Pictures

The pictures below (grouped together under Figure 74) are shown in the order as presented in the results tables in Appendix A.7.

A   B

C   D-Up

D-Down   E

F   G
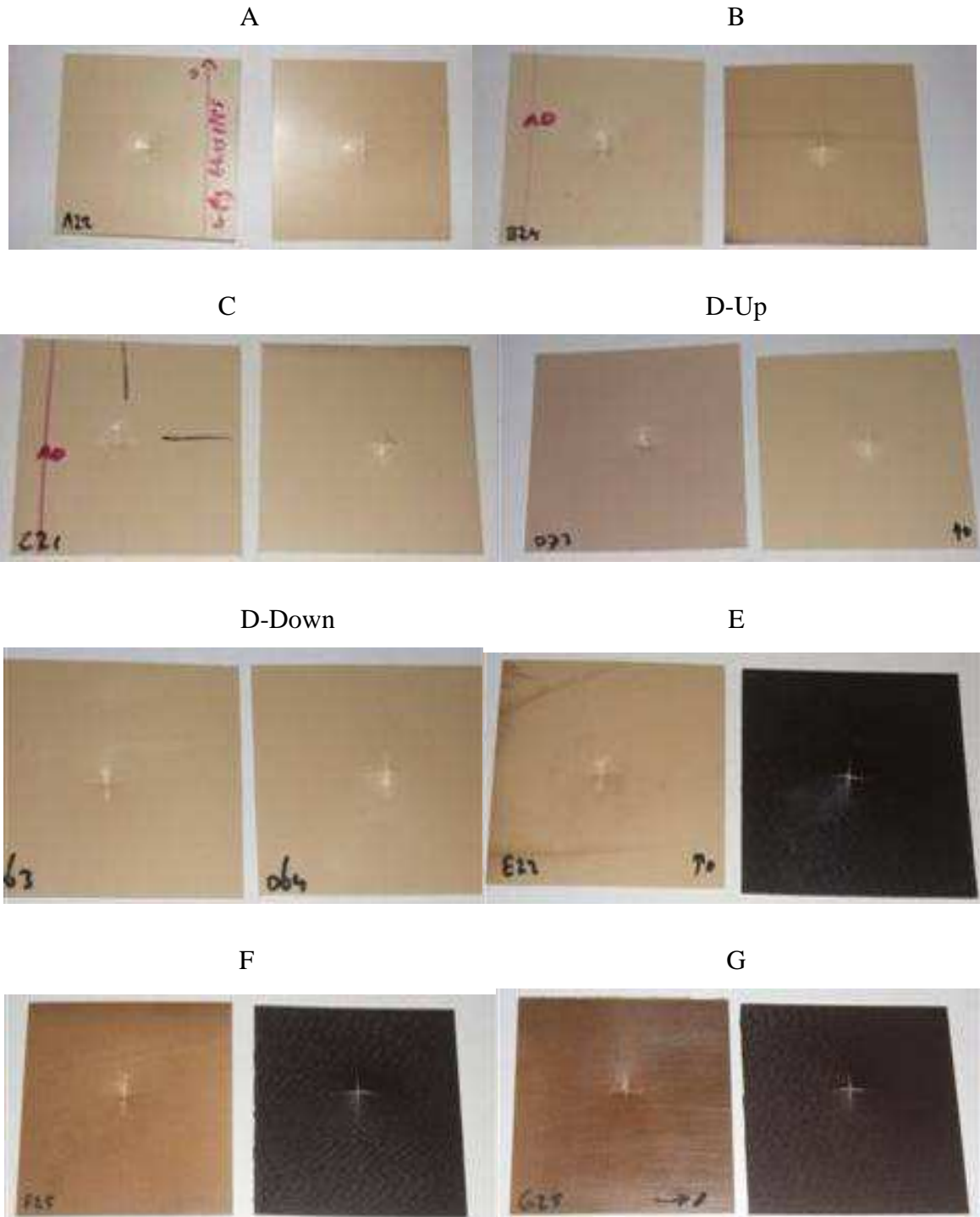
H
I

J
K

L
M

N
O

P   R

S   T

U   W

X   Y

Z   AA

AB   AC
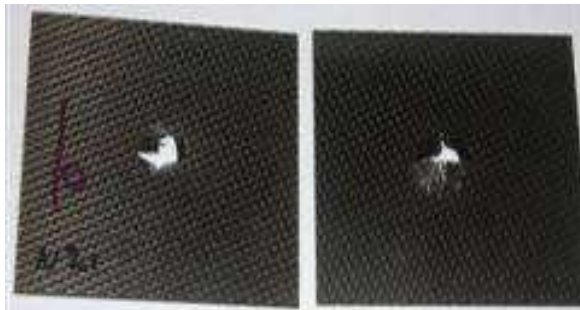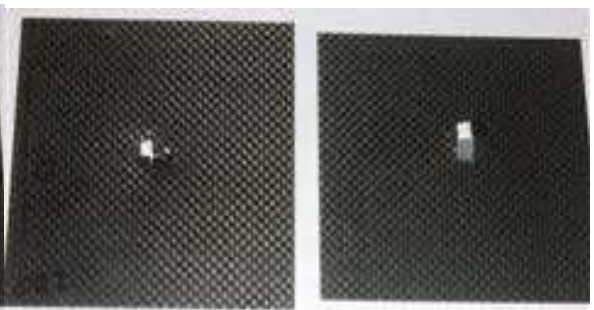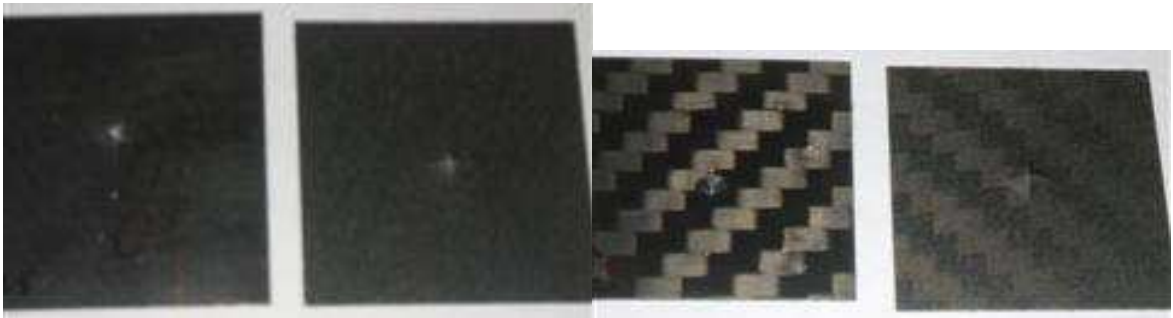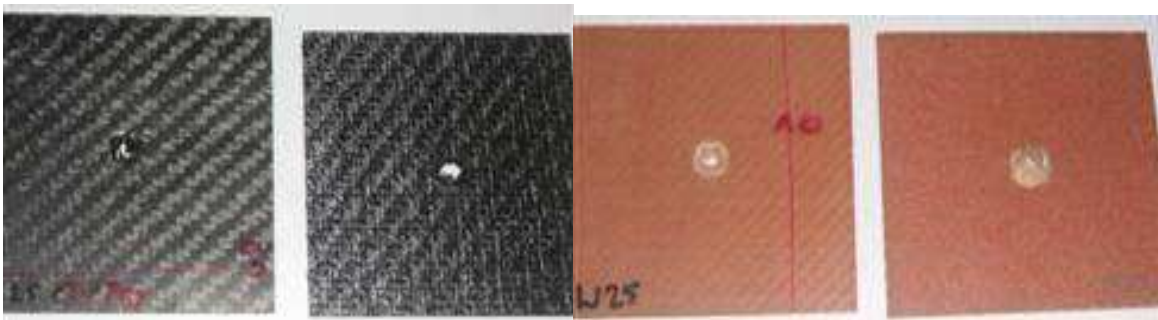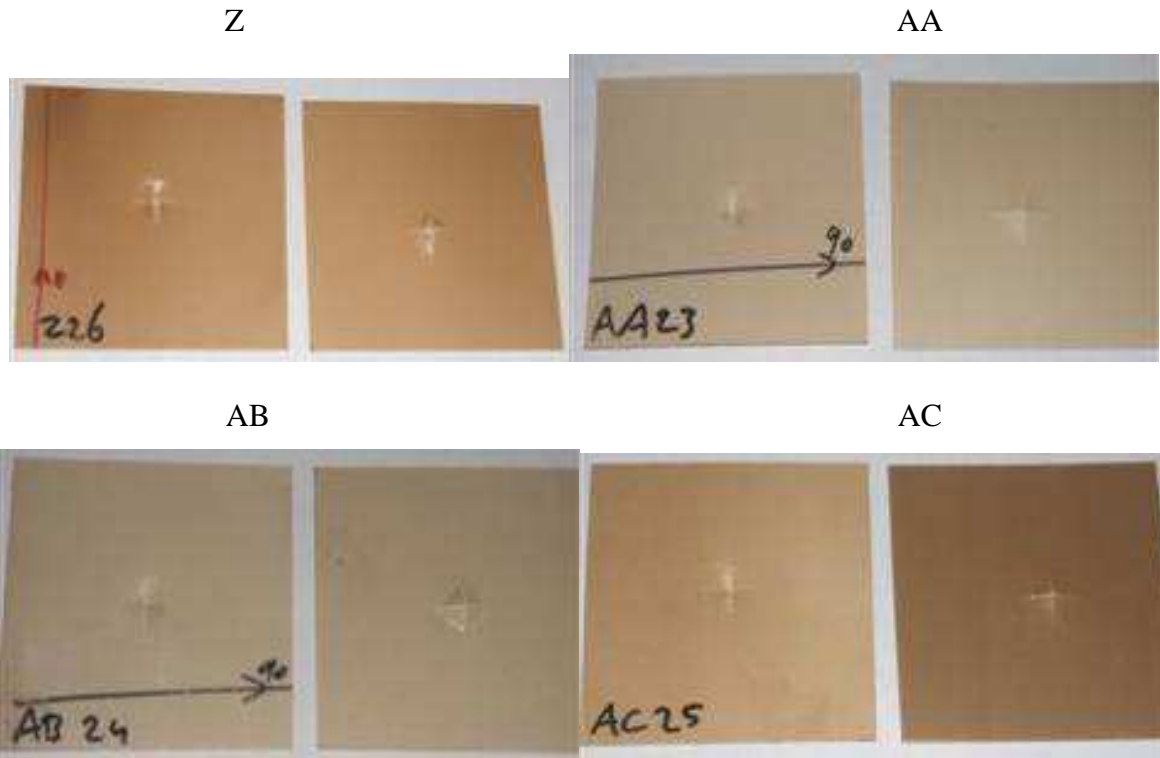
Figure 74: Test samples after impact testing

(Figure spread over four pages)

APPENDIX B: FE MODEL RESULTS

B.1   Loads and Boundary Conditions
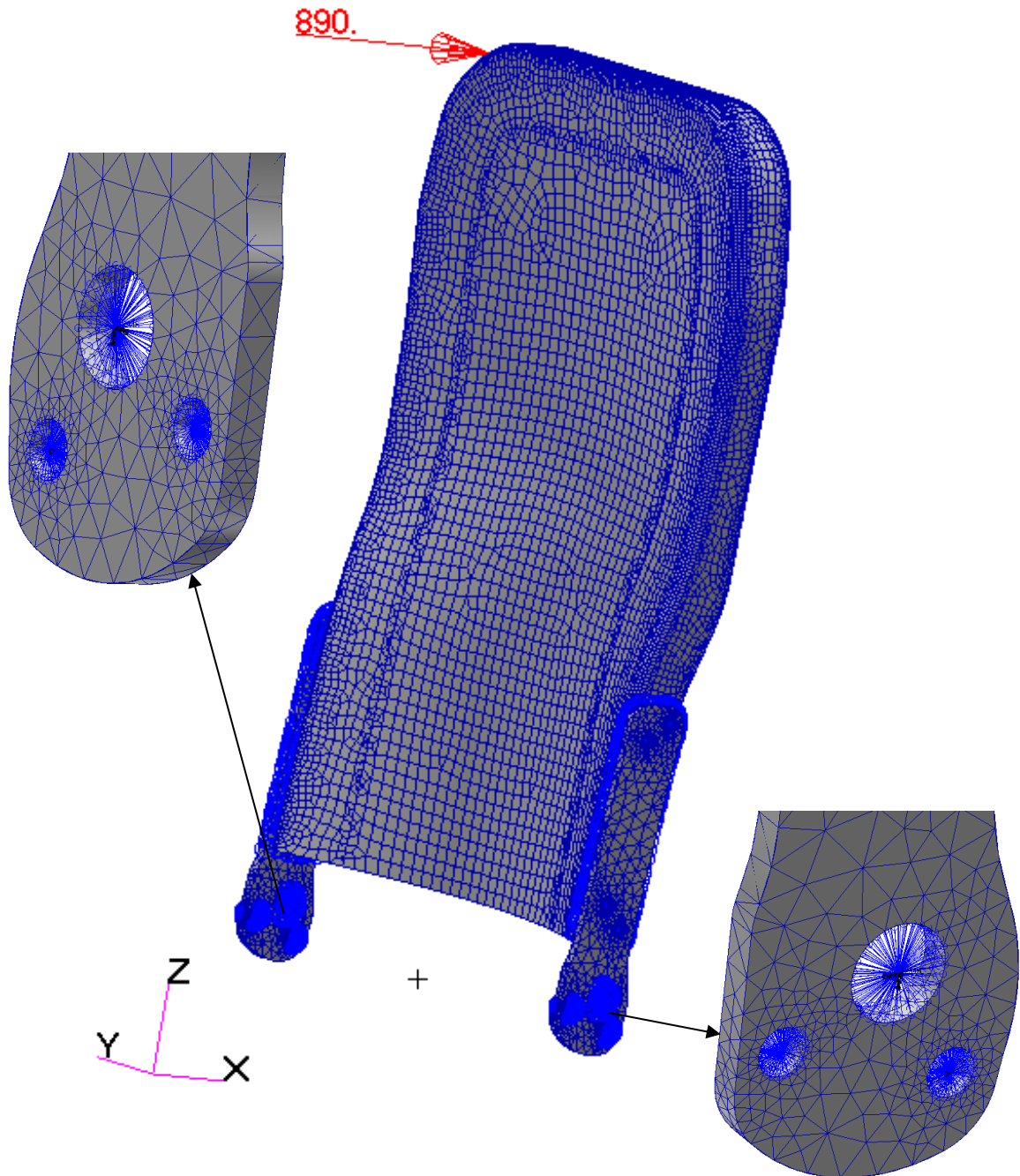
Figure 75: FE model loads and boundary conditions

B.2   Displacement Plots
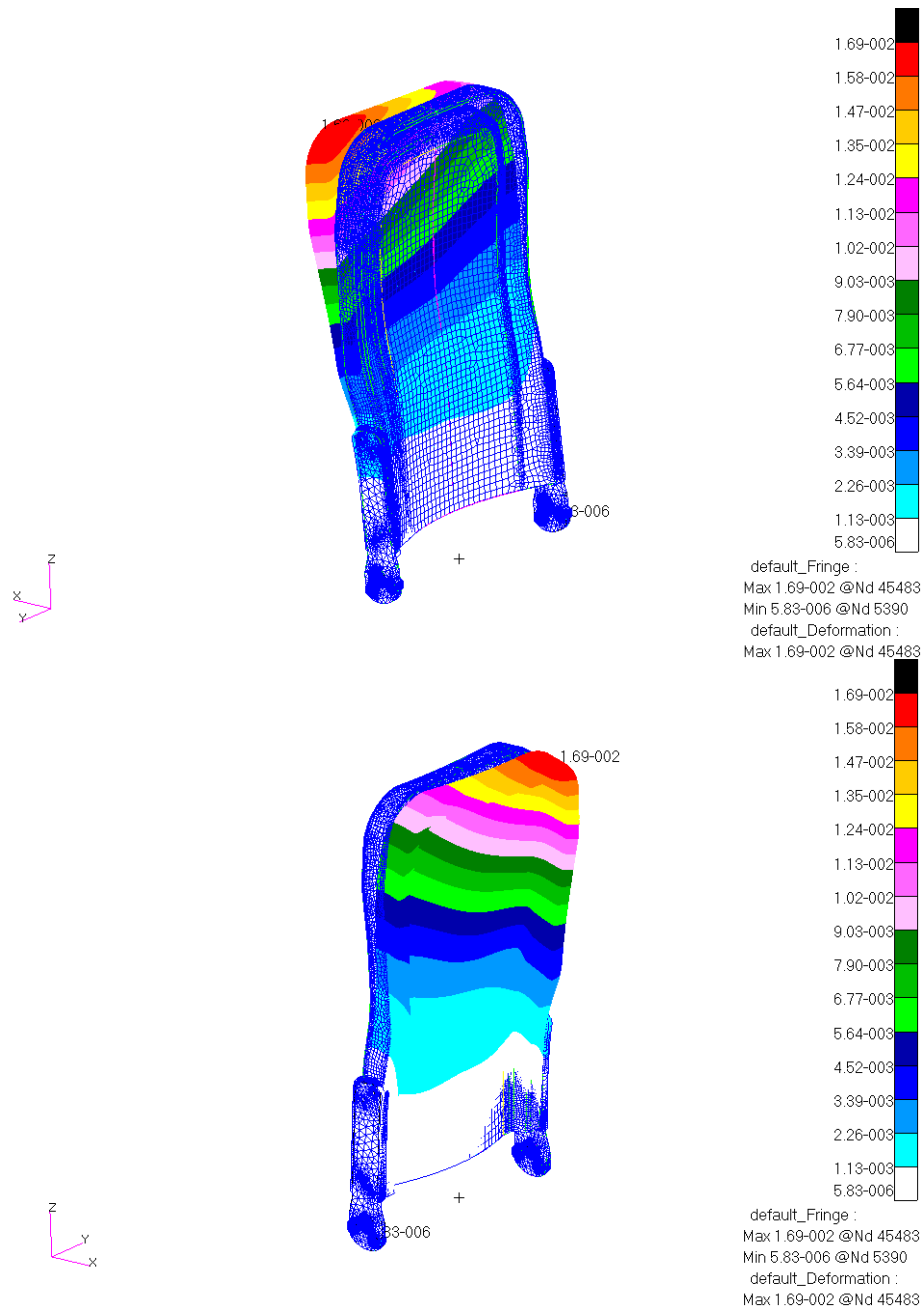
Figure 76: Displacement plot

Figure 76 shows the front view (top) and back view (bottom) of the displaced backrest under load. The displacement (in meters) is magnified five times for clarity. As shown the in the figure the maximum displacement for the LPET backrest is 16.9 mm at the corner where the load is applied.

B.3   Maximum Lamina Stresses

Spectra scale in Pa [N/m^2]

B.3.1   LPET Model

Figure 77: Maximum longitudinal lamina stress in LPET model

Figure 78: Maximum transverse lamina stress in LPET model

Figure 79: Maximum in-plane lamina shear stress in LPET model

B.3.2 Epoxy Model
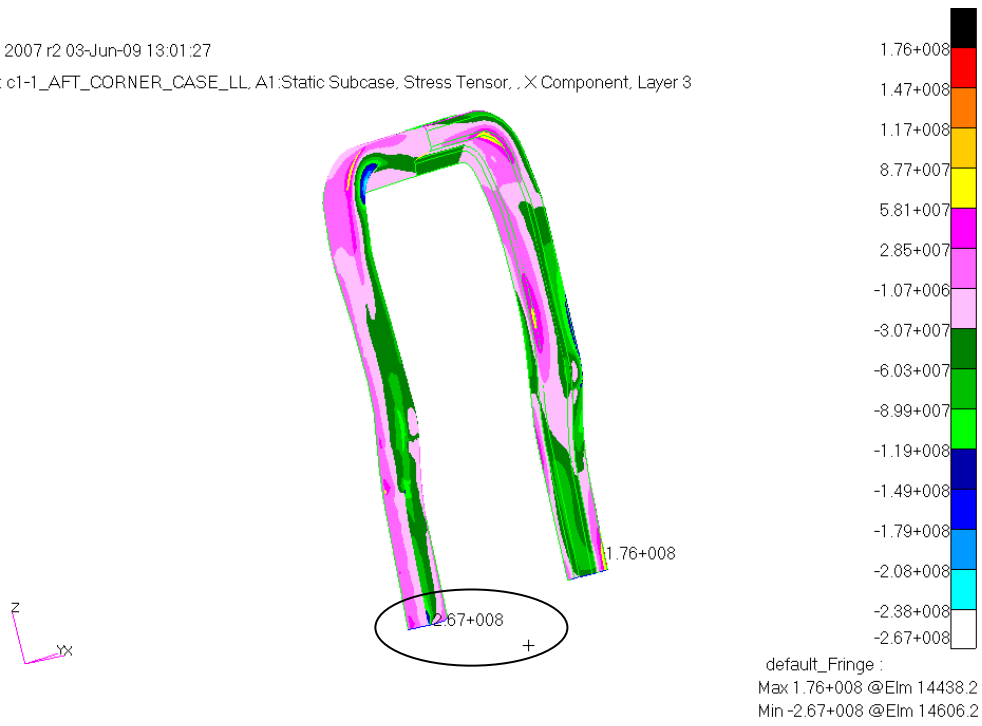
Figure 80: Maximum longitudinal lamina stress in Epoxy model

Figure 81: Maximum transverse lamina stress in Epoxy model

1.69+007
1.41+007
1.13+007
8.47+006
5.67+006
2.87+006
7.43+004
-2.73+006
-5.53+006
-8.33+006
-1.11+007
-1.39+007
-1.67+007
-1.95+007
-2.23+007
-2.51+007

-2.51+007
007

default_Fringe :
Max 1.69+007 @Elm 20187.3
Min -2.51+007 @Elm 23856.1

Figure 82: Maximum in-plane lamina shear stress in Epoxy model

B.4 Tables of Lamina Stresses

Lamina numbering of FE model was used.

Highlighted cells indicate the maximum stress in each direction for each lamina.

Table 26: Table of maximum and minimum lamina stresses – LPET model.

Backrest - Stress Values [MPa]

Material - Commingled LPET
- Carbon Biax [1] (modelled as 2 UD layers)
- Glass Twill [2]
- Carbon UD [3]
- Epoxy Glue [4]
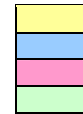
Load Case - Limit Load (890 N at top corner)
(layer number refers to Patran number)   (excluding middle section)

Tubular Section

Layer	1	2	3	4	5	6	7	8	9	10	11	12	13	14	15	16
Material	3	3	1	1	2	2	1	1	4	3	3	1	1	2	1	1
σ_{L+}	6.04	3.96	177	158	25.2	25.7	200	176	5.77	164	162	123	253	43.2	195	190
σ_{L-}	192	184	255	172	45.7	43.6	187	168	7.4	180	176	161	172	34.6	197	161
σ_{T+}	13.3	9.33	12.8	7.94	24.7	29.4	10.3	15.5	3.27	35.9	24.8	19.1	9.73	25.7	10.7	16.3
σ_{T-}	9.04	5.5	17	15.4	23.7	18	10.4	14.4	3.24	10.5	6.98	8.87	9.58	25.6	9.19	11.6
τ_{LT+}	8.11	6.85	34	19.8	5.13	5.55	18.9	39.2	1.4	7.98	8.35	28.1	35.8	6.76	30.7	29.5
τ_{LT-}	4.76	4.47	24.5	32.9	5.67	7.28	36.9	20.4	1.35	11.9	9.87	38.8	28.3	6.52	29.2	31.5
τ_{Lz}									5.63							
τ_{Tz}									6.5							

Inside Section

Layer	1	2	3	4	5	6	7	8	9	10	11	12
Material	1	1	2	1	1	4	1	1	2	2	1	1
σ_{L+}	84.2	66.7	18.8	53.3	63.8	3.21	49.2	25.6	11.1	9.48	19	44.2
σ_{L-}	22.5	10	1.48	8.39	13.1	0.605	11.8	21.1	4.83	5.73	43.1	30.7
σ_{T+}	4.91	5.42	2.11	4.46	3.04	0.392	1.87	2.98	2.83	3.14	2.54	1.21
σ_{T-}	0.689	1.09	6.85	0.8	0.505	0.807	1.13	1.03	8.54	8.94	1.95	3.14
τ_{LT+}	1.38	12.7	0.909	11.8	1.8	0.302	2.59	9.76	1.38	1.59	8.21	3.84
τ_{LT-}	13	1.42	1.29	1.64	11.5	0.311	10.1	2.76	0.446	0.385	3.66	7.9
τ_{Lz}						1.01						
τ_{Tz}						0.817						

Table 27: Table of maximum and minimum lamina stress – Epoxy model

Backrest - Stress Values [MPa]

Material - Epoxy Prepreg   - Carbon UD [1]   ▨ (yellow)
   - Glass Twill [2]   ▨ (blue)
   - Epoxy Glue [4]   ▨ (green)

Load Case - Limit Load (890 N at top corner)
(layer number refers to Patran number)   (excluding middle section)

Tubular Section

Layer	1	2	3	4	5	6	7	8	9	10	11	12	13	14	15	16
Material	1	1	1	1	2	2	1	1	4	1	1	1	1	2	1	1
σ_{L+}	7.91	3.91	176	143	31.9	32.5	186	145	3.89	156	153	124	226	53.5	175	185
σ_{L-}	185	179	267	148	53.8	51	201	151	4.56	165	161	149	148	40.3	168	161
σ_{T+}	15.4	11.6	14.1	10.7	26.7	33.2	11.4	16.6	2.66	42.2	30.7	21.5	10.4	30	11.6	18.3
σ_{T-}	9.65	6.46	17.9	19.1	37.6	22.9	12	17.8	2.53	13.7	8.48	9.92	11.4	30.1	10.9	12.6
τ_{LT+}	7.34	6.38	20.7	15.9	4.83	5.24	13.1	24	1.12	7.48	7.94	16.9	23.1	6.24	19.9	18.3
τ_{LT-}	4.25	3.82	19.1	20	4.34	5.77	22.6	17	1.08	9.93	8.31	25.1	17.1	4.89	18	20.9
τ_{Lz}									4.52							
τ_{Tz}									5.54							

Inside Section

Layer	1	2	3	4	5	6	7	8	9	10	11	12
Material	1	1	2	1	1	4	1	1	2	2	1	1
σ_{L+}	71	60.2	22.8	47.3	54.2	2.11	44.6	28	13.8	11.3	19	41.5
σ_{L-}	20.7	8.92	1.9	7.51	11.9	0.387	9.66	17.1	6.04	7.55	38.3	26
σ_{T+}	5.46	5.96	2.84	4.81	3.49	0.282	2.53	3.38	3.25	3.74	2.88	1.56
σ_{T-}	0.821	1.26	6.99	0.903	0.588	0.366	1.13	1.01	9.48	10.4	2.23	3.51
τ_{LT+}	0.876	7.78	0.652	7.12	1.15	0.233	1.52	6.09	1.11	1.27	4.97	2.47
τ_{LT-}	7.96	0.904	0.998	1.05	6.93	0.177	6.28	1.62	0.397	0.34	2.33	4.79
τ_{Lz}						0.86						
τ_{Tz}						0.745						

B.5   Von Mises Stress Results in Pivots

Spectrum scale in Pascal [Pa or N/m^2]

Patran 2007 r2 03-Jun-09 13:09:45

Fringe: c1-1_AFT_CORNER_CASE_LL, A1:Static Subcase, Stress Tensor, , von Mises, (NON-LAYERED)

4.60+008
4.29+008
3.98+008
3.68+008
3.37+008
3.07+008
2.76+008
2.46+008
2.15+008
1.85+008
1.54+008
1.24+008
9.31+007
6.25+007
3.20+007
1.46+006

default_Fringe :
Max 4.60+008 @Elm 6886.10
Min 1.46+006 @Elm 825.6

Right Pivot
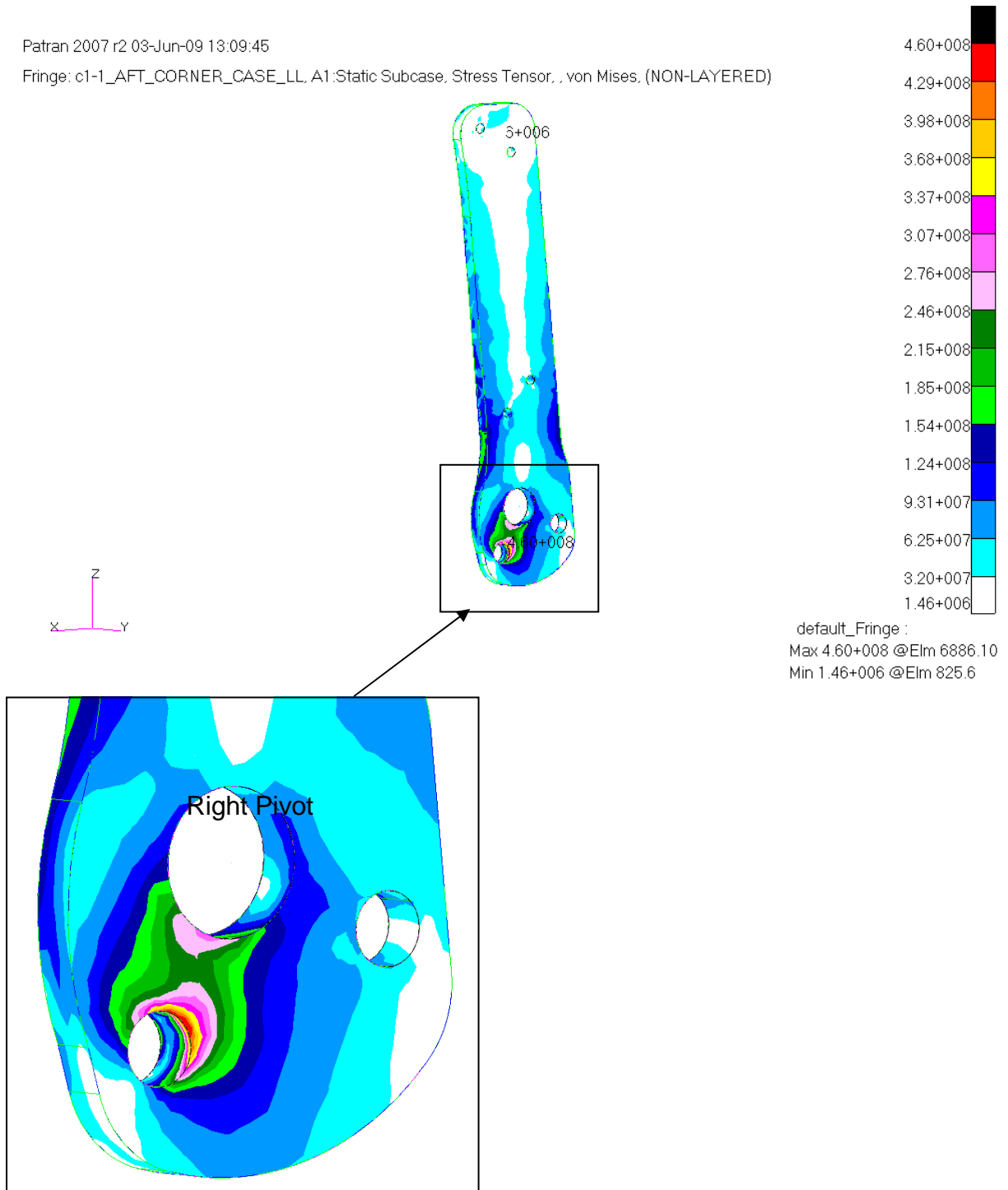
Figure 83: Maximum Von Mises stress in pivots

APPENDIX C : BACKREST TEST RESULTS

Table 28: Corrected backrest deflection results

	x_0 [mm]	x_{200lb} [mm]
E01	4.6	24.0
E02	11.6	21.4
E03	10.8	21.5
E04	10.4	21.3
E05	14.2	22.1
TP01	12.0	21.5
TP02	12.1	21.9
TP03	12.1	23.6
TP04	13.2	20.9
TP05	12.5	23.9

Table 29: Backrest masses

	Mass [kg]
E01	2.215
E02	2.205
E03	2.235
E04	2.230
E05	2.245
TP01	2.395
TP02	2.220
TP03	2.255
TP04	2.405
TP05	2.195

AVERAGE	2.226	kg
SD	0.016	

AVERAGE	2.294	kg
SD	0.099	

Table 30: Backrest calculated stiffness

	[lbf/mm]	[N/mm]
E01	8.3	37.1
E02	9.3	41.6
E03	9.3	41.4
E04	9.4	41.7
E05	9.1	40.3
TP01	9.3	41.5
TP02	9.1	40.6
TP03	8.5	37.7
TP04	9.6	42.5
TP05	8.4	37.2

AVERAGE	40.4	N/mm
SD	1.95	

AVERAGE	39.9	N/mm
SD	2.36	

Table 31: Backrest specific stiffness

	[N/mm.kg]
E01	16.7
E02	18.9
E03	18.5
E04	18.7
E05	17.9
TP01	17.3
TP02	18.3
TP03	16.7
TP04	17.7
TP05	16.9

AVERAGE	18.15	N/mm.kg
SD	0.86	

AVERAGE	17.38	N/mm.kg
SD	0.62	